SYNTHESIS OF β-ALUMINA-TYPE COMPOUNDS AND THEIR TRANSFORMATION VIA THE TCON PROCESS

by

Dominic Loiacona

Submitted in Partial Fulfillment of the Requirements

for the Degree of

Master of Science

in the

Chemistry Program

YOUNGSTOWN STATE UNIVERSITY

December 2010

SYNTHESIS OF β-ALUMINA-TYPE COMPOUNDS AND THEIR TRANSFORMATION VIA THE TCON PROCESS

Dominic Loiacona

I hereby release this thesis to the public. I understand that this thesis will be made available from the OhioLINK ETD Center and the Maag Library Circulation Desk for public access. I also authorize the University or other individuals to make copies of this thesis as needed for scholarly research.

Signature:

Dominic Loiacona, Student Date

Approvals:

Dr. Tim Wagner, Thesis Advisor Date

Dr. Clovis Linkous, Committee Member Date

Dr. Virgil Solomon, Committee Member Date

Peter J. Kasvinsky, Dean of School of Graduate Studies and Research Date

Abstract

Fireline TCON, Inc., a ceramics company in Youngstown, Ohio, has developed a unique method for producing co-continuous ceramic/metallic composite materials. These TCON composite materials are usually produced from a reaction of silica with molten aluminum via a process known as reactive metal penetration, producing an interpenetrating phase composite of aluminum oxide and aluminum metal, where silicon is alloyed with aluminum in the metal phase. These composite materials have a variety of interesting properties, such as extremely high tolerance of heat, resistance to corrosion, and high strength.

Theoretically, the TCON process can be altered in order to utilize a wide variety of metal oxides other than silica as sacrificial oxides. A class of compounds known as β-aluminas are of particular interest, as these compounds contain open channels within their crystal structure, which may facilitate the TCON reaction or produce a TCON composite with different morphology and properties than have previously been reported. Specifically, the possibility of producing a nano-scale composite is being investigated, due to the nano-scale features of the β-alumina crystalline structure itself. Several different β-alumina compounds have been prepared and transformed via the TCON process. Phases present in the product were analyzed via PXRD, and the morphology of the composite was analyzed via SEM. Several related spinel phases were prepared and transformed for comparison to results for transformed β-alumina.

In addition, attempts have been made to produce novel β-alumina structures that would be beneficial as sacrificial oxides in the TCON process. Novel compounds such as $SrTi_5Mg_6O_{17}$ that would transform under TCON conditions would result in a number of

beneficial properties in the produced composite. These benefits include the presence of aluminum-titanium alloys, which have excellent strength-to-weight ratios.

Acknowledgements

First and foremost, I would like to thank my research advisor, Dr. Tim Wagner, for all of his advice and guidance throughout the course of this project. I would also like to thank Dr. Matthias Zeller for his guidance on the powder XRD, and the extra time he devoted to solving some of the issues we had with the refinement program, which was an integral portion of this research. I would also like to thank Dr. Virgil Solomon for the time and effort he devoted to helping me use the SEM, another integral portion of this research, as well as for being a part of my thesis committee. I would like to thank Dr. Clovis Linkous for the time he spent fitting the tube furnace that I regularly use with a ventilation system so that a wider variety of reactions can be ran in the furnace, in addition to being part of my thesis committee. Also, I would like to thank Mark Peters and Eddie Stride of Fireline for all of their help and the use of their molten aluminum furnace, and for allowing this research project to exist in the first place.

I would like to thank the Youngstown State University Chemistry Department as a whole, for providing me with the education and the skills necessary for me to succeed as a chemist. Thank you to all of the professors who have instructed me or offered me guidance along the way. Thank you to all of my fellow graduate students for all of your support, as well as for the fun times. Thank you to Tim Styranec for procuring for me all the equipment and chemicals that made my research possible. Thank you to Ray Hoff for fixing all of the equipment that I may or may not have been responsible for breaking.

Last but not least, I would like to thank my family and friends for all of their support. Thanks to my loving wife Pam for all of your support, and for listening to me rant for hours about chemistry, even though you have no idea what I'm talking about.

Thank you to my parents for your emotional and financial support throughout my education. Thank you to my friends and to my brother for always providing me with a chance to take a break from my studies and have some fun. And of course, thank you to the rest of my family for all of your guidance and support.

Table of Contents

Chapters

List of Figures

List of Tables

CHAPTER I – INTRODUCTION

A. Introduction to Solid State Chemistry

Traditionally, solid state chemistry has been the study of extended inorganic solids. Some of the many disciplines overlapping with solid state chemistry include metallurgy, crystallography, mineralogy, and ceramic chemistry. Recently, the field has expanded to include novel areas, such as metal oxide framework materials, or even biomaterials. One of the key differences between solid state chemistry and traditional wet chemistry is that in solid state chemistry, extremely high temperatures are often required to drive a chemical reaction. Materials chemistry, sometimes used interchangeably with solid state chemistry, focuses more on structure-property relationships, and the design of materials for specific applications.

When describing crystal structure, it is important to understand the concept of a crystal lattice. A lattice is an array of points, each of which has an identical environment. The space of any lattice can be divided into identical parallelepipeds by connecting these lattice points. This parallelepiped is called the unit cell, and a crystal can be defined as an effectively infinite stacking of these unit cells in three-dimensional space. When defining the unit cell for a particular crystal structure, the unit cell chosen is that which has the highest symmetry (1). Refer to Figure 1.1 for a diagram of the unit cell of NaCl, which is a typical face centered cubic unit cell.

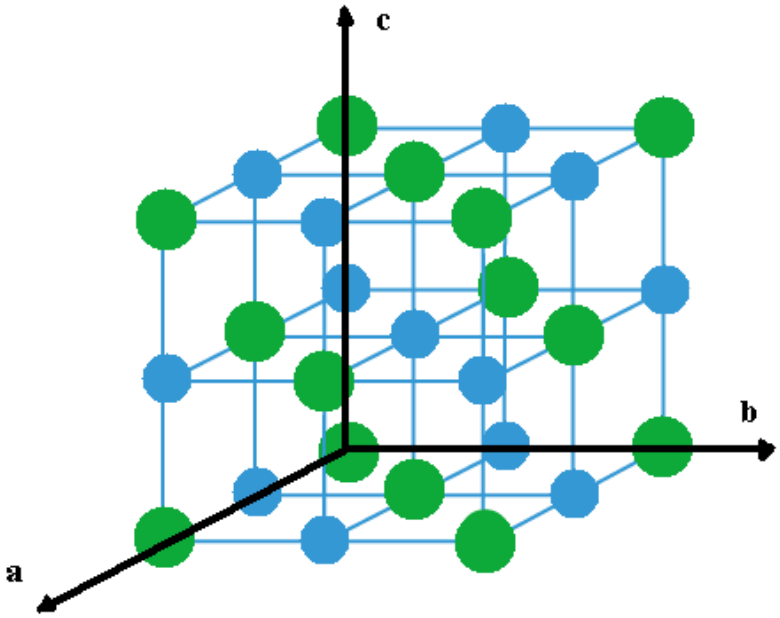

***Figure 1.1*. Unit cell of Sodium Chloride, which is face centered cubic. chloride ions are green, sodium ions are blue.**

When every lattice point is at a vertex (or corner), the unit cell is said to be primitive. While a cubic crystal system or any other such primitive crystal system contains eight vertexes, each lattice point only occupies one eighth of the unit cell's volume, so it is said that a primitive unit cell only contains one (8 x 1/8) total lattice point. Any primitive parallelepiped cell belongs to one of seven crystal systems (1).

Of these seven crystal systems, fourteen different total lattices are possible, which are termed Bravais lattices. It is possible to have fourteen Bravais lattices in only seven crystal systems since each crystal system can contain more than one Bravais lattice, due to the positioning of the lattice points within the crystal system. For example, the cubic crystal system contains three Bravais lattices; primitive, body centered, and face centered. The body centered cubic Bravais lattice contains a lattice point directly in the center of

the unit cell that is identical to the lattice points found at the vertices of the unit cell. Similarly, the face-centered cubic Bravais lattice contains a lattice point in the center of each face of the cube within the unit cell. In the above example, sodium chloride would be considered a face centered cubic unit cell, since a chloride ion exists at each corner of the unit cell, as well as in the center of each face of the unit cell (1). Refer to Figure 1.2 for unit cell diagrams of the fourteen Bravais lattices.

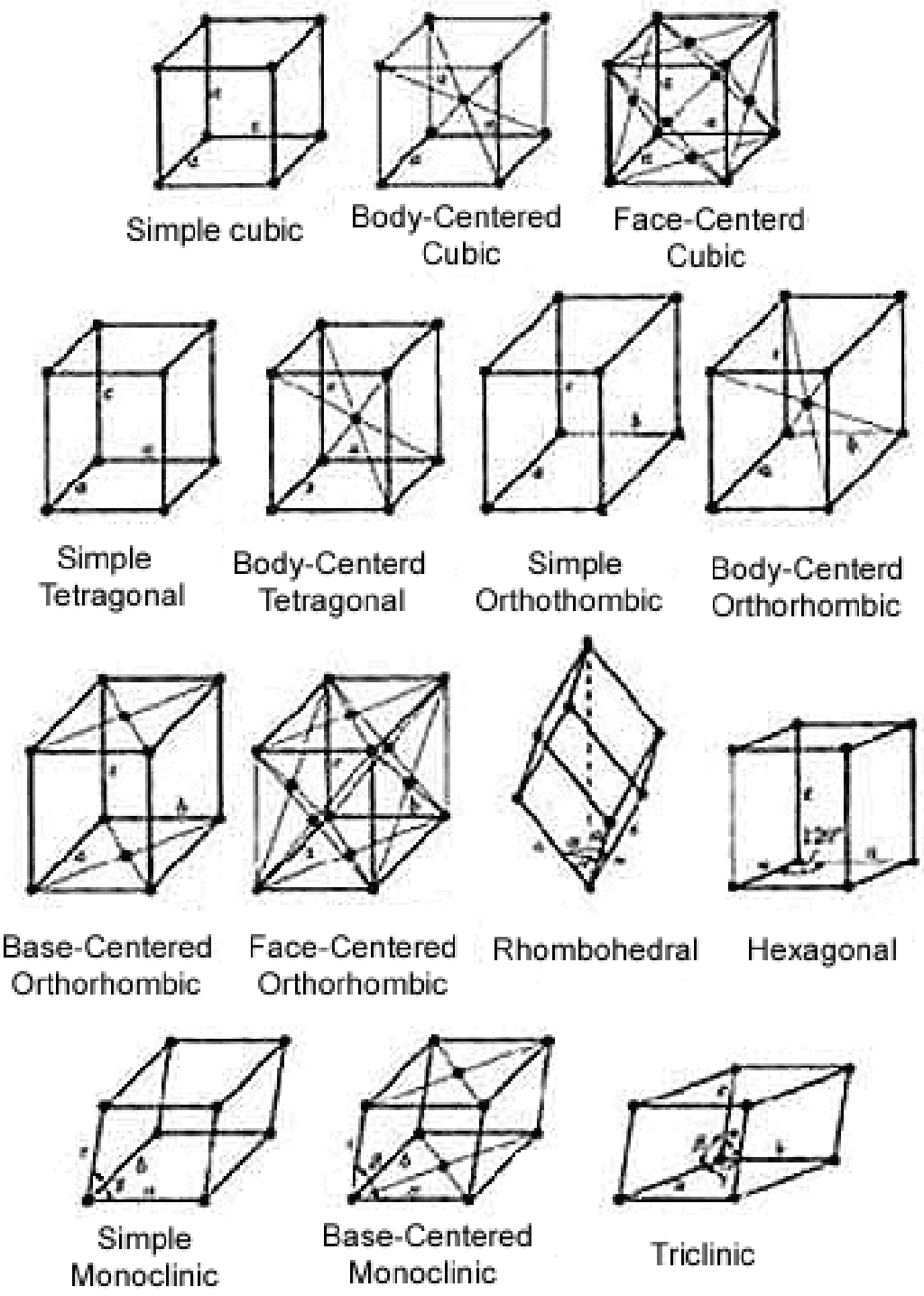

***Figure 1.2*, Unit cells of the fourteen possible Bravais lattices (1)**

A variety of parameters that define dimensions and angles can be used to describe any unit cell. Geometrically, unit cells contain three parameters, *a, b,* and *c*, which measure the dimensions of the unit cell in 3-dimensional space. The origin point of the unit cell parameters is conventionally placed at the bottom, back, left corner of the unit cell. The angles α, β, and γ are used to describe angles of the unit cell with respect to these parameters. Specifically, the Greek letter which denotes angle is the counterpart of the English letter omitted from the edge combination; i.e. the angle β measures the angle between unit cell parameters *a* and *c*. These unit cell parameters and angles, and how they relate to one another, are used to define crystal systems. For example, a cubic crystal system is one where $a = b = c$, and $\alpha = \beta = \gamma = 90°$ (1).

Locations within a unit cell are not given by relative position in terms of *a, b,* and *c*, but rather, by coordinates *x, y*, and *z*. These coordinates are fractions of *a, b,* and *c*, within the range of 0 to 1, and usually displayed as fractions. Therefore, a point within a unit cell can be defined in the format of (*x y z*) (1).

A lattice plane can be designated by selecting an arbitrary lattice point as the origin and indicating the intercepts of the plane with the three crystallographic axes in units of *a, b,* and *c*. This notation is the Weiss index of lattice planes; however, more commonly the Miller Index system is used, due to the reciprocal space nature of crystallography, since the Miller index is simply the reciprocal of the Weiss index. The Miller index is used to denote a set of equally spaced parallel planes, including one through the origin. The notation *hkl* is used when describing Miller indices, where *h* gives the number of equal divisions of the *a* edge, *k* the divisions of the *b* edge, and *l* the divisions of the *c* edge of the unit cell. A bar over the number in the Miller index

indicates a negative value (1). Understanding the concept of crystal planes is important to understanding and performing powder XRD, which was utilized extensively throughout this research and will be discussed in a later chapter. Refer to Figure 1.3 for a diagram of several common examples of crystallographic planes and their Miller indices as they exist in the cubic crystal system.

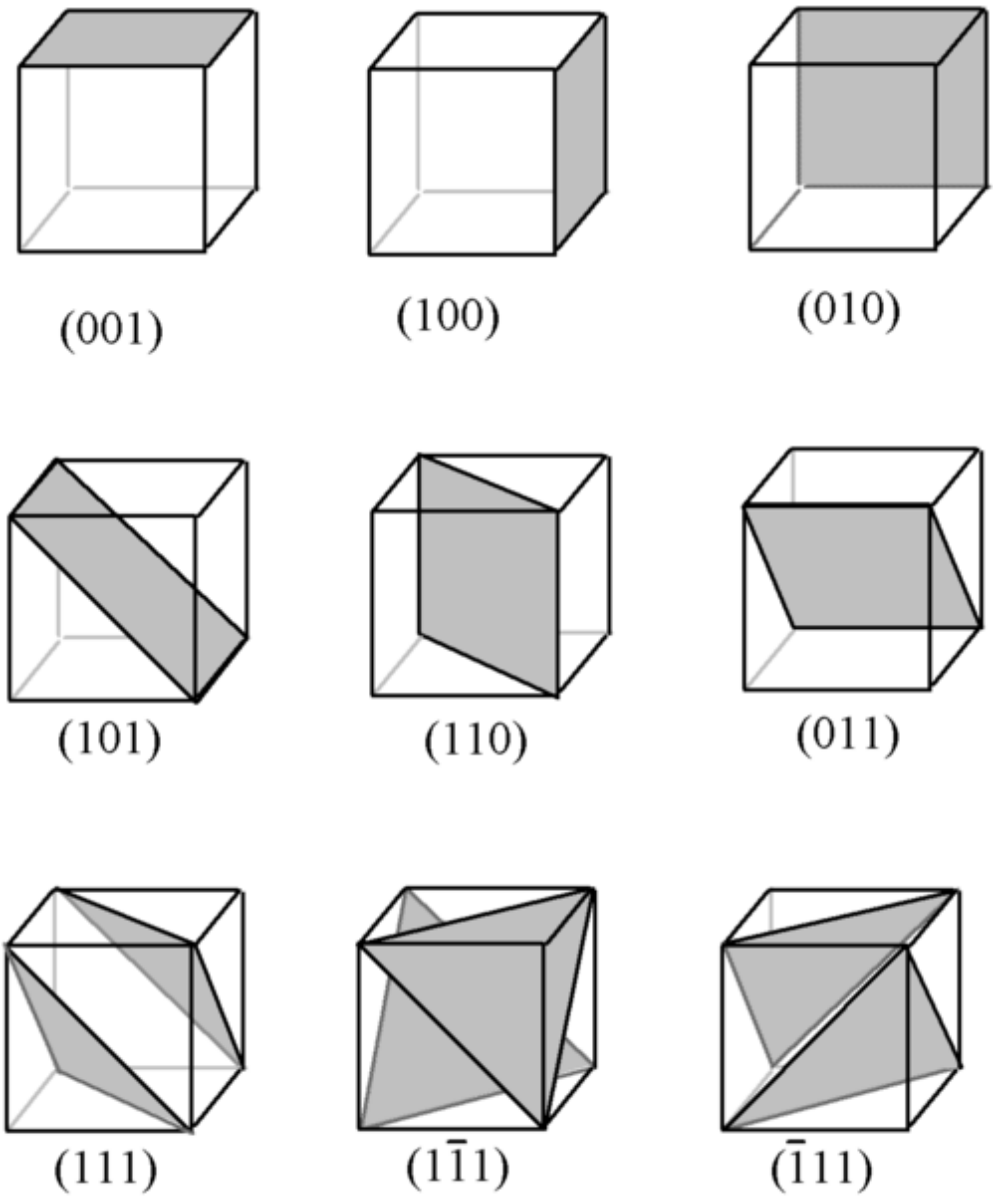

***Figure 1.3*, Example of common crystallographic planes and their Miller indices. Shown are unit cells in the cubic system**

B. Reactive Metal Penetration and the TCON© Process

Fireline-TCON, Inc., a subsidiary of Fireline Inc., has developed a unique process for developing interpenetrating phase ceramic-metallic composite materials. These materials exhibit a very high strength, as well as excellent refractory properties (tolerance of high temperatures). Also, these materials are extremely resistant to erosion and corrosion by molten aluminum, and can easily be made into a wide variety of shapes. TCON products have numerous applications, primarily in industries where transport of molten metals is required, but also including automotive braking components and force protection materials for vehicle and body armor systems (2).

These ceramic/metallic composites can be described as a continuous ceramic network interpenetrated by a continuous network of reinforcing metals, and is therefore a co-continuous composite material. Each constituent phase in the composites is topologically interconnected throughout the microstructure, so it can be expected that each phase will contribute its own properties to the macroscopic properties of the composites. The ceramic phase, for example aluminum oxide in the form of corrundum, provides low density, high modulus (a measure of stiffness), and high temperature resistance to the composites. The metallic aluminum phase offers good toughness, and good thermal and electrical conductivity (3).

Currently produced TCON materials can usually be characterized by the following chemical reaction (2);

$$\mathbf{(4 + x)Al + 3SiO_2 \rightarrow 2Al_2O_3 + xAl + 3[Si]_{Al}}$$

Equation 1.1

An object made of silica is submerged in molten aluminum, and an interpenetrating phase composite material of silica and aluminum is formed, where the silicon is alloyed with the aluminum in the metal phase. In the reaction above, the silicon dioxide is referred to as the "sacrificial preform", since it will be consumed during the reaction. The molten metal is a reductive agent, since silicon from the sacrificial preform is reduced, and aluminum is oxidized to alumina. In terms of volume, the aluminum oxide forms about 63% of the base matrix, and the aluminum-silicon alloy about 37% (2). Refer to Figure 1.4 for an SEM micrograph of a TCON composite, demonstrating the co-continuous nature of the phases.

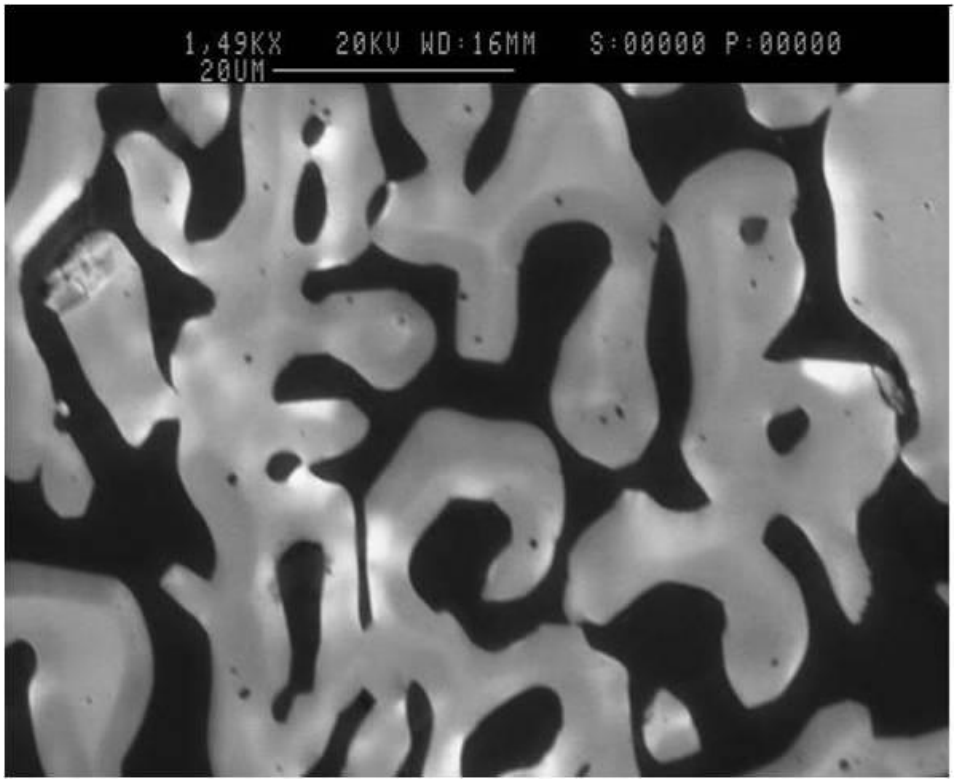

***Figure 1.4*. SEM micrograph of TCON material. Lighter areas are aluminum oxide, darker areas are metal alloy. (2)**

The TCON process is actually very simple. A preform is made via standard ceramic procedures, and submersed in a transformation furnace containing molten

aluminum metal. Reaction time is dependant on the thickness of the preform, as the aluminum oxide phase initially forms on the surface of the preform and grows into the silica. Growth rate constants were found to be around 1.6 mm/hr at 1000 ºC for Al_2O_3/Al composites (3). Further reaction occurs in a reaction front between the sacrificial silica preform and the growing Al_2O_3/Al composite. Refer to Figure 1.5 for a diagram of the reactive metal penetration reaction. After the reaction is complete, the object is removed from the furnace, and excess aluminum is removed. The original shape and dimensions of the preform are maintained, with the exception of a very small reduction in size, about 1%. The resulting composite material has a strength equal to about 5 to 10 times that of the origional starting ceramic material (2). Refer to Figures 1.6 and 1.7 for images of the molten aluminum furnace, and examples of TCON products, respectively.

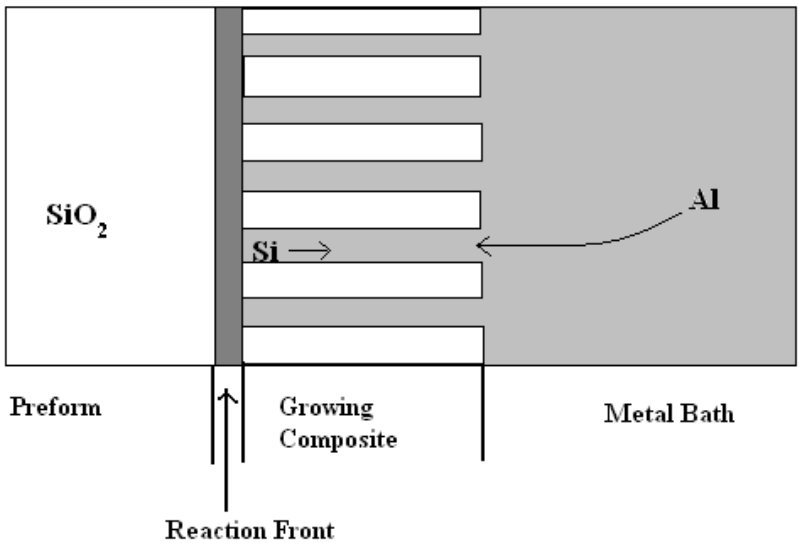

Figure 1.5. **Schematic illustration of the reaction and growing mechanism during the formation of the alumina/aluminum composite by immersing silica in molten aluminum via reactive metal penetration. The liquid Al channels in the aluminum oxide network serve as transport paths for Al and Si. (3)**

Figure 1.6. **Molten aluminum furnace at Fireline TCON Inc, in Youngstown Ohio (2).**

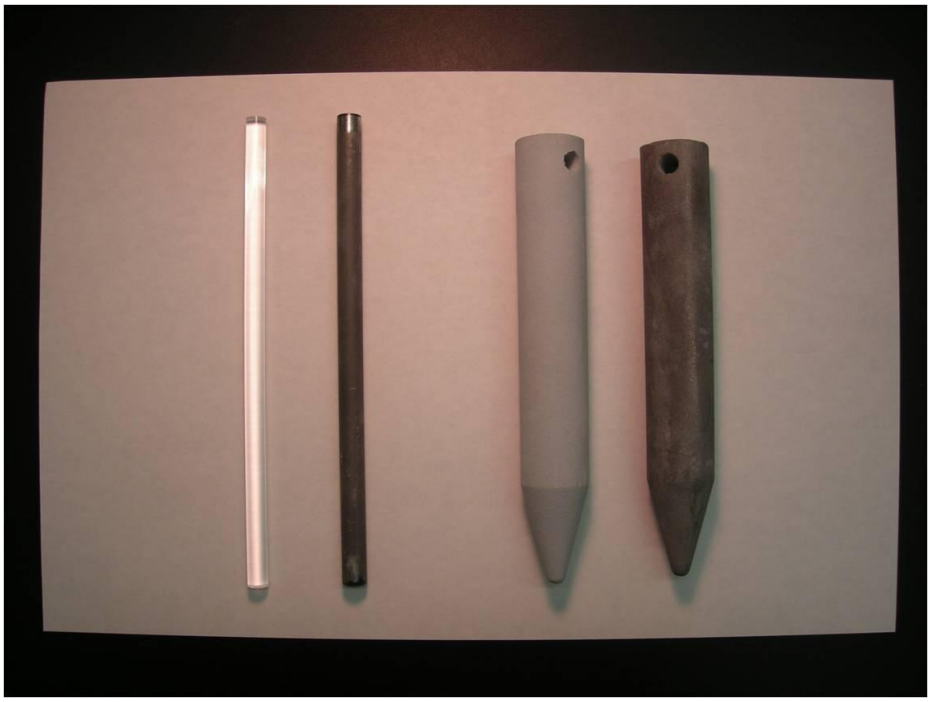

Figure 1.7. **Silica objects transformed via the TCON process. On the left is a silica rod before and after TCON transformation, on the right is a ceramic object before and after transformation. The TCON materials in both cases are the darker ones (2).**

In addition to silica, other ceramic materials could theoretically be used as sacrificial preforms, and indeed, this thesis is largely concerned with investigating novel ceramic materials for this role. A wide variety of oxides, carbides, nitrides, borides, or sulfides can be utilized. Also, the molten metal is not limited to just aluminum. Magnesium, iron, nickel, cobalt, titanium, tantalum, tungsten, yttrium, niobium, zirconium, hafnium, and various alloys can be employed as reductive agents for the processing (3). For example, a similar process has been observed in the formation of an interpenetrating MgO/Mg composite by immersing silica preforms in molten magnesium (3).

Taking this into account, a generalized chemical reaction can be made to describe any composite formed via reactive metal penetration, as per Liu and Kuster (3);

$$\frac{2}{y}\,Sa_xO_y(s) + \frac{2p}{q}\,Me(l) \longrightarrow \frac{2q}{q}\,Me_pO_q\,(s) + \frac{2x}{y}\,Sa(s \text{ or } l)$$

Equation 1.2

Sa denotes the metal element in the sacrificial oxide, and Me is the reductive metal. Liu and Kuster (3) outline the criteria for the formation of an oxide/metal composite through the described process are as follows;

1. The produced oxide (Me_pO_q) must have a smaller volume than the sacrificial oxide (Sa_xO_y). This is necessary so that the reaction can proceed as molten metal seeps through the voids left in the material as the reaction proceeds to completion through the entire object.

2. The produced oxide must be more stable than the sacrificial oxide. In other words, the free energy of formation of the produced oxide must have a more negative value than that of the sacrificial oxide.
3. The processing temperature must be higher than the melting point of the reductive metal (Me) but lower than its boiling point. The processing temperature must also be lower than the melting or sublimating point of both the sacrificial and the produced oxides.

This gives a very wide range of possible sacrificial oxides that can be utilized as performs in a molten aluminum furnace at 1000 °C, such as CuO, NiO, MnO, WO_2, MoO_2, SiO_2, Cr_2O_3, Fe_3O_4, Ta_2O_5, Nb_2O_5, $NiCr_2O_4$, $MgFe_2O_4$, $FeCr_2O_4$, $NiAl_2O_4$, and $CoAl_2O_4$ (3). Again, since these are the sacrificial oxides, the produced composite will almost always be Al_2O_3/Al, with the metal elements of the sacrificial oxide being alloyed with aluminum in the metal phase. Refer to Figure 1.8 for a graph that displays some of the possible sacrificial oxides that can be used in a reaction with molten aluminum. There are a few exceptions to this generalization, such as when using NiO as the sacrificial oxide, which actually reacts with molten Al to form $NiAl_2O_4$ as the produced oxide. (3).

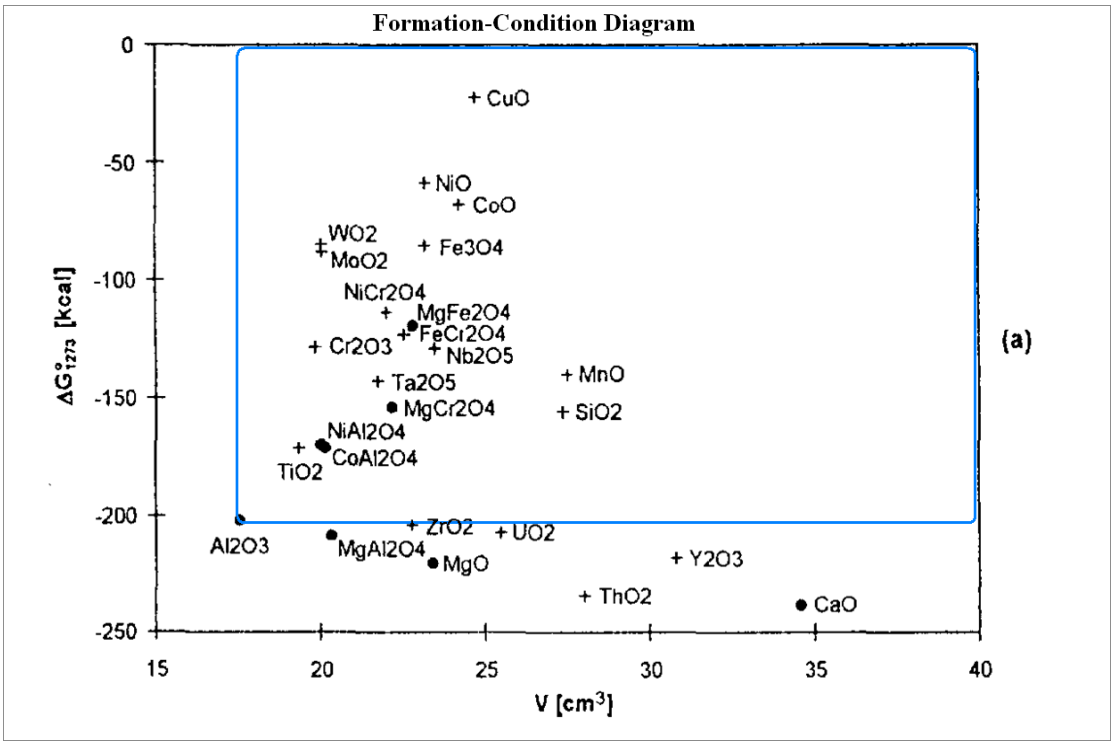

***Figure 1.8*. Formation-Condition Diagram of Reactive Metal Penetration reactions. The necessary reaction conditions for reactive metal penetration to occur require that the sacrificial oxide be both above and to the right of Al_2O_3 in this chart. Since Al_2O_3 is both one of the densest, and one of the most stable oxides, an extremely broad range of sacrificial oxides can react with molten aluminum to form the desired composite material (3).**

Since such a wide range of ceramic materials can theoretically be utilized in the TCON process, part of the focus of the Wagner group at Youngstown State University is on the preparation of novel ceramic materials for use in this process.

C. Structure of Ceramic Compounds

1. General Properties of Ceramic Materials

Ceramic materials are of great interest to materials science. In fact, ceramics itself is one of humanity's oldest technologies, with a history of about ten thousand years. This number has even more meaning when compared to something like polymer technology, which has existed for less than a hundred years (4). Ceramic compounds are generally perceived as being inorganic crystalline oxides. However, other classes of materials that are considered ceramics include nitrides, carbides, borides, silicides, and halides. So depending on how broadly one would like to define the word, nearly any ionic crystalline compound can be called a ceramic material. Some ceramicists even consider non-crystalline, amorphous solids such as glass to be ceramic compounds (4). But traditionally, ceramic compounds are mostly considered to be inorganic crystalline oxides, which is the definition that will be used throughout this research, if only for the reason that all ceramic materials dealt with herein can be defined in this manner.

Even though ceramic compounds encompass such a broad range of materials, most of them share some common properties with one another. Ceramics tend to be extremely hard, with the oxides of most metals being harder than the metals themselves. However, ceramics tend to be brittle, and not malleable like their metallic counterparts (4). Another common trait of ceramic materials is their extremely high melting points, which is of obvious importance to this research, since the sacrificial oxides utilized in the TCON process must be solids at temperatures that the TCON process is performed at.

2. Corundum and Similar Compounds

The most stable form of aluminum oxide, also known as alumina, is corundum, or α-alumina. This compound exists in nature in the form of sapphire, ruby, and emery, with minor impurities contributing to the color of these gems. In its pure form, Al_2O_3 is colorless, and is known as white sapphire when occurring naturally. Corundum is particularly well known for its hardness, and as such is commonly used as an abrasive. The absolute hardness of corundum is 400, compared to diamond's value of 1600 and quartz's value of 100 (4).

The structure of corundum is based on hexagonal close-packing of oxygen ions, with aluminum ions in two-thirds of the octahedral holes. The unit cell of corundum is trigonal, with a space group of R3c. The unit cell parameters are a=4.75 Å and c=12.982 Å, with Z=6. The corundum structure is also seen in a variety of other compounds, the most common of which are Fe_2O_3, Cr_2O_3, Ti_2O_3, and V_2O_3 (4). Refer to Figure 1.9 for a diagram of the unit cell of corundum.

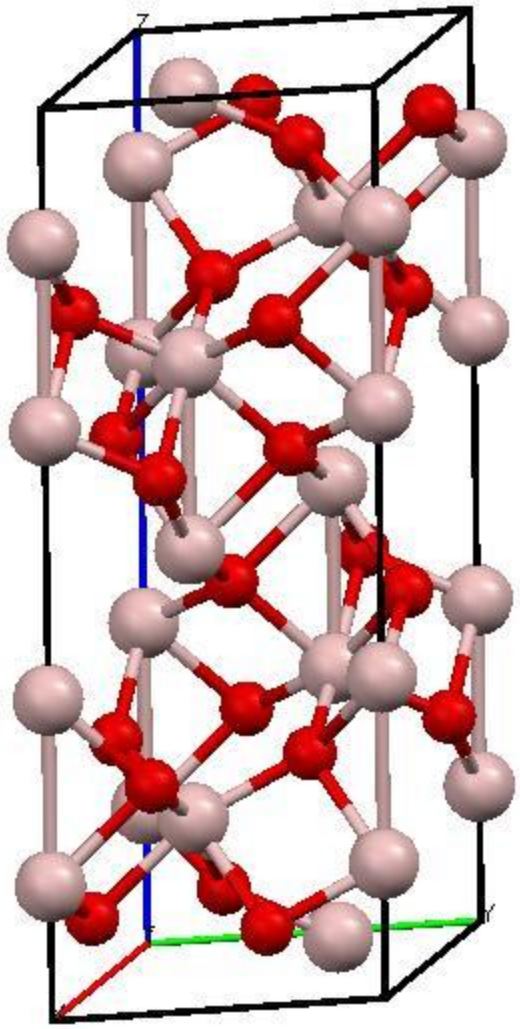

Figure 1.9. **Unit cell of corundum, α-Al_2O_3, prepared by the Mercury software package. Oxygen ions are red, Aluminum atoms are off-white.**

3. Perovskites

Perovskite itself is a mineral of the formula $CaTiO_3$; however, the term perovskite is also widely applied to compounds with a similar structure. As such, any mentioning of the word "perovskite" henceforth in this research will be in reference to the structure type, and the broad range of compounds which exhibit this structure, not to the actual

compound $CaTiO_3$. All perovskites have a similar formula, which can be generalized as ABO_3, where A is a +2 charged cation, and B is a +4 charged cation. These compounds exhibit a variety of interesting electrical and magnetic properties, such as colossal magnetoresistance, ferroelectricity, and superconductivity (4).

The ideal structure of perovskites is cubic, and can be considered a face-centered cubic array of oxygen ions and +2 charged cations, with the +4 species occupying one-quarter of the octahedral interstices. Some compounds that adopt a perovskite structure are $SrTiO_3$, $BaTiO_3$, $CdTiO_3$, and $PbTiO_3$, as well as other similar compounds in which titanium is replaced by zirconium, tin, or other ions (4). Perovskite itself, $CaTiO_3$, is orthorhombic at room temperature, and converts to the cubic phase at high temperature. Refer to Figure 1.10 for the ideal cubic perovskite structure, as represented by compounds such as $SrTiO_3$.

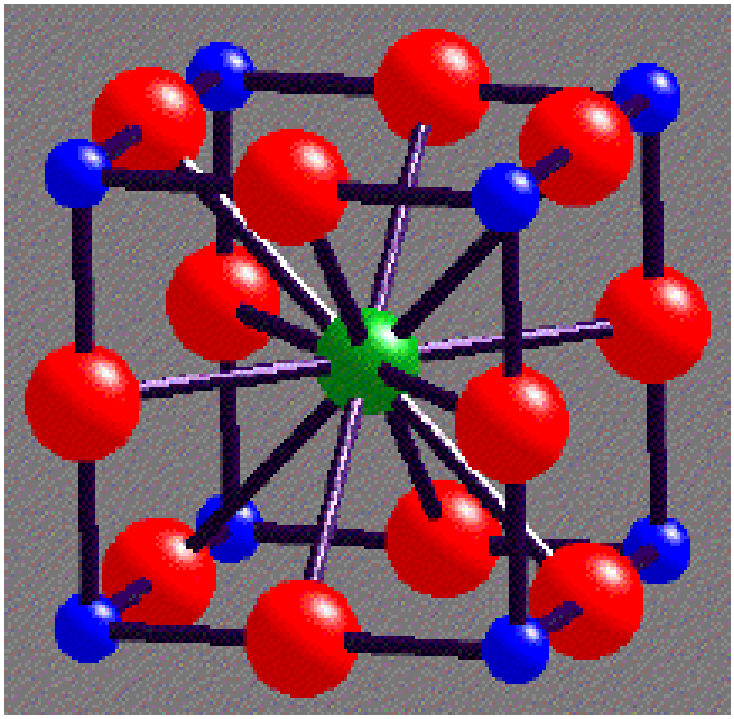

Figure 1.10. **Unit cell of $SrTiO_3$, which adopts the ideal cubic perovskite structure. Strontium ions are green, Titanium ions are blue, and Oxygen ions are red. (2)**

Another class of mineral, which is similar to both perovskites and corundum are the ilmenites. Ilmenite itself is a mineral with the formula $FeTiO_3$, but just as with perovskites, any mention of the word "ilmenite" henceforth in this research will be in reference to the structure type, and the broader range of compounds that exhibit this structure, and not just the specific compound $FeTiO_3$. It is clear that ilmenites have the same generic formula as perovskites, ABO_3; however, the +2 cation is too small to form a close-packed array with oxygen anions. As such, the structure adopted will be more similar to that of corundum, with the octahedral interstices being occupied by two species instead of one. Some other examples of ilmenites include $MgTiO_3$, $CoTiO_3$, $NiTiO_3$. As with perovskites, other compounds exist in which titanium is replaced with other +4

charged cations (4). Refer to Figure 1.9 above for the unit cell of corundum, which ilmenites adopt.

4. Spinels

Spinel, also known as magnesium aluminate, $MgAl_2O_4$, has donated its name to a structure with both frequent occurrence and great importance in ceramic science. The unit cell is cubic and contains 32 oxygen ions, with 8 magnesium ions in tetrahedral sites, and 16 aluminum ions in octahedral sites. Refer to Figure 1.11 for the unit cell of spinel. It can be seen that the cubic unit cell is split up into 8 smaller cubelets, of which alternate cubelets are identical. In fact, the only difference between the two types of cubelets is their orientation (5). Refer to Figure 1.12 for a depiction of this structural arrangement.

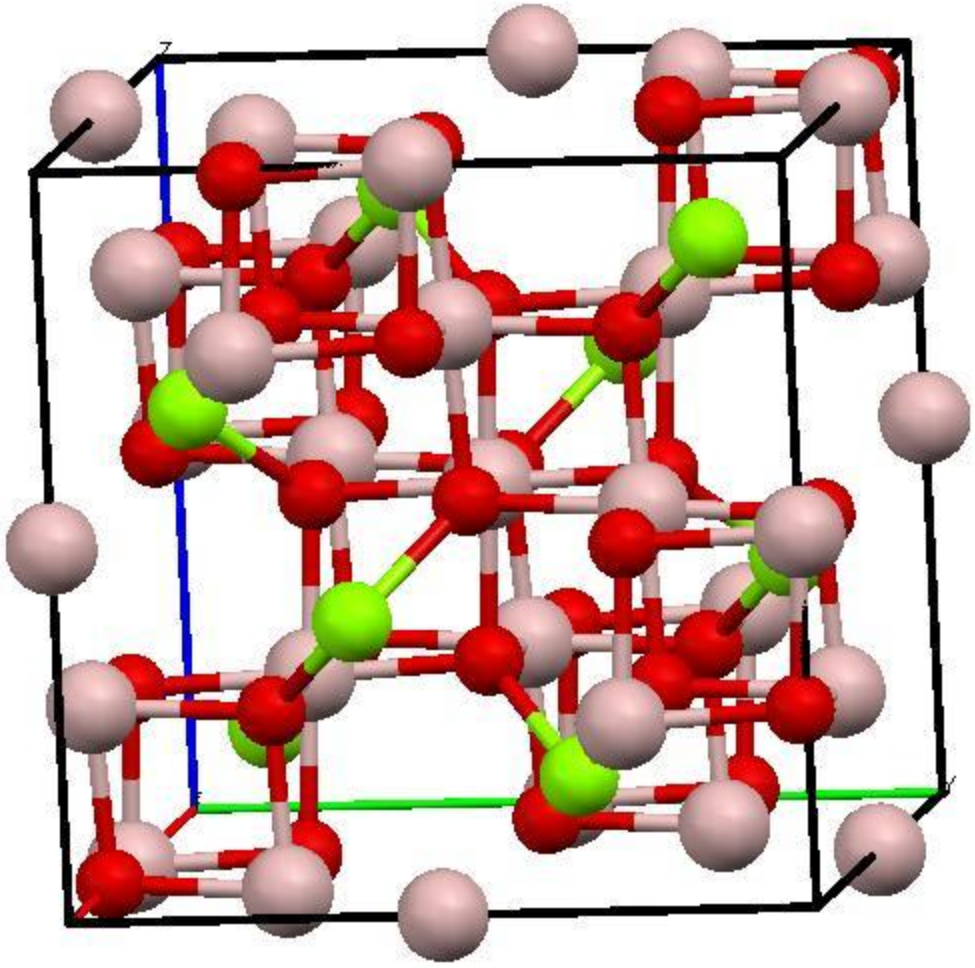

***Figure 1.11*. Unit cell of spinel, $MgAl_2O_4$. Magnesium ions are green, Aluminum ions are off-white, and Oxygen atoms are red.**

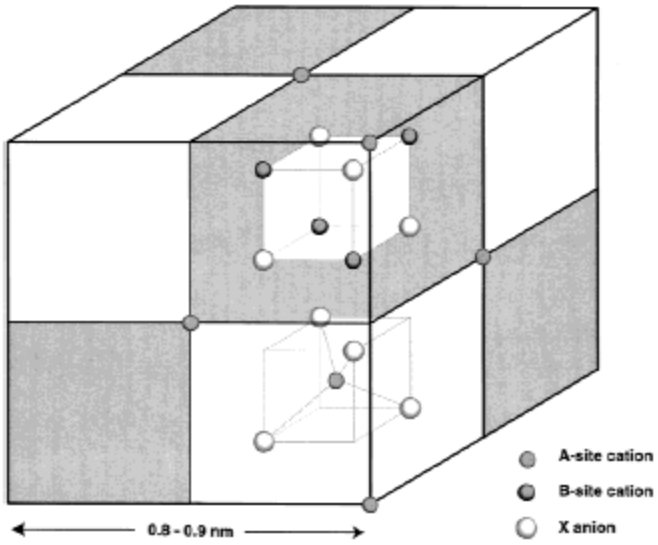

Figure 1.12. **Unit cell of spinel structures, displaying primitive tetragonal and conventional cubic unit cells of spinel. The primitive unit cell consists of two octants of the conventional unit cell, one within the other. Atom positions are only shown for the primitive unit cell. Atomic positions throughout the whole conventional unit cell alternate as displayed by the pattern of white and shaded cubelets. One A site cation is not displayed, is exists on the center of the base of the cubic unit cell. (5)**

As before with perovskites, any mention henceforth of "spinel" is in reference to the broad range of compounds which adopt a structure similar to that of the compound itself spinel, $MgAl_2O_4$. That being said, the great deal of flexibility found in the differing combinations of cations forming a spinel-like structure should be mentioned. While a spinel most traditionally has the formula AB_2O_4, with A possessing a +2 charge, and B possessing a +3 charge, this is not always the case. There are many examples of spinels, such as $TiMg_2O_4$, where instead of one +2 cation and two +3 cations, there are two +2 cations, and one +4 cation. Also, there are compounds in which one +6 cation exists with two +1 cations to form a spinel structure. Indeed, the only true requirement of the cation charges is that they have a sum of +8 so as to satisfy the total of -8 charge from the oxygen anions (4). For this reason, spinels henceforth in this research will be referred to

as being 2,3,3 spinels, 2,2,4 spinels, and 1,1,6 spinels, reflecting the charges of the cations involved.

Another interesting spin on the structure of spinels is that there are “normal” spinels, and “inverse” spinels. A normal spinel is one in which the divalent cations occupy the tetrahedral sites and the trivalent ions occupy the octahedral sites. An inverse spinel is one in which the tetrahedral sites are occupied by only half of the trivalent cations, and the octahedral sites are shared between the divalent cations, and the other half of the trivalent cations. In applications where this difference is important, it is customary to write the formula for the spinel with the cations in the octahedral sites in brackets. For example, $MgAl_2O_4$ existing as a normal spinel would be written as $Mg(Al_2)O_4$. $MgFe_2O_4$, a spinel commonly found in its inverse form, would be written as $Fe(MgFe)O_4$ (4).

Spinels of the 2,3,3 variety are generally classified as being aluminates (based on Al_2O_3), ferrites (based on Fe_2O_3), and chromites (based on Cr_2O_3). The divalent ion can be, but is not limited to, Mg, Fe, Zn, Mg, Ni, Cu, or Co. Spinels of the 2,2,4 variety are usually based on SnO_2 and TiO_2, compounding with the above divalent ions (4). Other compounds which adopt a type of spinel structure include γ-Fe_2O_3 and γ-Al_2O_3. In fact, when we write these compounds in the form $M_{8/3}O_4$, in order to more closely resemble traditional spinel formulae, we can see that these compounds will exhibit a defective spinel structure, as there are not enough cations to fill all of the available sites. Because of this, one ninth of the cation sites are left empty in these structures (4).

5. β-Alumina and Similar Compounds

Hexagonal aluminates having a β-alumina, magnetoplumbite, or similar structure have commonly been referred to as hexaaluminates. Of these compounds, the most well-known is sodium β-alumina, often commonly just called β-alumina, since this is the compound for which the structure is named after. The general chemical formula for β-alumina is $NaAl_{11}O_{17}$, and this compound is known for its superior ionic conductivity. As such, this compound and those like it have a variety of applications in conductivity, fluorescence, laser processes, nuclear waste disposal, and high temperature combustion catalysis. It should be noted that the term β-alumina comes from a misnomer upon discovery of the material. It was originally thought to be an alternate phase of Al_2O_3, and since common corundum is known as α-alumina, it was termed β-alumina. It was known; however, that the structure was defective with sodium, and not pure aluminum oxide. Only later was it discovered that sodium is actually critical to the structure of the compound (6).

The unit cell of β-alumina is hexagonal, with a space group of P63/mmc. The unit cell parameters are generally reported as being close to $a=b=5.60$ Å, and $c=22.50$ Å. β-alumina's structure consists of alternating planes of spinel blocks of aluminum oxide and conduction layers of sodium oxide, where Na^+ ions are mobile and account for the material's superior conductivity. While stated before that the chemical formula for β-alumina is $NaAl_{11}O_{17}$, β-Alumina is actually better described as a non-stoichiometric compound, since β-alumina and compounds like it tend to contain much more sodium than the chemical formula would imply. Sodium β-alumina contains excess Na^+ ions on the conduction plane, and if we were to be entirely accurate, the chemical formula would

be better expressed as $Na_{1+x}Al_{11}O_{17+ x/2}$, where x is usually close to 0.25. To compensate for the additional positive charge of the excess sodium ions, a complex Frenkel defect mechanism is present in the structure, wherein a pair of interstitial Al^{3+} ions, which have migrated from the spinel block by the Frenkel defect mechanism, are bridged by interstitial oxygen ions formed by this complex defect mechanism (7). Refer to Figure 1.13 for a schematic of the ideal (i.e. stoichiometric) β-alumina structure, seen as multiple unit cells. Refer to Figure 1.14 for a single unit cell of β-alumina. Refer to Figure 1.15 for a more detailed comparison of the spinel $MgAl_2O_4$ structure in comparison to the spinel-like blocks found in β-alumina structure.

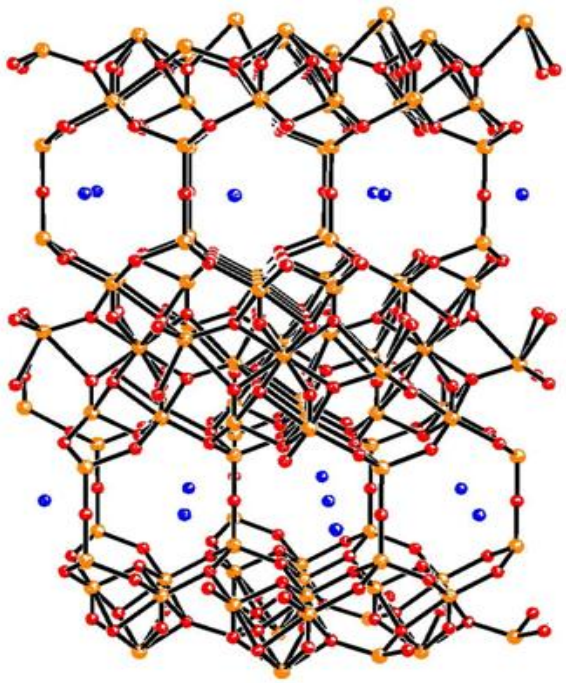

Figure 1.13. **β-Alumina crystalline structure, displaying alternating spinel layer and conduction layer. blue = sodium, yellow = aluminum, red = oxygen (2).**

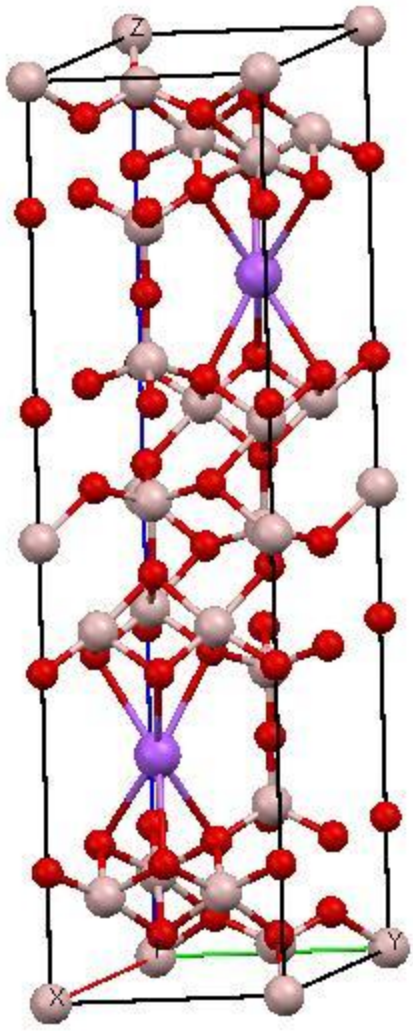

***Figure 1.14*. Unit cell of β-alumina. Oxygen atoms are red, aluminum atoms are off-white, and sodium ions are purple.**

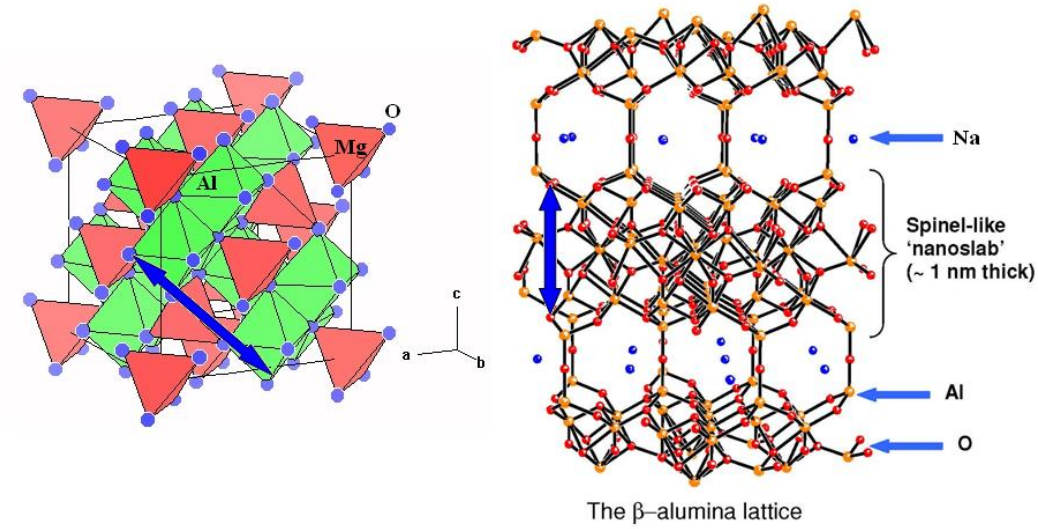

Figure 1.15. **Comparison of spinel-like blocks found in β-alumina structure (right) to the actual spinel structure (left). The blue arrows correspond to one another, showing the angle in which spinel structure exists in β-alumina (2).**

There are in fact additional structures of β-alumina that should be mentioned, which are referred to as β”-alumina, β”’-alumina, and β””-alumina. Of these different compounds, only β”-alumina has also been observed throughout this research, and this unit cell can be seen below in Figure 1.16. There is only one true difference between these two structures. Both structures consist of a spinel block in between a conduction plane; however they differ in their stacking sequence of adjacent spinel blocks, which is displayed more clearly below in Figure 1.17. This slight structural difference results in significantly different unit cell parameters, with the c axis being 33.62 Å long instead of 22.50 Å as it is in standard β-alumina. Also, β”-alumina has a different space group, R-3m, and is rhombohedral rather than hexagonal. This difference in stacking sequence results in a slightly different stoichiometry for the two compounds. β”-Alumina stacking allows for a higher level of sodium ions to be present, and therefore allows β”-alumina to be a better conductor than β-alumina. Because of the similar nature of these two

compounds, it is often difficult to synthetically produce only one, and more often than not a mixture of products is formed (8).

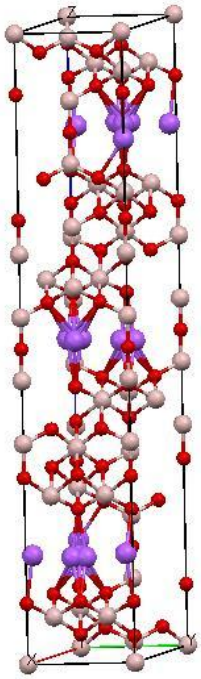

Figure 1.16. **unit cell of β"-alumina. Oxygen ions are red, aluminum ions are off-white, and sodium ions are purple.**

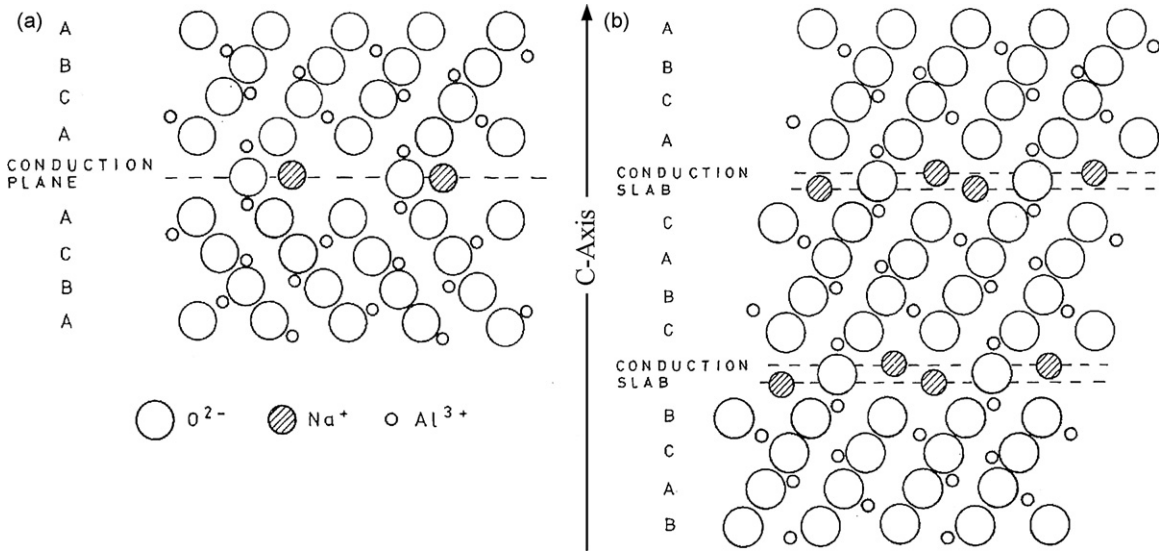

Figure 1.17. **Projection of β-Alumina (a) vs. β"-Alumina (b) along the (1 1 $\bar{2}$ 0) plane, displaying stacking sequence differences (8).**

Compounds with a similar structure to sodium β-alumina also exist, most generally when another cation takes the place of sodium in the conduction plane. The only true stipulation as to which cations can form β-alumina-type compounds is that the cation must be large enough for the conduction plane to exist. Other β-alumina type compounds that exist include $LiAl_{11}O_{17}$, $AgAl_{11}O_{17}$, $TlAl_{11}O_{17}$, $KAl_{11}O_{17}$, $RbAl_{11}O_{17}$, and $GaAl_{11}O_{17}$. While these compounds all substitute Na^{+} with another cation containing a +1 charge, it is also possible to further substitute sodium with +2 charged cations. An appropriate compensation for the additional charge can be made by replacing an Al^{3+} ion with an appropriate ion such as Mg^{2+}. One such example of this is in the compound $SrMgAl_{10}O_{17}$, where strontium exists on the conduction plane in place of sodium, and magnesium acts as a charge compensator (7).

D. Aluminum and Aluminum Alloys

While aluminum compounds have been known since ancient times, elemental aluminum metal has only been capable of being isolated since the beginning of the 19th century, and even then, only in minute quantities. By the middle of the century, it had become more widely available, but was still quite expensive. For example, the cost of the six-pound ornamental aluminum pyramid that was placed on the top of the Washington Monument in Washington D.C. in 1884 was similar to that of silver. It was not until 1886 that aluminum production became economically feasible by means of the Hall-Heroult process (9).

Aluminum is the most abundant metal in the earth's crust, most commonly in the form of bauxite, a hydrated oxide of aluminum, iron, and silicon. Aluminum oxide is extracted from this ore via the Bayer process, in which the bauxite is treated with hot sodium hydroxide. The alumina is then dissolved in a bath of molten cryolite (sodium aluminum fluoride), and then electrolyzed. The final product is molten aluminum, which is degassed, alloyed if desired, and cast into ingots (9).

While bauxite is mined in many parts of the world, aluminum smelting is only usually only done in areas where electricity costs are low, since the electrolytic process requires a great amount of energy. Aluminum is a very reactive metal, and as such, a great deal of energy is required to separate oxygen from aluminum when it is in the oxidized state. In fact, an atomically clean aluminum surface will oxidize when exposed to air within seconds. Luckily, this thin layer actually serves to protect the rest of the object, preventing further oxidation and endowing aluminum with excellent corrosion resistance in most environments. However, this does result in the need for aluminum welding procedures to require shielding from air (9).

Aluminum and its alloys have face-centered cubic crystal structures, and therefore have excellent formability properties. The strength obtainable by heat treating some alloys can be greater than in many structural steels. An alloy is a complete or partial solid solution of two or more elements, wherein a metallic matrix exists with alloying elements dissolved within the matrix, with the purpose of altering the physical or mechanical properties of the material. Aluminum metal has a high degree of reflectivity, good electrical and thermal conductivity, and low density. The low density of aluminum, combined with some high strength alloys available, give very high strength-to-weight

ratios, which are responsible for these alloys being the primary structural materials in the aerospace industry. The elastic modulus, or stiffness, of aluminum is only approximately one-third as high as that of steel, a factor which should be considered in component design in order to prevent deformation while in service. The major commercial uses for Aluminum are as follows in terms of percent tonnage of aluminum produced: the transportation industry at more than 20%, the container and packaging at more than 20%, the construction industry at more than 15%. Consumer durables, electrical products, and the machinery and equipment industry each provide between 5% and 10% of the market (9).

Throughout the course of this research, sacrificial oxides utilized in the TCON process are chosen for the compound's ability to be transformed via favorable thermodynamics and volume change, desired morphological features of the finished TCON product, and desired aluminum alloys that will hopefully be present in the metallic phase of the TCON product. It is important to understand that aluminum alloys exist in one of two different categories; wrought alloys and cast alloys. Alloys are traditionally formed by mixing alloying elements in with the molten metal, and are then cast into the desired shape and allowed to solidify by cooling. A wrought alloy is simply one that has been mechanically worked after casting, and as such, may exhibit different properties than an alloy that has not been wrought (9). Since the metallic phase of TCON materials is never wrought, only the properties of cast alloys will be discussed. Refer to Table 1.1 for a list of elements that were attempted to be alloyed with aluminum as a consequence of the TCON reaction, and the effect of these alloying elements on traditional cast aluminum alloys.

Table 1.1		
Effect of Alloying Elements on Aluminum		
Alloying Element	**Effect on aluminum phase compared to pure aluminum**	**Commercial/Industrial Application**
Silicon	Higher castability and corrosion resistance. Lower strength. Non-heat treatable. Among the most important commercial casting alloys (9).	Intricate die castings which may require pressure tightness. Sand and permanent mold castings, including cooking utensils and food handling equipment (9).
Lithium	Lower density. High elastic modulus. High toughness. Superior fatigue crack growth resistance. In the strongest heat-treated conditions, mechanical properties are highly anisotropic. Early cracking in high stress regions (10).	Aircraft and spacecraft applications. Currently not widely used, partially due to high cost, typically 3-5 times expensive than traditional aluminum alloys (10).
Magnesium	Higher corrosion resistance. Higher strength. Lower density. Low castability. Good machinability and weldability. Low impurity content is important (9).	Due to corrosion resistance, used in marine applications and food handling applications (9).
Titanium	Greatly increases strength via grain refining effect. Decreased friction and wear (11).	Aircraft and spacecraft applications where low friction and high resistance to wear is required. Titanium-Aluminum alloys (where aluminum is the alloying element in titanium) are also of great interest (11).
Strontium	Increases strength, ductility, and other mechanical properties as a grain refiner (12).	Applications include use in aircraft parts, internal combustion engine parts (13).
Nickel	Increases strength and electrical conductivity (14).	Applications include use as a replacement for copper conductors due to copper shortage, as well as anything requiring high strength and conductivity (14).

E. Composite Materials

A composite material, also sometimes called a complex material or a heterophase material, is a solid which is made by physically combining two or more existing materials to produce a multiphase system with different physical properties from the starting materials due to synergistic effects. It is important to note what exactly is meant by a "phase" in the context of composite materials, because the term is used in the study of composite materials as more of a descriptive term, rather than in the thermodynamic sense. A phase is defined as a structurally homogeneous part of a material system. Some chemical interaction often occurs in the process of creating a composite material, so that one phase or more may differ from the starting materials, but in other cases the phases themselves remain unchanged. In addition, an interphase region may be formed at the phase boundaries, which may differ in physical properties from the starting materials (15).

Perhaps one of the earliest examples of a composite material is that of a mud or clay brick, with the addition of straw or other fibrous plant matter. This was discovered to be a drastic improvement when compared to the use of mud or clay alone. The straw assists in the evaporation of moisture from the interior, and helps distribute the cracks that form more evenly. These two factors increase the strength of the wall drastically. In fact, sun-baked bricks made in this way by the Israelites in 800 B.C. have a compressive strength of 1000 p.s.i., which is one-fourth the strength of modern fired bricks. This is impressive when considering that in nearly three thousand years, bricks have only quadrupled in strength (15).

Composite materials are categorized into two broad classes, depending upon the base relationships within the material. The first of these classes encompasses composites with one continuous phase, often called the matrix, and one or more dispersed phases embedded within the matrix. The second class includes composites with two or more continuous phases. These types of composite materials are often called co-continuous, and are generally more difficult to produce than composites that are only continuous with respect to one of the phases (15). The TCON process produces co-continuous composite materials, since the product is continuous in both the metal and ceramic phases. This is part of what makes TCON materials so useful, since the result of this morphology is a higher degree of synergy between the properties of the ceramic and metallic phases (2).

CHAPTER II – BACKGROUND ON EXPERIMENTAL METHODS

A. General Synthetic Techniques

A variety of methods are available for use in the synthesis of ternary, quaternary, and more complicated metal oxides. Binary oxides (those involving only oxygen and one type of cation, such as Fe_2O_3) are readily available for purchase from a variety of vendors, since this is the most common naturally occurring state of most metals. More complicated metal oxides must usually be synthesized in the lab. Some synthetic techniques employ binary metal oxides, while other methods utilize compounds involving metallic elements, such as sulfates, nitrates, alkoxides, and so on.

All of these synthetic techniques, in one way or another, are designed to produce an intimate mixture of the reagents involved, in order to facilitate a reaction. The central problem to solid-state synthesis is that in order for reagents to react, they must be in close enough contact with one another for a reaction to take place. While this may seem obvious, it is not usually an observable problem in traditional wet chemistry. In solid-state synthesis, simply mixing and heating solid reagents will not provide a guarantee that a reaction will take place to completion, or that a homogeneous product will form. While solid reagents may appear to the eye to be thoroughly mixed after swirling them together with a spatula, they are not necessarily well mixed on the molecular level. Because of this, steps must be taken to ensure that reagents are homogeneously mixed before a reaction takes place, as will be further discussed later.

Another common technique found in many of these methods is the use of a mechanical press to press the reagent powders into pellets. Pelletizing helps to ensure that within the sample, reagents are in intimate contact with one another, by forcibly removing most of the air in the sample, which causes voids. It also helps to ensure that the sample is not reacting with the container it is in by use of a sacrificial pellet. A sacrificial pellet is one that lies on the bottom of the stack of pellets, and thus is the only one in the stack to be in contact with the container that the pellets are placed in during sintering, usually a combustion boat or a crucible of some kind. In the case of an unanticipated reaction being possible between the container material, and the compounds found in the pellets, only the sacrificial pellet will be contaminated, while the other pellets will remain relatively pure. This is one example of how the concept of reagent contact in solid-state chemistry is actually an advantage rather than a burden.

Finally, most of these techniques involve some form of sintering and/or calcining of the sample. Sintering is a method of forcing powder particles to adhere to one another at the molecular level, so as to form a solid object from a powder perform, such as a pressed pellet. This is done by heating the sample to a high temperature, but below the melting point of the oxide, until a solid pellet is obtained. This technique is commonly employed in the ceramic industry. Calcining is a thermal treatment process applied to solids to bring about thermal decomposition, phase transition, or removal of a volatile fraction. Throughout this research, calcining has been utilized by converting metal sulfates, carbonates, and other such salts into metal oxides, as well as in removing complexed water molecules and other such moieties from the compounds involved in the reaction. Equation 2.1, seen below, is an example of calcining, in which high

temperature causes strontium carbonate to decompose to strontium oxide and carbon dioxide, which exits the system as a gas.

$$SrCO_3 \rightarrow SrO + CO_2$$

Equation 2.1

1. Standard Ceramic Methods

The simplest synthetic method for making complex metal oxides is via standard ceramic methods. Simple, binary metal oxides are readily available for purchase from a variety of vendors; however, most ternary and more complicated metal oxides must be synthesized in the lab. This method is very simple and straightforward. First, simple metal oxides are ground together via mortar and pestle in the desired stoichiometric proportions. Grinding accomplishes three goals, the more obvious two being to reduce grain size of the crystallites in the sample, and to mix the compounds so that the various compounds involved are actually in contact with one another. The final goal accomplished by grinding is that it creates defects in the crystalline structure of the reagents. These defects help to facilitate reactions between the reagents involved. Grinding of reagents throughout this research has generally been done for between ten and thirty minutes.

Following grinding, a technique that is often employed in order to facilitate homogeneous mixing of reactants is to create an evaporating slurry. This involves adding a volatile liquid that the reagents are insoluble in, and then mixing the slurry together. As the liquid evaporates, the powders settle at the bottom of the container, more intimately mixed than can be accomplished through typical grinding and mixing alone. A

commonly used liquid for these purposes in this research has been acetone. Acetone is used because of its high volatility, and ability to evaporate quickly at room temperatures. Also, acetone does not adsorb to the surfaces of the reagents involved nearly to the extent that water would, so it does not usually require that the slurry be dried in an oven after the acetone has evaporated.

After the mixture is allowed to sit overnight to allow for the acetone to evaporate completely, the resulting powder mixture is re-ground for a few minutes, and then pelletized. The pellets are placed in a tube furnace or a box furnace to be calcined and/or sintered. After heating, the sacrificial pellet is removed from the rest of the pellets. One of the pellets is ground so that the products can be verified via powder XRD.

Note that it is often beneficial to utilize metal carbonates rather than oxides alone as precursors in solid-state reactions. The advantage to employing metal carbonates in the reaction is that they will calcine into a metal oxide and carbon dioxide. As carbon dioxide escapes from the sample pellets, channels are formed throughout the pellet, which promote reactivity.

2. Co-precipitation

Co-precipitation is another technique that helps to ensure a homogenous, intimate mixture of the reagents in the sample. This method involves dissolving ionic metal compounds, such as nitrates or sulfates, in a solvent. Once dissolved, the conditions of the solution are altered so as to force the solutes out of solution. For example, this can often be accomplished by addition of another solvent in which the compounds are

insoluble. As they precipitate out of solution, the compounds will be very homogenously mixed, much more so than if the compounds were simply ground together.

After precipitation, the solvent is decanted, and the remaining slurry is dried overnight. Depending on the specific reaction desired, it may or may not be desirable to pelletize the resulting precipitate. The precipitate is calcined and sintered in a furnace. Since co-precipitation usually involves ionic compounds containing polyatomic anions, which decompose under calcining conditions to volatile products and metal oxides, the product formed after the initial sintering is usually quite porous. This of course is due to all of the volatile, gaseous compounds that form and escape from the sample while in the furnace, so the sample often "puffs up" considerably. At this point, the product is verified via powder XRD or XRF to consist only of metal oxides and to be devoid of compounds that should have calcined, such as metal sulfates, thus ensuring a complete reaction. If the reaction is not complete, it can simply be repeated until all undesirable compounds have been removed via calcination. The sample is then reground and re-sintered into a solid, homogenous pellet.

3. Sol-Gel

The Sol-Gel process is a widely used technique in the ceramic sciences. The name derives from the word *sol*, which is a dispersion of colloidal particles in a solvent, and *gel*, which is an interconnected, rigid network with pores of submicrometer dimensions and polymeric chains whose average length is greater than a micrometer.

The term “gel” can refer to several diverse combinations of substances that can be classified into four distinct categories; well-ordered lamellar structures, completely disordered covalent polymer networks, predominantly disordered polymer networks formed through physical aggregation, and particular disordered structures. This process is useful in creating a more homogeneous and pure sample than traditional ceramic powder methods (16).

The sol can be produced through a variety of different chemical procedures, involving a number of different reagents such as alkoxides, chlorides, nitrates, and so forth. A gel-like two-phase system containing a liquid and solid phase is formed. The solid phase can range anywhere from being comprised of discrete particles to continuous polymer networks. The liquid phase is removed, usually by drying, and the remaining solid phase is sintered, yielding the product (16).

B. Powder X-Ray Diffraction

Powder X-ray diffraction, or PXRD, is a powerful analytical technique for analyzing crystalline materials. Throughout this research, PXRD has been used extensively to identify the phases present in the sacrificial oxide pellets prepared for reaction in the TCON furnace. Powder XRD has also been used to verify phases that exist within the finished TCON product after transformation. In addition, Rietveld

analysis has been done in order to ensure product purity, and in the case of impure samples, to quantify the amount of each phase present.

X-ray diffraction is based on constructive interference of monochromatic X-rays interacting with a crystalline sample. A cathode ray tube generates the radiation, which is collimated and directed towards the sample. Crystalline substances act as three dimensional diffraction gratings, especially for X-rays since X-ray wavelengths are similar in length to the spacing of planes in a crystalline lattice. The interaction between the incident rays with the sample produces constructive interference when the right geometric conditions are met. Bragg's Law, seen in Equation 2.2, can be used to describe these conditions, and is defined as follows; λ is the wavelength of the incident X-ray, n is a positive integer (usually 1), d is the distance between lattice planes, and θ is the angle at which diffraction has occurred (17);

$$\mathbf{n\lambda = 2dsin(\theta)}$$

Equation 2.2

So when the X-ray wavelength and the incident angle are known, we can calculate the distance between these two atomic planes within the crystalline lattice. See Figure 2.1 for a diagram explaining how Bragg's Law is derived.

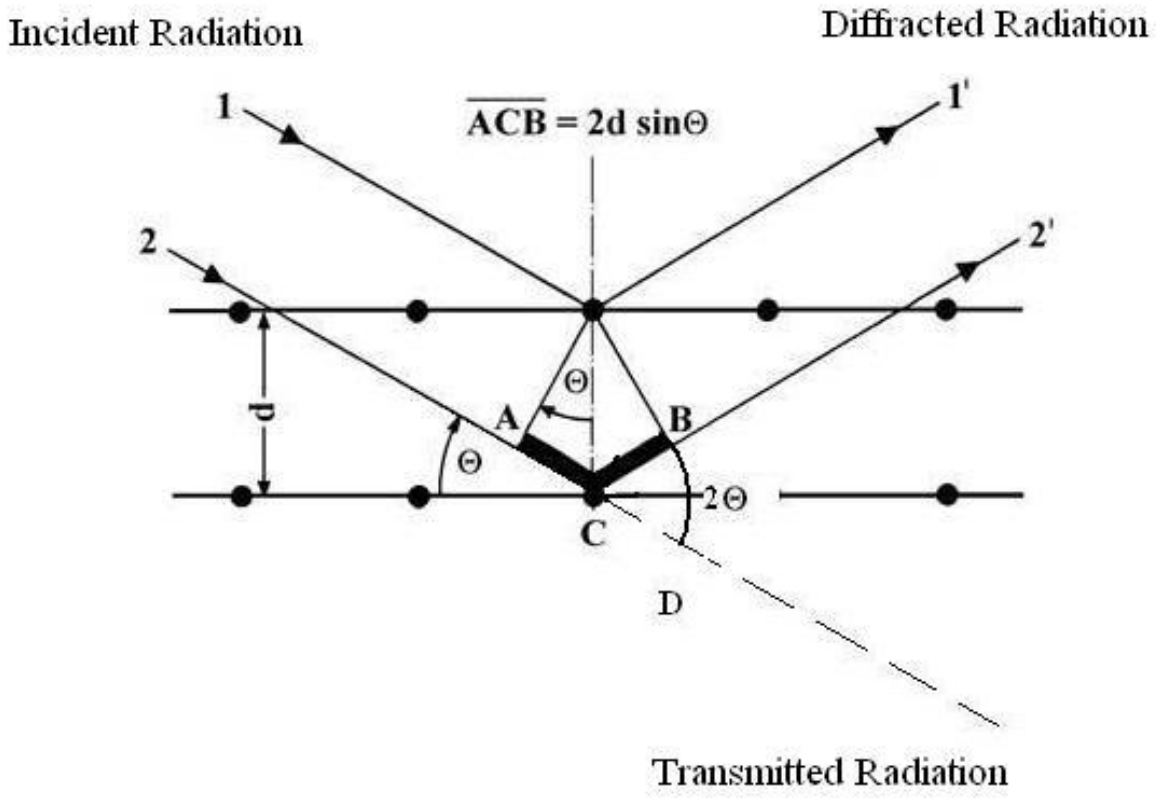

Figure 2.1. **Representation of Bragg's Law, illustrating how powder XRD allows us to calculate lattice spacing between planes in a crystalline solid. The line ACB is understood to be equal to nλ, where n = 1. Note that the angle BCD, the angle between the transmitted ray and the diffracted ray, is 2θ (18).**

The PXRD itself consists of three main components, an X-ray tube where the rays are generated, the sample holder, and the X-ray detector. A cathode ray tube generates the X-rays by heating a filament to produce electrons, accelerating the electrons towards a target by applying voltage, and bombarding the target material, copper at YSU, with electrons. When electrons have sufficient energy to dislodge inner shell electrons from the copper, a characteristic X-ray spectrum is produced, the most common rays of which are denoted K_α and K_β. This spectrum of produced X-rays is unique to every element. PXRD requires monochromatic X-rays, that is, X-rays of a single wavelength in order to be able to use Bragg's Law to calculate d-spacings, so these X-rays must be filtered so

that only one is emitted towards the sample. Filtering is done with either foils or crystal monochromaters. $K_{\alpha 1}$ and $K_{\alpha 2}$ radiation are actually so close in wavelength that an average of the two is often the radiation used, and the rest is filtered out, never interacting with the sample. CuK_{α} has a wavelength of 1.5418 Å (17). However, the Bruker D8 system in use at YSU is equipped with a primary beam monochromater which filters out $K_{\alpha 2}$, permitting transmittion of only $K_{\alpha 1}$ X-rays to the sample.

As X-rays are generated and directed towards the sample, the detector is rotated around the sample in order to adjust 2θ (2θ is generally used in place of θ since 2θ is the angle between diffracted X-rays and the directed X-ray beam after it passes through the sample). When possible, the sample itself is also rotated. This helps to increase randomness of the orientation of the crystallites within the sample, reducing the amount of preferred orientation displayed in the final pattern. The device that maintains the angle and rotates around the sample is termed the goniometer. At YSU, patterns are typically collected in a range of 2θ from 10º to 90º, although scans at higher angles are possible. When Bragg's Law is satisfied, constructive interference occurs, a peak in intensity occurs. The intensity of the diffracted beam is recorded as counts per second (cps). Refer to Figure 2.2 for a diagram of what is known as a diffraction cone. Since powder samples consist of many randomly aligned crystallites throughout the sample, X-rays experiencing constructive interference are diffracted in a cone pattern. The X-ray detector in a powder diffractometer essentially scans through a trace of this cone, in order to construct a pattern (17).

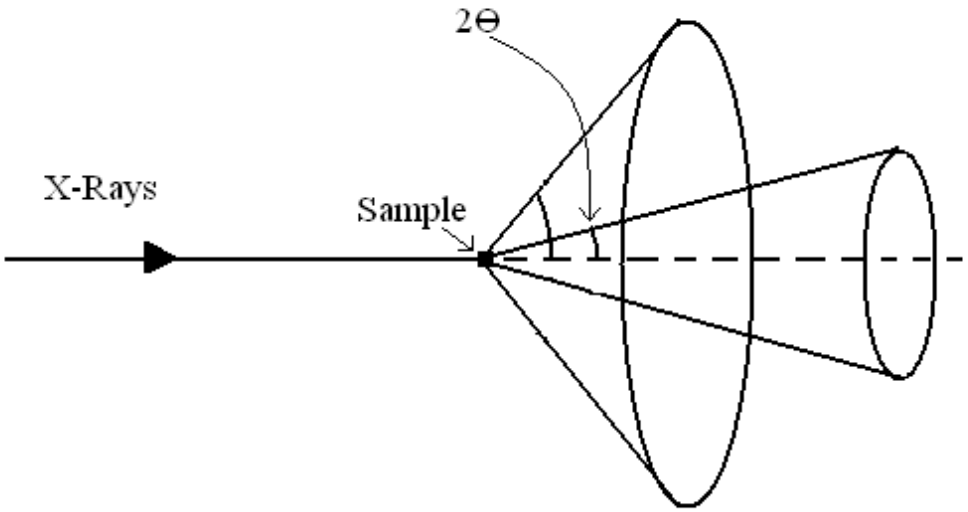

***Figure 2.2*. Diffraction cone, displaying diffraction of X-rays in a randomly oriented polycrystalline sample (19).**

After the pattern has been fully taken, it can be analyzed by comparing experimental peaks with patterns from a standard reference database of PXRD files, which is distributed by the ICDD (International Centre for Diffraction Data). Database patterns, called Powder Diffraction Files, or PDFs, for compounds suspected to be present in the sample are compared to the experimental data present, until all experimental peaks have been accounted for. It is important to note that each peak present corresponds to a specific set of planes within the crystal lattice, and can be defined as such (e.g. the (001) planes). While we cannot explicitly identify new phases via PXRD, new phases can generally be indexed by comparison to a known phase with a closely related structure.

Although typical PXRD analysis of matching peaks can account for which compounds are present, it cannot give us an accurate measurement of the ratios of the compounds in the sample. Rietveld refinement is a technique that is applied to powder patterns, and utilizes a least squares method to refine a theoretical line pattern until it matches the actual pattern of the sample. This theoretical pattern is calculated from the .cif files of the compounds present in the sample, so as to calculate a variety of properties of the sample that PXRD alone cannot provide. Perhaps the most valuable aspect of Rietveld refinement is that it can calculate the percentage mass of each component present in the sample. Rietveld refinement is also useful in verifying that the compounds believed to be present are actually the compounds present, as often times different compounds with similar structures can have very similar powder patterns.

C. Scanning Electron Microscopy

Scanning Electron Microscopy, or SEM, is a powerful analytical technique for characterizing the morphology and microstructure of solid materials. The instrument operates by focusing a beam of high-energy electrons to generate a variety of signals at the surface of the sample. The signals that are generated from these electron-surface interactions reveal information about the surface of the sample, such as morphology, chemical composition, crystalline structure, and orientation of the crystalline structure. Since data is collected over a selected area of the surface, a two-dimensional image can be generated that displays these characteristics. Areas from 1 cm to 5 micron in width, or

a magnification ranging from 20X to 30,000X, can be imaged in scanning mode using conventional SEM techniques. SEM is also useful for doing point analysis on the sample, in order to determine elemental composition of the sample at the point and help identify the various phases present (17). Refer to Figure 2.3 for a schematic of a typical SEM.

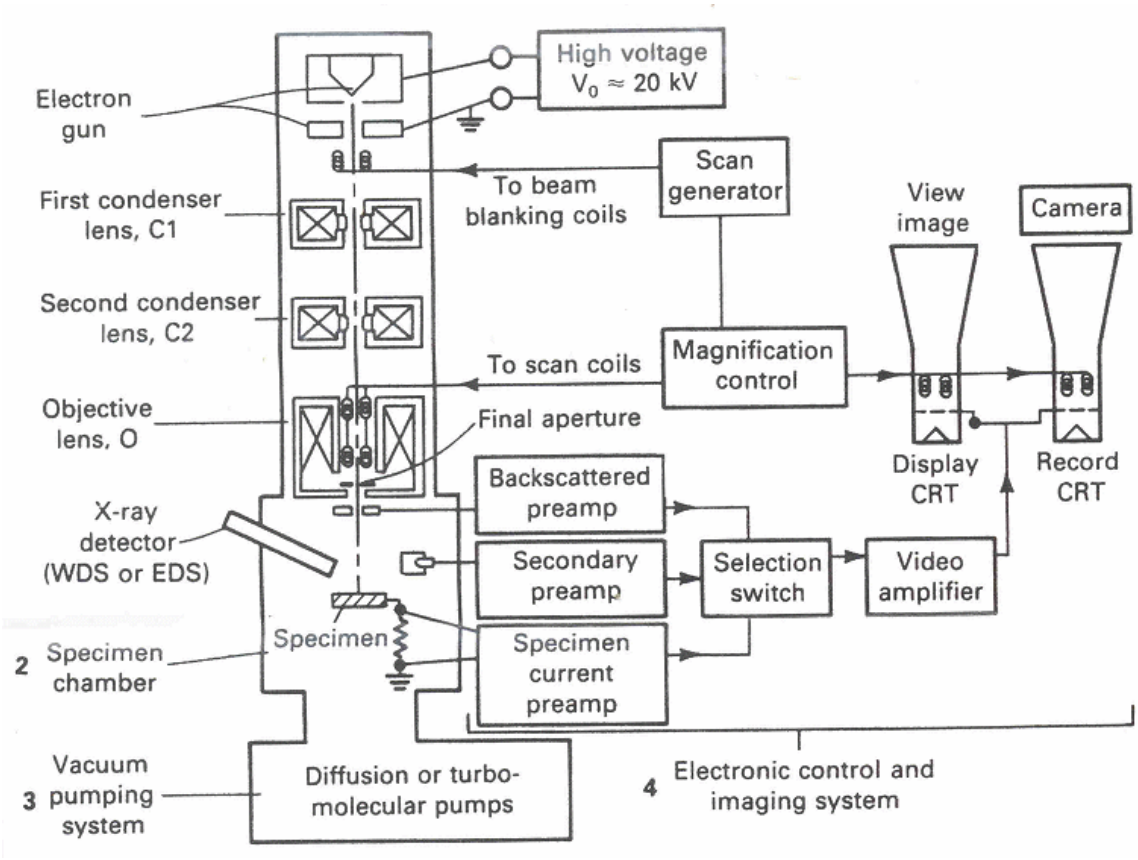

Figure 2.3. **Schematic of a typical Scanning Electron Microscope. Image courtesy of Jeol Ltd.**

In an electron microscope, electrons are generated by means of an electron gun, which operates by applying voltage to a filament, causing an emission of electrons. Several types of electron guns are commercially available, which differ in the types of

filament used (17). At YSU, the filament in the SEM used throughout the bulk of this research is a single crystal of lanthanum hexaboride, LaB_6, contained within a high vacuum. Another commonly used filament is tungsten. Emitted electrons are attracted towards an anode plate, the voltage of which is controlled by the operator. Next, the electrons pass through a Wehnelt cylinder, which is biased negatively relative to the filament. This acts as a grid that repels the emitted electrons and focuses them into a spot of a programmable diameter and divergence half-angle (17).

Focusing lenses in electron microscopes are comprised of copper wire solenoids, which produce a magnetic field that is shaped by the surrounding iron fixture into an optimum geometry to produce the lensing action. As an electron moves through the magnetic field, it experiences an inward radial force. The effect of these electromagnetic focusing lenses is similar to that of traditional optical lenses; however, in optical lenses, the focal length is fixed by the physical curvature of the lens surface, and cannot be altered. With electromagnetic lenses, the focal length can be altered by the operator by affecting two main variables; the gun voltage, which affects electron velocity, and the amount of current flowing through the coils, which affects flux density of the magnetic field (17).

Within the SEM instrument, two sets of scanning coils, one for raster and the other for deflection, are located in the bore of the objective lens cage. These coils cause the electron beam to scan over a square area on the sample surface, which maps directly to the final image displayed on the computer screen (17).

A variety of electron-surface interactions occur in the SEM that can be useful for imaging and analyzing the sample, and these can include either elastic or non-elastic scattering processes. The common signals used to generate an image in the SEM are typically either secondary electrons, or backscattered electrons. Detectors can also make use of cathodoluminescence, auger electrons, and characteristic X-rays, each of which offer their own advantages and disadvantages (17). Of these signals, the ones utilized in this research include secondary electron imaging, backscattered electron imaging, and characteristic X-rays for Energy Dispersion Spectra.

Secondary electron imaging is the most commonly used method of image generation in the SEM. Secondary electrons are generated as an ionization product of the electron beam scanning across the surface of the sample. These ejected electrons result from strong interactions between the primary beam electrons and electrons of the specimen's atoms. They are called secondary electrons since they are not electrons from the beam, the primary radiation, but are from the sample itself (17).

Another useful signal detector in SEM is the backscattered electron detector. Backscattering is an elastic collision phenomenon which occurs when an electron from the beam interacts with the nucleus of an atom in the sample in such a way that is is elastically scattered back towards the detector. The useful aspect of this technique is that the chance of an atom backscattering electrons in this way is proportional to the atom's atomic weight, since the electron is more likely to hit a large nucleus than a small one. Because of this, backscattering will image heavier atoms as being brighter areas on the screen, and smaller atoms as darker areas on the screen. In the case of a non-elemental sample, the backscattering effect is averaged amongst all atoms present in the phase. In

other words, Al_2O_3 will appear darker than pure Al due to the presence of the smaller atom oxygen (17).

In one of the variations of X-ray fluorescence, characteristic X-rays are produced by a primary electron from the electron beam displacing an electron from the inner shell of an atom, causing the secondary electron to eject from the atom. When an outer, higher-energy electron in the atom fills the electron hole caused by the inner-shell electron escaping, the difference in energy is compensated for by being released in the form of an X-ray (17). Refer to Figure 2.4 for a diagram describing the phenomenon of X-ray fluorescence.

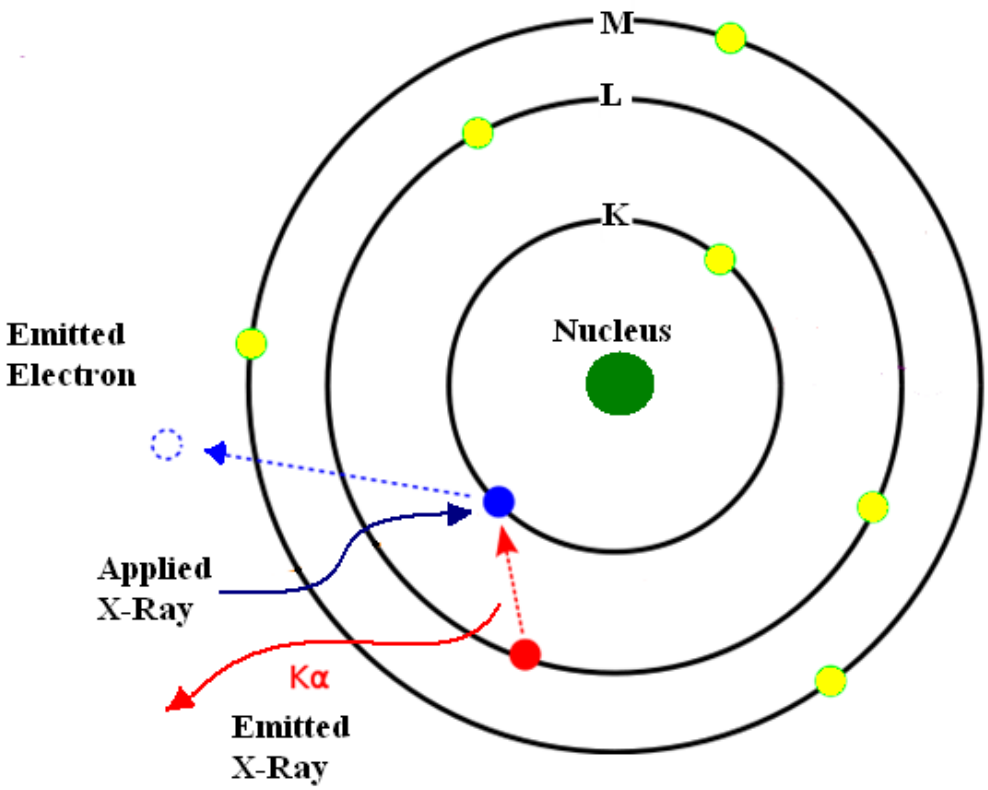

Figure 2.4. **Diagram of X-ray fluorescence, and how fluorescent X-rays are generated by the ejection of an inner-shell electron.**

Depending on which inner-shell electron was ejected from the atom, and which outer-shell electron loses energy to replace the ejected electron, a variety of differing X-rays can be generated. A K_α X-ray is produced when a K electron is ejected, and an L electron replaces it, and is the most commonly observed fluorescence peak. A K_β X-ray is produced when a K electron is ejected, and replaced by an M electron. An L_α peak is produced when an L electron is ejected, and replaced by an M electron. Each element has its own unique spectrum of energies produced by this fluorescing technique, and thus this is one of the most useful ways to identify elements present, and quantify their abundance (17).

These characteristic fluorescing X-rays can be imaged with the use of energy-dispersive X-ray spectroscopy. The advantage to this technique is that it can allow for more detailed elemental identification than backscattering electron detectors. An energy-dispersive detector is used to separate the characteristic X-rays produced by different elements into an energy spectrum, so that the abundance of each element within the phase can be quantified. While this technique can give us elemental abundance, it cannot give us the compounds in which these elements exist. However, it can give us a relatively good idea, just from the ratios of the elements present, and suspicions of specific phases present can be verified through other methods such as powder XRD (17).

CHAPTER III – STATEMENT OF PROBLEM

Because such a wide variety of ceramic materials can be integrated into the TCON process as sacrificial oxides, one of the focuses of the Wagner research group at YSU is to introduce new ceramic materials as TCON precursors in order to produce novel composites. This thesis project has two primary objectives: the first is to incorporate a Ti-Al alloy phase into TCON composites, and the second is to investigate β-alumina ceramics as TCON precursors in order to determine whether the nanoscale features of the β-alumina lattice manifest as nanostructure in the resulting composite material. Some of the compounds investigated serve to enable study of both objectives.

The β-alumina structure is of interest for this process due to the presence of the open conduction planes of the structure. These channels are responsible for the compound's excellent ionic conductivity, but are of different interest in regards to the TCON project. Our hypothesis is that these open channels may help facilitate the reaction of a β-alumina sacrificial oxide with molten aluminum. It may be possible that these open-channeled structures would allow this research group to create composite materials with an entirely different morphology from the existing TCON products, which are composite materials on the order of the micro-scale. Theoretically, a transformed β-alumina compound could react in such a way that the molten aluminum seeps through the conduction planes of the β-alumina, facilitating reaction with the spinel-block layers of the compound. If this hypothesis is correct, β-alumina transformation would be an excellent platform for the production of a nano-scale type composite material, as the

conduction planes of the β-alumina structures are only a few nanometers apart from one another (2).

β-alumina compounds targeted for synthesis and subsequent use as TCON precursors include both known and novel phases. In order to gauge the role that the layered structure of β-alumina plays in TCON composite microstructure, spinel phases related in composition to some of the β-alumina phases will also be investigated. The criterion for choosing which β-aluminas will be synthesized was based upon which alloying elements would produce a desired effect on the aluminum phase of the TCON composites. Elements such as lithium, magnesium, titanium, nickel, and strontium have a wide variety of positive effects on aluminum alloys, as seen in Table 1.1. Known β-alumina compounds chosen for this research contain useful aluminum-alloying elements, such as $SrMgAl_{10}O_{17}$ and $LiAl_{11}O_{17}$. As such, standard Na β-alumina is not being used in this research, as sodium does not form a useful alloy with aluminum. It should be noted that this is by no means a definitive list of elements which are useful alloy elements with aluminum, it is simply a list of the elements utilized in this research.

CHAPTER IV – MATERIALS, METHODS, AND RESULTS FOR THE SYNTHESIS OF CERAMIC PRECURSORS

The first step in producing ceramic/metallic TCON composites is to synthesize the sacrificial oxide, and then to verify that the targeted sacrificial oxide sample was successfully prepared. These samples are most commonly verified by PXRD and Rietveld refinement. One of the most credible methods of verifying sample composition in crystalline powders is by comparing experimentally refined unit cell parameters to known unit cell parameters taken from .cif files. Table 4.1 lists the oxides targeted as TCON precursors in this study, along with their expected unit cell parameters, and Rietveld-refined unit cell parameters. The remainder of this chapter summarizes details on the synthesis, procedure, and characterization of each of the oxides targeted. Also provided is the rationale for targeting each of the samples as TCON precursors. Results of the TCON transformation are then presented in Chapter V.

Table 4.1

Experimentally Derived Unit Cell Parameters Compared to ICSD Unit Cell Parameters for TCON Targeted Sacrificial Oxides

TCON Sacrificial Oxide	**Synthesis Verified?**	**ICSD Unit Cell Parameters (Å)** **(card #)**	**Experimentally (i.e. Rietveld determined) Unit Cell Parameters (Å)** **(c/a ratio)**
$SrMgAl_{10}O_{17}$	Yes	a = 5.6286 c = 22.3484 (155524)	a = 5.6234 c = 22.3951 c/a = 3.982
$NaAl_{11}O_{17}$ (β-Alumina)	Yes**	a = 5.602 c = 22.626 (67545)	a = 5.6067 c = 22.5516 c/a = 4.022
$NaAl_{11}O_{17}$ (β"-Alumina)	Yes**	a = 5.6037 c = 33.6210 (74473)	a = 5.6090 c = 33.8706
$LiAl_{11}O_{17}$	Yes	N/A	N/A (composition verified via PXRD phase identification and EDS)
$SrTi_5Mg_6O_{17}$	No	N/A	N/A
$SrNiAl_{10}O_{17}$	Yes	N/A (compare to $SrMgAl_{10}O_{17}$, which is very similar)	a = 5.6239 c = 22.4285 c/a= 3.988
$TiMg_2O_4$	Yes	a = 8.4376 (65792)	a = 8.4472
$NiAl_2O_4$	Yes	a = 8.0481 (158683)	a = 8.0490
$SrAl_{12}O_{19}$* **	-	a = 5.5666 c = 22.0018	c/a = 3.952

- **Inorganic Crystal Structure Database, version 2010-2**

** = Two phases of $NaAl_{11}O_{17}$ were found in each $NaAl_{11}O_{17}$ sample, β and β" alumina, so unit cells of both are being reported.

***$SrAl_{12}O_{19}$ was not used as a sacrificial oxide. It is included in this table to compare experimentally found c/a ratios to the known c/a ratio of a similar magnetoplumbite phase.

A. $SrMgAl_{10}O_{17}$

1. Background

$SrMgAl_{10}O_{17}$ was the first successfully synthesized and partially TCON transformed β-alumina-type compound in this research. The obvious benefit of transforming this compound via the TCON process is to help prove or disprove our hypothesis that conduction planes found in β-alumina compounds affect the final product's morphology. Another benefit to transforming this compound is that magnesium has a variety of beneficial effects when incorporated into aluminum alloys. Among those that would be important to the TCON process would be that magnesium improves both the strength and corrosion-resistance of aluminum alloys (9). While strontium is the vitally important large cation of this particular β-alumina structure, it also has some positive effects on aluminum as an alloying element. Strontium acts as a grain refiner when alloyed with aluminum, and as such, will improve ductility and strength of the material (12).

Strontium hexaaluminate, $SrO•6Al_2O_3$ (or $SrAl_{12}O_{19}$), which is closely related to β-alumina in structure, differs only in the composition of the conduction plane (e.g. $SrAlO_3^-$ vs. SrO, respectively). Incorporating Mg^{2+} into the lattice makes possible the β-alumina-like composition, $SrMgAl_{10}O_{17}$. The divalent Mg^{2+} ion incorporates itself into the β-alumina structure by replacing an Al^{3+} cation in the spinel block at a tetrahedral site.

2. Synthesis Procedure

Producing $SrMgAl_{10}O_{17}$ was a relatively simple synthesis, performed via the oxide-grind method. Synthesis of this compound was adopted from Iyi and Gobbels (20). Reagents used were MgO, Al_2O_3, and $SrCO_3$. The three reagents were measured in stoichiometric proportions to allow for the following chemical reaction in Equation 4.1 to take place:

$$5\ Al_2O_3 + 1\ MgO + 1\ SrCO_3 \rightarrow SrMgAl_{10}O_{17} + CO_2$$

Equation 4.1

The reagents were ground in a mortar for approximately ten minutes, and then ground and mixed under acetone for another ten minutes. The acetone was allowed to evaporate overnight. The resulting powder mixture was pelletized, calcined, and sintered at temperatures between 1500 and 1600 ºC. The article by Iyi and Gobbels (20) actually calls for a sintering temperature of 1700 ºC; however, the reaction was ran at a lower temperature out of concern for wear to the heating element capacity of the tube furnace.

After the first samples were proven to have a successful TCON reaction (this will be discussed in Chapter V), a third sample was prepared. The release of carbon dioxide from the pellets caused a somewhat porous group of pellets to be produced. While the benefit of using a carbonate in the reaction is understood, porosity of the pellet is undesirable, as a more homogenous pellet is desired that is as free of voids in the structural morphology as possible. For this reason, the third sample was synthesized similarly to Samples 1 and 2, but following synthesis completion, it was reground and

resintered in order to remove this porosity. From each sample, a pellet was ground to be analyzed via powder XRD and Rietveld refinement.

Note that reaction conditions had to be slightly altered for the production of Sample #3. The Thermolyne furnace was under repair, so the Lindberg had to be used, which has a maximum temperature capability of only 1500 °C. Also, the Lindberg furnace is in close proximity to other students' workspaces, so it was undesirable to have the furnace ramped up to 1500 °C in the middle of the summer if people had to be near it. For that reason, the furnace was only run over the weekend and at nights, so a shorter reaction time had to be used. A summary of reaction conditions used to synthesize $SrMgAl_{10}O_{17}$ is given in Table 4.2.

Table 4.2

Reaction Conditions of the Synthesis of $SrMgAl_{10}O_{17}$

Sample #	Reagents	Mass of Reagents	1st Sintering Conditions	2nd Sintering Conditions	Furnace Used
1	Al_2O_3 $SrCO_3$ MgO	2.50g 0.75g 0.20g	1600ºC for 96 hours	X	Thermolyne 59300 (WB Room 5028)
2	Al_2O_3 $SrCO_3$ MgO	4.22g 1.22g 0.33g	1600ºC for 96 hours	X	Thermolyne 59300 (WB Room 5028)
3	Al_2O_3 $SrCO_3$ MgO	3.03g 0.88g 0.24g	1500ºC for 56 hours	Reground and Repelletized 1500ºC for 6 hours	Lindberg 54233 (WB Room 5005)

3. Results

Rietveld refinement of the produced samples ultimately verified synthesis of the target $SrMgAl_{10}O_{17}$ compound, although it was necessary to first catalog a bug in the Rietveld program used, Topas version 3.0. While it was evident that we produced the target compound, the refinement program was not giving a good fit for the pattern. This was a problem, since even if the sample is known to be the target compound with some impurity present, it is impossible to know the percentage by mass present of each compound without a well-fitting refinement. However, due to diligent efforts by Dr. Zeller and some outside help from Bruker-AXS, it was found that the problem was a simple reading error in the Topas program. The program was not correctly reading special positions of the .cif file such as '0.33333' to be equivalent to the entry 1/3, so the refinement would always be slightly off. This was fixed, and the resulting refinements fit very well (using data from ICSD card # 155524). Figures 4.1 and 4.2 show the powder pattern and Rietveld refinement of Sample 1, and Table 4.3 summarizes the results. It is seen in Table 4.3 that even using a simple oxide grind method produced a sample of about 95% purity by mass.

Another verification that the β-alumina phase was successfully prepared as opposed to the magnetoplumbite phase is through examination of the c/a ratio of the unit cell parameters refined for the sample. For β-alumina compounds, the c/a ratio will usually be greater than 4.0, due to the relatively elongated c-axis by the β-alumina structure relative to magnetoplumbite structure. This is because the magnetoplumbite structure contains conduction planes that have five bridging bonds per unit cell as opposed to one in β-alumina (7). As indicated from the Rietveld-refined parameters in

Table 4.1, the c/a ratio of $SrMgAl_{10}O_{17}$ Sample 1 was determined to be 3.982. Even though this ratio is not quite 4.0, it is still larger than the c/a ratio for magnetoplumbite-type $SrAl_{12}O_{19}$, which is 3.952 (from ICSD # 69020), and so does provide further evidence that the targeted β-alumina-type $SrMgAl_{10}O_{17}$ phase was produced.

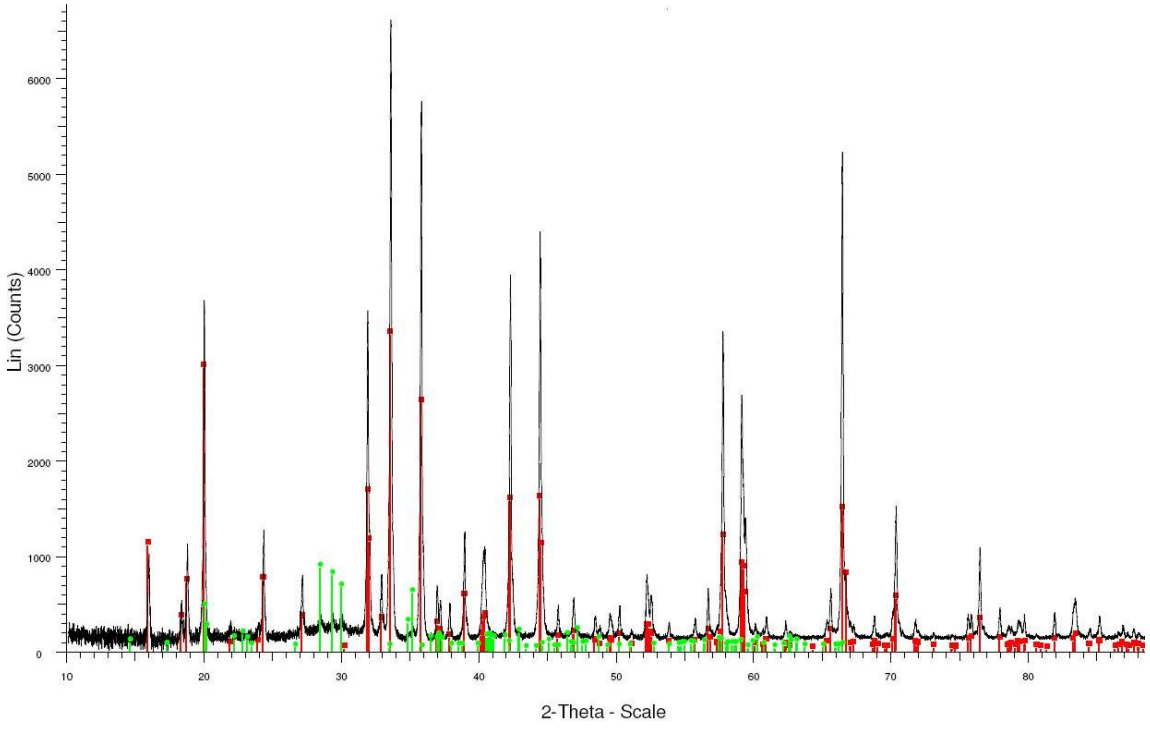

***Figure 4.1*. Powder XRD pattern of $SrMgAl_{10}O_{17}$ Sample #1. Red lines indicate peaks diffracted by the target compound (PDF File 04-010-0738), green lines indicate peaks diffracted by a side product, $SrAl_2O_4$ (PDF File 00-034-0379).**

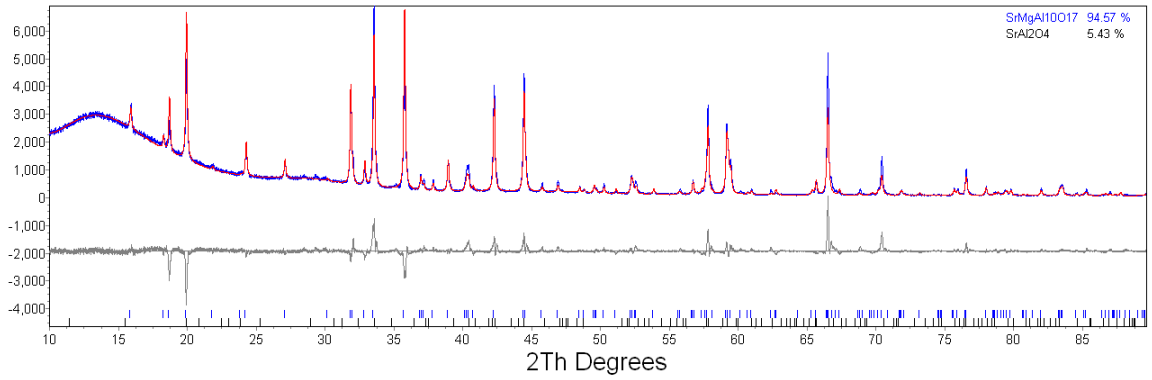

***Figure 4.2*. Rietveld refinement of $SrMgAl_{10}O_{17}$ Sample #1. Sample #1 was found to be 94.57% by mass the target compound, and 5.43% by mass the impurity $SrAl_2O_4$. Shown is the experimental pattern in blue, the theoretically calculated pattern in red. Below is the difference between the two in grey.**

Table 4.3		
Mass Percentage of Phases Present in $SrMgAl_{10}O_{17}$ Samples, Quantified via Rietveld Refinement		
$SrMgAl_{10}O_{17}$ Sample	**$SrMgAl_{10}O_{17}$ % by mass**	**$SrAl_2O_4$ % by mass**
1	94.57	5.43
3	95.25	4.75

*** Rietveld analysis was not performed on Sample #2, since reaction conditions were identical to those that were used to make Sample #1.**

B. $NaAl_{11}O_{17}$

1. Background

Sodium β-alumina cannot itself be used as a sacrificial oxide in the TCON process, as the presence of sodium in sacrificial oxides transformed via the TCON process can yield very negative properties in the finished product. These properties include a great deal of cracking and crumbling, even with only a minute amount of sodium present. Sodium β-alumina cannot be used even to simply prove whether or not ceramic precursors with β-alumina conductive channels have an effect on the TCON process, simply because it would be undesirable to put any sample containing sodium in

the molten aluminum furnace out of concern for contamination of future samples. However, it is possible to perform an ion exchange reaction on sodium β-alumina with molten salts to produce β-alumina compounds that would be useful as TCON precursors. Because of this, $NaAl_{11}O_{17}$ has been produced during the course of this research for use as a reagent in the production of $LiAl_{11}O_{17}$, which is a composition that is applicable to the TCON project as a sacrificial oxide.

2. Synthesis Procedure

Gel-to-Crystallite Synthesis of $NaAl_{11}O_{17}$

The first method of synthesis of $NaAl_{11}O_{17}$ attempted in this study was gel-to-crystallite conversion. This approach was chosen primarily for its ease in providing a thorough, homogeneous mixture of precursor products for successful sintering of sodium β-alumina. This method was adapted from a paper wherein the authors attempted to synthesize several different compounds of formula $MAl_{11}O_{17}$, where M = Li, Na, K, Rb, Ca, and Eu (21). Of these compounds, the method outlined is only successful for Na, K, and Rb. Hydrated aluminum gels of formula $Al_2O_3 \bullet nH_2O$, where $80 < n < 120$ are precipitated from aqueous solutions of $Al(NO_3)_3$ by titration with 0.10 M NaOH. The resulting gel is reacted under reflux conditions with NaOH in an ethanol/water solution for six hours. The product should have the formula $NaAl_{10}O_2(OH)_{28}0.5H_2O$, which is then dried, sintered and calcined to yield the final product, sodium β-alumina (22).

Unfortunately, this method of synthesis was largely unsuccessful, as we were unable to reproduce the reported synthesis. The products were analyzed via XRD, and did not appear to contain any β-alumina type compounds. In fact, virtually no identifiable compounds were present.

Sulfate Co-Precipitation

After the Gel-to-Crystallite conversion technique for synthesis of β-alumina could not be reproduced, a method involving sulfate co-precipitation was attempted. The journal article by Kang and Park (23) that this technique is adapted from actually involves deriving aluminum and sodium sulfates from kaolin, a clay mineral. The purpose of this process was ultimately to synthesize β-alumina from inexpensive starting materials; however, for the purpose of this research, we began the synthesis with hydrated sulfates of aluminum and sodium.

Aqueous solutions of $Na_2SO_4 \bullet 10\ H_2O$ and $Al_2(SO_4)_3 \bullet 18H_2O$ were first prepared. The molar ratio of these two reagents was varied, with the desire to alter the final ratio of Na_2O to Al_2O_3. The ideal ratio for Na_2O to Al_2O_3 was reported to be 1-to-1. Once the solution is prepared, it was slowly dropped into pure ethanol, and agitated via magnetic stirring. While these materials are soluble in water, they are not soluble in ethanol, or concentrated solutions of ethanol and water, and precipitate out of solution. The precipitate was allowed to age for 24 hours. It was then decanted, and dried at 80 °C for another 24 hours (23). The resulting precipitate, now a waxy, white substance, is pelletized, and heated in a tube furnace at various temperatures and times, which are

reported in Table 5.3. The calcination reaction can be characterized by the Equations 4.2 and 4.3;

$$(4.2)\ 2\ Na_2SO_4 \bullet 10\ H_2O + 11\ Al_2(SO_4)_3 \bullet 18H_2O \rightarrow 2\ Na_2SO_4 + 11\ Al_2(SO_4)_3 + 218\ H_2O$$

$$(4.3)\quad 2\ Na_2SO_4 + 11\ Al_2(SO_4)_3 \rightarrow 2\ NaAl_{11}O_{17} + 35\ SO_3$$

Equations 4.2 and 4.3

In the above chemical reactions, it is evident how a great deal of mass is lost in the H_2O given off in the first step, and in the SO_3 given off in the second. This causes the pellets to puff up considerably, as these gasses leave the system. The pellets therefore must be reground, repelletized, and re-sintered so as to produce a dense, solid pellet. This second sintering process requires no more than a few hours, just long enough for the particles to anneal.

3. Results

Synthesis of $NaAl_{11}O_{17}$ proved to be one of the more difficult procedures performed throughout the course of this research. The first method attempted, gel to crystallite synthesis, was unable to be reproduced in the laboratory, and sodium β-alumina was not obtained. The second synthesis attempted, sulfate co-precipitation, was eventually a success. However, this method had to be altered drastically from the referenced journal article in order to get a semi-pure product. The authors of the referenced journal article reported that calcining and sintering was done at 1400 ° C for

one hour (23). When these conditions were reproduced, an extremely high percentage weight of sulfur was detected via XRF, presumably in the form of the metal sulfate salts. Obviously, no sulfur should be present if the reaction progressed to completion, as all sulfur products formed by this reaction should be gaseous or volatile enough at these temperatures to leave the sample, so reaction conditions were altered by increasing sintering times to around 15 hours until no sulfur was present in the pellet after calcining and sintering.

Also, it was found that when the ratio of Al_2O_3 to Na_2O is indeed 1-to-1, as recommended by the referenced paper, the result is the formation of a great deal of the side product, $NaAlO_2$, which is undesirable. We found nearly half of the sample to be $NaAlO_2$ by mass, and the rest consisting of a mixture of β and β" alumina. In terms of stoichiometry, this is logical, but it was assumed that perhaps most of the sodium content may remain in solution and would therefore not be in the precipitated sample. This level of impurity is unacceptable for the purposes of this research, so the molar ratio of Al_2O_3 to Na_2O was altered until a more acceptable mixture of products was obtained.

As indicated in Table 4.4, six trials were completed in all, with ratios of Al_2O_3-to-Na_2O varied from 1:1 in Samples 4, 5, and 6 in order to get a higher percentage of $NaAl_{11}O_{17}$ in the product. This minor variation to the procedure was proven successful, since Samples 4 and 6 are mostly the desired products, with only a small percentage of $NaAlO_2$. Figures 4.3 and 4.4 show the PXRD pattern and corresponding Rietveld refinement for Sample 6, respectively. Table 4.5 then summarizes the Rietveld analysis of the remaining samples, except for Sample 5. Although Sample 5 appeared to be mostly the desired product from the heights of the powder pattern peaks, a Rietveld

refinement of the data gave a poor fit, and no results were reported. This did not appear to be due to a bad molar ratio of reagents, but rather some other unidentified problem, perhaps a contaminant of some kind. Further studies may be done in the future to try to further reduce the amount of $NaAlO_2$ present.

Finally, it should also be noted that for the results shown in Table 4.4, Sample 4 has the lowest level of impurity. Sample 6 contains slightly more impurity; however, it also contains a higher ratio of β-alumina to β”-alumina. Recall it was previously mentioned that the β’’-alumina phase is often co-formed along with the β-alumina phase in the synthesis of β-alumina phases. It is not yet known whether β-alumina or β”-alumina will be more desirable in terms of TCON reactions, but it may be something to look further into in the future.

Table 4.4

Reaction Conditions of Sulfate Co-Precipitation Sodium β-Alumina Synthesis

Trial	**$Al_2(SO_4)_3 \cdot 18H_2O$ (grams)**	**$Na_2SO_4 \cdot 10\ H_2O$ (grams)**	**Approximate $Al_2O_3 : Na_2O$ Molar Ratio**	**Reaction Conditions (1^{st} sintering)**	**Reaction Conditions (2^{nd} sintering)**
1	23.480	11.141	1:1	1400 °C for 1 hour	-
2	23.480	11.141	1:1	1400 ° C for 2 hours	-
3	24.056	11.070	1:1	1500 ° C for 14 hours*	-
4	23.574	7.2695	3:2	1500 ° C for 13 hours*	1500 ° C for 1.5 hours
5	26.012	4.140	3:1	1500 ° C for 12 hours	1500 ° C for 3 hours
6	26.440	6.886	2:1	1500 ° C for 16 hours	1500 º C for 3 hours

*** Indicates a total reaction time at given temperature, rather than a consecutive number of hours. In cases where an unacceptable amount of sulfur was retained in the product, pellets were recalcined until sulfur was no longer detectable.**

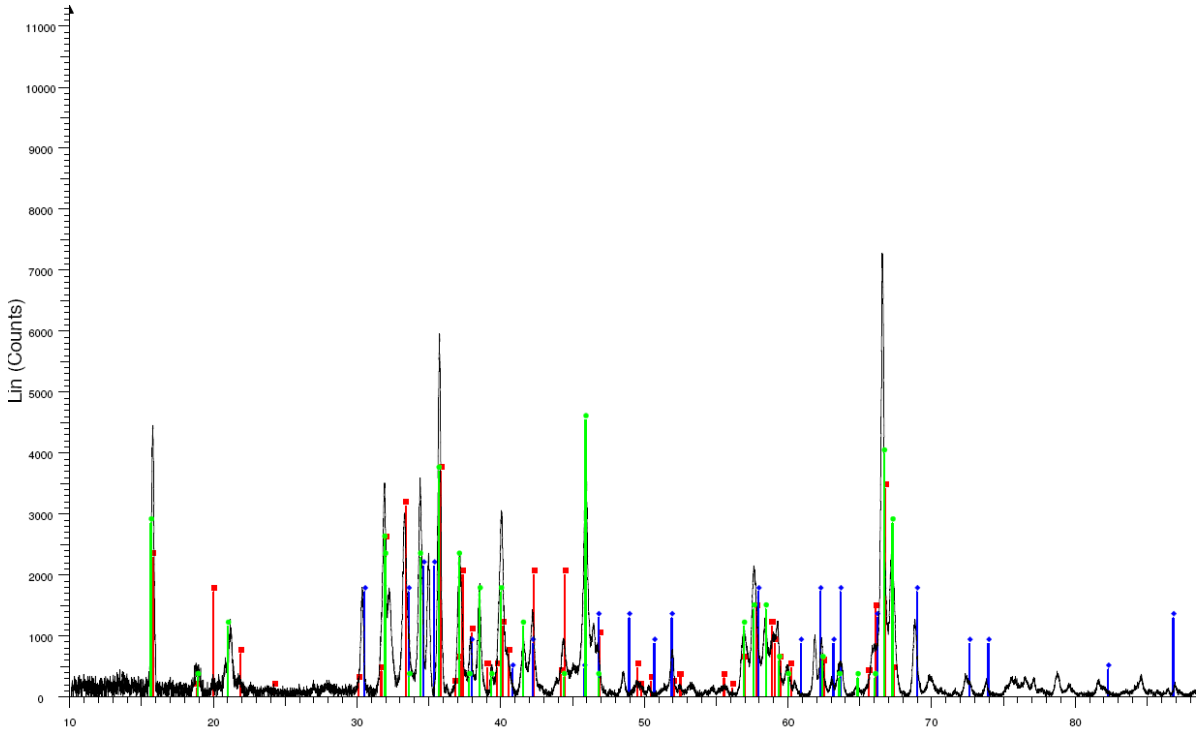

Figure 4.3. **powder XRD pattern of $NaAl_{11}O_{17}$ Sample 6 produced by sulfate co-precipitation. Red lines correspond to Na β-alumina (PDF File 00-025-0775), green lines to Na β"-alumina (PDF File 00-019-1173), and blue lines to the side-product, $NaAlO_2$ (PDF File 00-002-0985).**

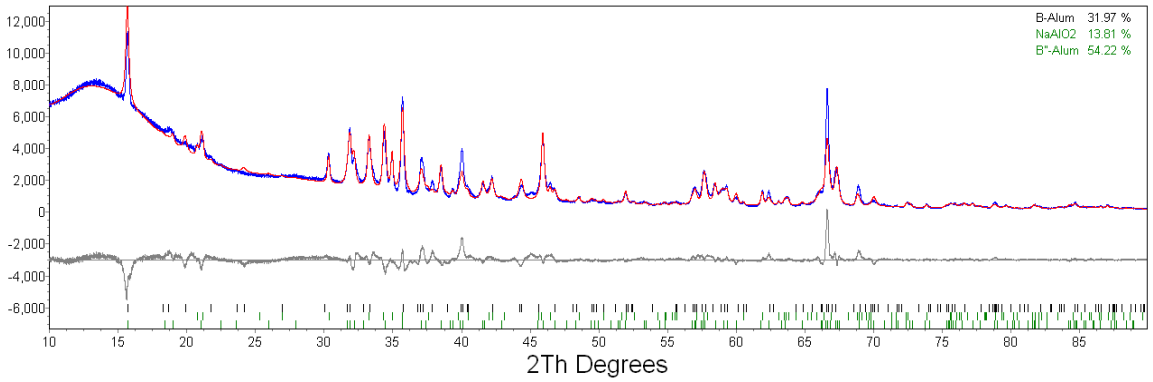

Figure 4.4. **Rietveld refinement of $NaAl_{11}O_{17}$ Sample 6 produced by the sulfate co-precipitation method. The sample was determined to be 31.97 % Na β-alumina, 54.22 % Na β"-alumina, and 13.81% $NaAlO_2$. Shown is the experimental pattern in blue, the theoretically calculated pattern in red. Below is the difference between the two in grey.**

Table 4.5			
Mass Percentage of Phases Present in Sulfate Co-Precipitation Synthesis of Na β-Alumina. Quantified via Rietveld Refinement			
Sample*	**Percent by mass Na β-Alumina**	**Percent by mass Na β"-Alumina**	**Percent by mass $NaAlO_2$**
1	28.72	28.57	42.72
2	-	-	-
3	24.45	31.50	44.05
4	18.89	73.90	7.21
5	-	-	-
6	31.97	54.22	13.81

Samples 2 and 5 have been omitted due to a poor Rietveld refinement, which is probably due to the presence of unidentified compounds within the sample.

C. $LiAl_{11}O_{17}$

1. Background

Another β-alumina compound that would be useful to the TCON process is $LiAl_{11}O_{17}$. Of the β-alumina compounds studied throughout the course of this research, $LiAl_{11}O_{17}$ is the one with the smallest conduction-plane cation, with the radius of Li^+ being only 0.74 Å, compared to that of Na^+, which is 1.02 Å. Nevertheless, it is still comparatively larger than the Al^{3+} ions that make up the spinel block of the structure, which are only 0.53 Å in radius, so it is still possible for this structure to exist (24). If successfully transformed via the TCON process, this compound would possibly allow for lithium to be an alloying element with aluminum. Lithium-aluminum alloys have several desirable properties, including lower density, higher elastic modulus, and higher toughness (10).

2. Synthesis Procedure

One challenge that presents itself is that $LiAl_{11}O_{17}$ cannot easily be synthesized directly. Rather, it is necessary to take a more indirect route, usually by first preparing $NaAl_{11}O_{17}$, and then performing an ion exchange reaction to produce $LiAl_{11}O_{17}$. The first approach considered involved a two-step ion exchange process reported by Wells (24), with the first step involving conversion from $NaAl_{11}O_{17}$ to $AgAl_{11}O_{17}$, and then second from $AgAl_{11}O_{17}$ to $LiAl_{11}O_{17}$. The primary reasoning behind this approach was reportedly that performing ion-exchange directly from Na β-alumina to Li β-alumina would not result in a reaction that progressed to completion. Since sodium is not a useful alloying element with aluminum, it is not desirable to have any sodium in a sacrificial oxide for use in the TCON reaction. Supposedly, a two-step ion exchange with silver β-alumina as an intermediate would result in a complete ion exchange, thus assuring that all sodium (and silver, for that matter) has been removed from the sample (25). However, the synthesis of $AgAl_{11}O_{17}$ proved to be very tedious, and so another approach was used.

The method of ion-exchange ultimately used in the project was adapted from Jayaraman and Periaswami (26), wherein single-crystals of Na β-alumina are reacted with molten lithium chloride to produce Li β-alumina crystals. For the purposes of this research, a sintered pellet of Na β-alumina was used in lieu of single crystals. A Na β-alumina pellet was placed in a quartz crucible, with roughly five grams of LiCl. The appropriate mass ratio of β-alumina to LiCl was about 1 to 5. The crucible was placed in a box furnace, reacted at 657 °C for 5 hours, and then allowed to cool to room temperature. At this point, the pellet was encased in solidified LiCl, which was washed away with an aqueous solution of 20% by volume ethanol. It was often also necessary to

chip away at the solid LiCl with a metal spatula. The resulting pellet was washed free of any residual salts, and dried overnight at 120 °C (26). Refer to Equation 4.4 for the chemical equation for ion exchange between Na β-alumina and Li β-alumina.

$$NaAl_{11}O_{17} + LiCl \rightarrow LiAl_{11}O_{17} + NaCl$$

Equation 4.4

3. Results

Several attempts were made to prepare $LiAl_{11}O_{17}$ via the ion-exchange reaction with $NaAl_{11}O_{17}$ and LiCl described above, and the various reaction conditions utilized along with corresponding results are given in Tables 4.6 and 4.7, respectively.

Table 4.6

Reaction Conditions of Ion Exchange Reaction to produce Li β-Alumina

Sample #	Sample of Na β-alumina used	Mass of Na β-alumina used in g	Mass of LiCl used in g	Time and Temperature of rxn	Additional Comments
1 (1 pellet)	Sulfate Co-precip. #5	0.95	5.01 g	657 °C for 5 hours	
2 (1 pellet)	Sulfate Co-precip. #4	0.91	5.00 g	657°C for 24 hours	
3 (1 pellet)	Sulfate Co-precip. #6	1.01	5.00 g	657°C for 3.5 hours	Washed w/ Acetone/ Ethanol soln.
4 (2 pellets)	Sulfate Co-precip. #6	1.81	9.89 g	657°C for 5 hours	Washed w/ Acetone/ Ethanol soln.

Table 4.7		
Results of Ion Exchange Conversion of $NaAl_{11}O_{17}$ to $LiAl_{11}O_{17}$		
Sample #	Phases present	Comments
1	Undetermined due to extreme hygroscopic nature	Extremely hygroscopic, reaction assumed to be incomplete and attempted again at longer reaction time
2	Undetermined due to pellet loss	Pellet destroyed, possibly due to long reaction time
3	Pre-wash : NaCl, LiCl, unidentified β-alumina phase, $LiAlO_2$ Post-wash : Primarily $LiAl_{11}O_{17}$, some $NaAl_{11}O_{17}$, some $LiAlO_2$	Initial pellet ground and washed with ethanol/acetone solution. Determined via PXRD to contain a β-alumina phase, determined via EDS to be mostly $LiAl_{11}O_{17}$ with some $NaAl_{11}O_{17}$

The first attempt to produce $LiAl_{11}O_{17}$ was initially thought to be unsuccessful, due to the extremely hygroscopic nature of the product. When left alone for only a few hours, the powder collected so much moisture that its appearance was more like that of a spilled solution than a powder. Because this procedure was adapted from a source that performed the reaction on single crystals rather than pellets, a longer reaction was performed for Sample 2. However, this was unsuccessful, as the pellet simply fell apart, and could not be salvaged.

Sample 3 was similar in hygroscopicity; however, a PXRD pattern was still collected by grinding the sample, and covering it in the PXRD sample cup with Parafilm to avoid moisture contamination. The pattern revealed four distinct phases; NaCl, LiCl,

$LiAlO_2$, and a β-alumina phase. NaCl is a product of the ion exchange in which sodium from either $NaAl_{11}O_{17}$ or $NaAlO_2$ impurity reacts with LiCl to form $LiAl_{11}O_{17}$ or $LiAlO_2$, and NaCl. LiCl is present due to being the reagent in excess, and it is also hypothesized that LiCl diffused throughout the voids in the pellet sample. $LiAlO_2$ is present from the impurity found in Na β-alumina samples, $NaAlO_2$ undergoing ion-exchange. Unfortunately, it cannot be easily determined from PXRD whether the β-alumina phase detected is Li β-alumina or Na β-alumina. This is because there is no powder pattern available in the ICDD database for $LiAl_{11}O_{17}$ to compare to our sample. Furthermore, although there is an ICDD pattern available for $NaAl_{11}O_{17}$, the unit cell parameters of Li and Na β-alumina are nearly identical, so it is very difficult to distinguish these patterns. Specifically, for $LiAl_{11}O_{17}$, a = 5.596 Å and c = 22.570 Å, while for $NaAl_{11}O_{17}$, a = 5.594 Å and c = 22.530 Å (27).

Due to the hygroscopic nature of the sample, it was next washed with a solution of 50% acetone/50% ethanol, dried overnight in a box furnace at 120 °C, and re-evaluated via PXRD. The resulting powder was no longer hygroscopic. The PXRD pattern revealed that the only phases still present after washing were $LiAlO_2$ and the unidentified β-alumina phase, with very small amounts of NaCl. Figure 4.5 shows the PXRD pattern obtained for $LiAl_{11}O_{17}$ after washing.

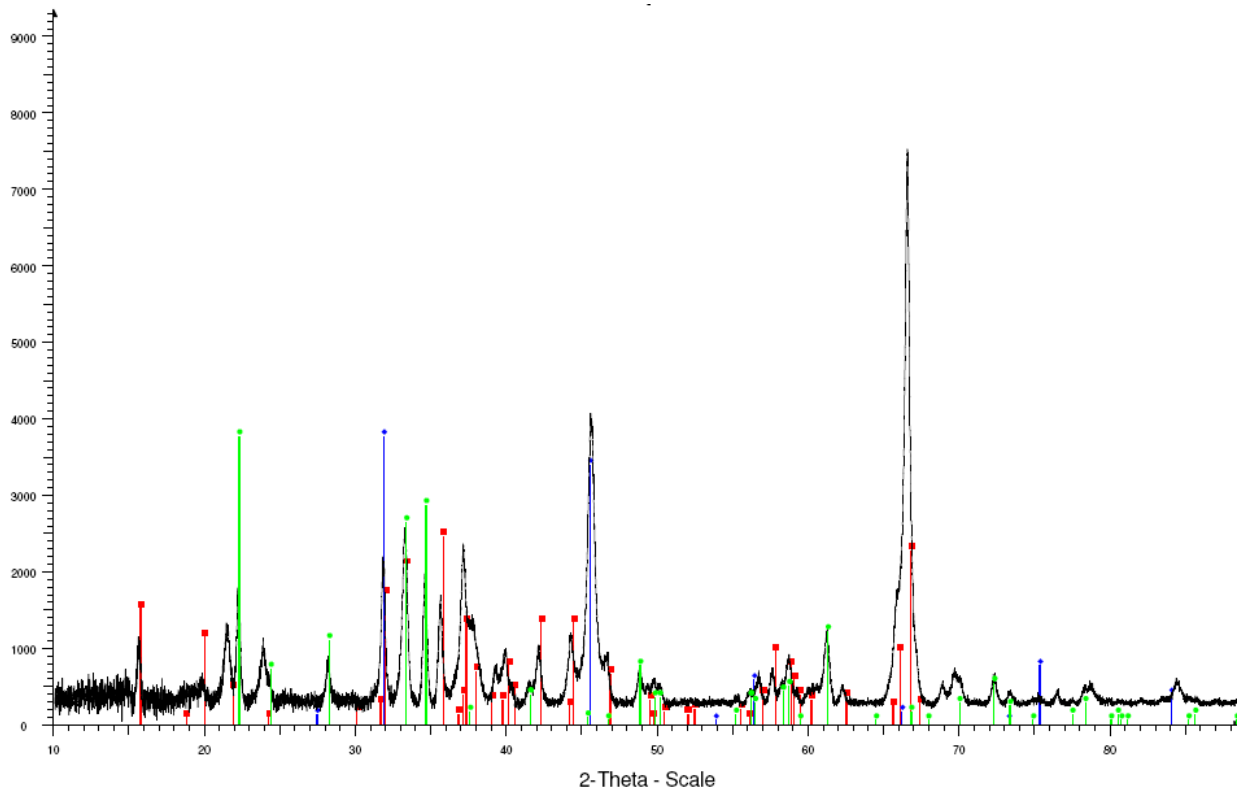

***Figure 4.5*. PXRD pattern of $LiAl_{11}O_{17}$ after washing. Phases shown are an unidentified β-alumina phase in red (PDF File of Na β-alumina used, 00-025-0775) , $LiAlO_2$ in green (PDF File 00-038-1464), and trace amounts of NaCl in blue, (00-001-0994). While NaCl peaks are large, Rietveld refinement suggests that NaCl is only present in minute quantities. It is also possible that the NaCl peaks are due to the presence of an unidentified β"-alumina phase, since Na β"-alumina phase was present in the sample before ion exchange.**

In order to verify that the β-alumina phase present is actually $LiAl_{11}O_{17}$ and not $NaAl_{11}O_{17}$, it is necessary to analyze that sample with a technique other than PXRD. Ideally, TEM would be an excellent analytical technique, but it is extremely time consuming. Alternatively, SEM/EDS analysis can be used. While EDS cannot detect extremely light elements such as lithium, it can detect every other element suspected to be present in the sample. Therefore, it is possible to simply look at a powder sample of $NaAl_{11}O_{17}$, and compare it to post-ion-exchange $LiAl_{11}O_{17}$. If there is a significant loss of sodium due to the ion exchange, it can be assumed that this is due to the reaction succeeding, and $LiAl_{11}O_{17}$ is present. A slight loss of sodium could simply be due to the ion exchange of the side product $NaAlO_2$ converting to $LiAlO_2$, so only an extreme change in sodium abundance helps confirm the presence of the target compound, Li β-alumina.

SEM/EDS was therefore used to quantify the amount of sodium present in both a sample of $NaAl_{11}O_{17}$, and the possible sample of $LiAl_{11}O_{17}$ after ion exchange, and the EDS results are summarized in Table 4.8. It was revealed that there was a great loss of sodium after the ion exchange reaction, which implies that $LiAl_{11}O_{17}$ was indeed produced. A small reduction in sodium could also be due to the conversion of $NaAlO_2$ to $LiAlO_2$, which PXRD confirmed; however, this reaction alone is insufficient in explaining the extreme loss of sodium found via EDS.

SEM images and EDS data for $NaAl_{11}O_{17}$ and $LiAl_{11}O_{17}$ are presented in Figures 4.6 and 4.7, respectively. Note the presence of carbon measured in both samples, which is present due to the carbon tape used to prepare the sample for SEM, and can be factored

out of the percentage abundance of the samples. Table 4.8 also gives atomic abundance data for these samples both before and after carbon is factored out.

Table 4.8

EDS Data on $NaAl_{11}O_{17}$ and $LiAl_{11}O_{17}$, Comparing Abundance of Na in order to Estimate Abundance of Li

Element Measured	Atomic abundance % in Na β-alumina before ion-exchange	Abundance % correcting for presence of carbon	Atomic abundance % in unidentified β-alumina after ion-exchange	Abundance % correcting for presence of carbon
Na	7.48	9.12	1.55	1.67
Al	26.53	32.36	32.89	35.43
O	47.97	58.51	58.39	62.90
C	18.02	0.00	7.17	0.00

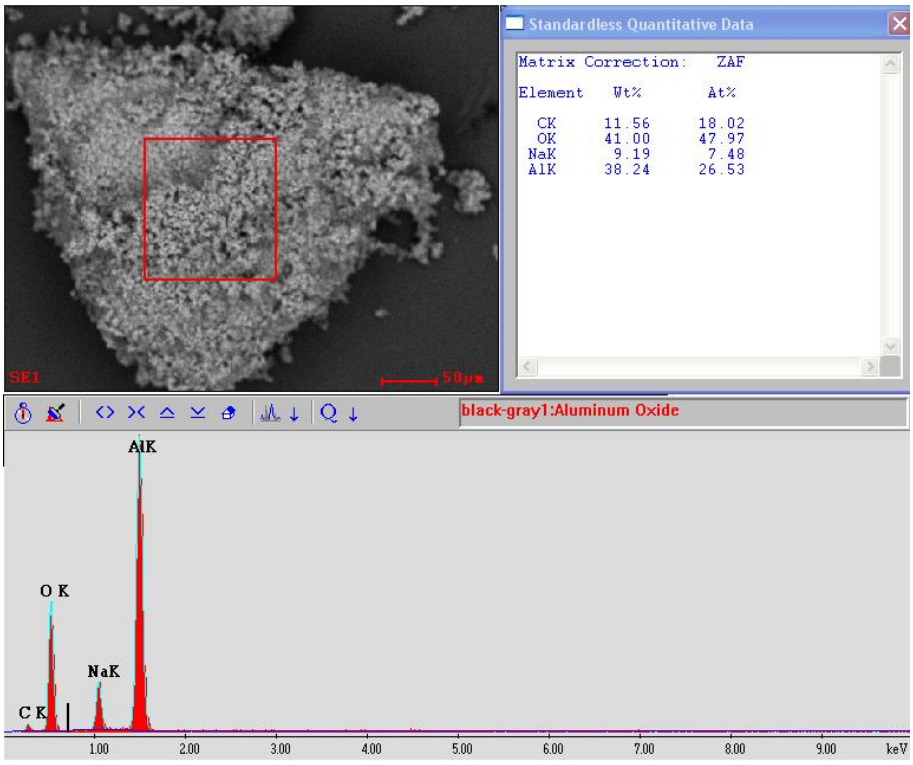

***Figure 4.6*, SEM micrograph and EDS data of $NaAl_{11}O_{17}$ before ion-exchange reaction, showing abundance of sodium, aluminum, oxygen, and carbon.**

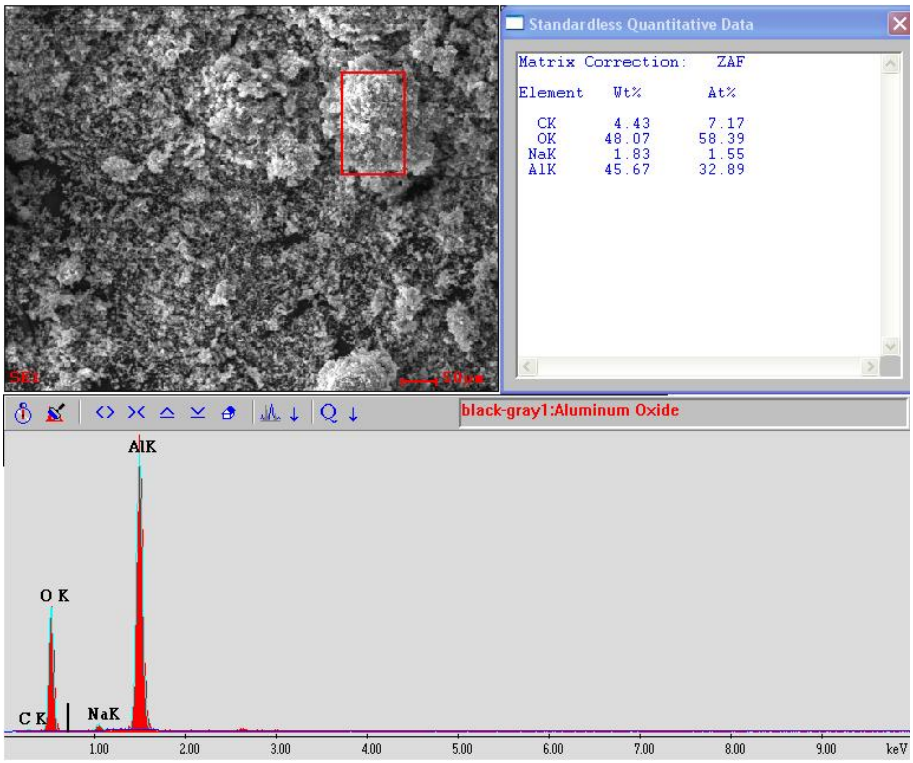

Figure 4.7. **SEM micrograph and EDS data of suspected $LiAl_{11}O_{17}$ after ion-exchange reaction, showing abundance of sodium, aluminum, oxygen, and carbon.**

As mentioned, the EDS data clearly shows a large reduction in the amount of sodium present after ion exchange. Sodium abundance is reduced from 9.12% to 1.67% by mole, which is clearly enough to account for the complete reaction of $NaAlO_2$ to $LiAlO_2$, as well as a reaction of most Na β-alumina to Li β-alumina. While we know that both of these compounds are likely present in the Li β-alumina sample, we cannot know actual percentages of each compound present. This cannot be reasonably calculated with non-stoichiometric compounds such as β-aluminas, where more sodium and/or lithium is present than the chemical formula implies. However, from the extreme loss of sodium observed, it can be reasonably concluded that most of the Na β-alumina was converted to Li β-alumina.

Further work can be done on this ion-exchange reaction in the future in order to ensure a complete reaction where no $NaAl_{11}O_{17}$ is present, such as by altering reaction times so that a complete reaction occurs without the destruction of the pellet. If $LiAl_{11}O_{17}$ does indeed transform via the TCON process, this will actually be quite necessary, as Na is very undesirable as an alloying element with aluminum, as previously mentioned.

It should also be noted that Li β-alumina is not actually stable above temperatures of 800 ° C, where it converts to a spinel-like phase, $LiAl_5O_8$ (26). Because of this unwanted reaction, it will be necessary to do heat treatment studies to quantify the amounts of $LiAl_{11}O_{17}$ and $LiAl_5O_8$ that are likely to be present during TCON transformation, as these temperatures are above 800 °C. It is likely that if the reaction is performed quickly enough, the transforming pellets will still be mostly Li β-alumina, and not the unwanted spinel. However, the transformation of $LiAl_5O_8$ could still be useful to study, since it could allow lithium into the metal phase with aluminum, and form $Al_2O_3/Al_{(Li)}$ composites.

D. $SrTi_5Mg_6O_{17}$

1. Background

If β-alumina compounds do indeed have a beneficial effect on TCON transformation, the need to synthesize different types of novel β-alumina compounds would drastically increase. One such proposed novel compound that would be useful as a sacrificial oxide is $SrTi_5Mg_6O_{17}$. Since this compound contains no aluminum oxide, it is possible that the TCON transformation of this β-alumina-type phase would be significantly different compared to other β-aluminas studied throughout this research, in which the majority of cations in the compound are Al^{3+}. A compound such as this with a higher density of non-aluminum cations in its spinel blocks would increase the amount of metal from the sacrificial oxide that end up alloying with aluminum once the reaction is complete. Because of this, it is possible that transformed $SrTi_5Mg_6O_{17}$ may exhibit an entirely different morphology than the other compounds studied.

If it were to exist, $SrTi_5Mg_6O_{17}$ would likely have the β-alumina structure, with its characteristic alternating structure of spinel blocks and conduction planes. In the case of $SrTi_5Mg_6O_{17}$, Sr^{2+} would exist in the conduction plane, being the largest cation with an atomic radius of 1.16 Å, compared to Na^+, the traditionally seen conduction plane cation, which has an atomic radius of 1.02 Å. The spinel block would contain Ti^{4+}, Mg^{2+}, and O^{2-}. The atomic radii of Ti^{4+} and Mg^{2+} are 0.61 Å and 0.72 Å, respectively, compared to the Al^{3+} cations found in other known β-alumina structures which have an ionic radius of 0.53 Å (24). Given this information, it is probable that the unit cell of $SrTi_5Mg_6O_{17}$ will be significantly larger than that of sodium β-alumina, since the cations are larger, and ionic radii are directly proportionate to bond lengths.

2. Synthesis Procedure

The oxide grind method was the preferred choice of synthetic techniques for the attempted preparation of this compound. If a successful reaction does occur, a more refined method such as sol-gel or co-precipitation can be done in the future in order to obtain a more pure product. The first few attempts were simply carried out using binary metal oxides, TiO_2 and MgO, with $SrCO_3$, as indicated in the reaction shown in Equation 4.5.

$$SrCO_3 + 5\ TiO_2 + 6\ MgO \rightarrow SrTi_5Mg_6O_{17} + CO_2$$

Equation 4.5

The powders were measured out in the appropriate molar ratios, and ground via mortar and pestle for about 10-15 minutes. Acetone was added, and the powders were ground again for another 10-15 minutes. The acetone was allowed to evaporate overnight. The powder was pelletized, and the pellets were calcined and sintered at several different temperatures.

After sintering, a pellet was ground in order to obtain a powder XRD pattern. Since this would be a novel compound if it were indeed synthesized, no previously cited powder pattern is available for comparison to our own sample, unlike the case of the known compounds being synthesized in this research. Instead, when analyzing these samples via powder XRD, the sample is compared with known compounds of similar or related composition, such as $SrMgAl_{10}O_{17}$ or $BaMg_6Ti_6O_{19}$, and if there are any peaks

that we cannot account for, further study will be done on the sample to determine whether or not the target compound was produced.

There are alternative routes to producing this compound that may be more successful than the grinding and sintering of simple binary oxides. One such route is the precursor method, which involves using more complex reagents than binary oxides, such as the spinel $TiMg_2O_4$. This approach offers two main advantages, the more obvious one being that the use of a spinel as a reagent may help to produce the spinel block layer of the β-alumina structure. The second advantage of this technique is that since the reactants are relatively similar in composition to the target phase, the reaction may have greater thermodynamic stability. For example, when using the binary precursors mentioned above, the only strontium compound that formed was $SrTiO_3$ due to its stability. By using more complex reagents, it is possible to, in a sense, "tie-up" certain elements so that their simpler, more stable phases are not as likely to form, increasing the change of producing the desired target compound.

Equations 4.6, 4.7, and 4.8 give proposed approaches of synthesizing the β-alumina type structure $SrTi_5Mg_6O_{17}$ using the precursor method.

(4.6) $3\ TiMg_2O_4 + 2\ TiO_2 + 1\ SrCO_3 \rightarrow 1SrTi_5Mg_6O_{17} + CO_2$

(4.7) $5\ MgTiO_3 + 1\ SrCO_3 + 1\ MgO \rightarrow 1\ SrTi_5Mg_6O_{17} + CO_2$

(4.8) $4\ MgTiO_3 + 1\ TiMg_2O_4 + 1\ SrCO_3 \rightarrow 1\ SrTi_5Mg_6O_{17} + CO_2$

Equations 4.6, 4.7, and 4.8

For the first attempt of utilizing the precursor method to produce the target compound, Equation 4.6 was the reaction used. This is the first logical reaction attempted out of the three above, for the simple reason that β-alumina structure contains a spinel block between each conduction plane, and so it is reasonable to assume that the spinel block of the β-alumina structure would form most easily from existing spinel-type compounds such as the 2,2,4 spinel $TiMg_2O_4$. The remaining required titanium would be provided by TiO_2 powder, and strontium from $SrCO_3$.

Of course, before this reaction could be attempted, it was first necessary to prepare the reactant spinel compound. Refer to Section E below in this chapter for the discussion, synthesis, and results of the production of the spinel $TiMg_2O_4$.

3. Results

Unfortunately, the synthesis of the target compound $SrTi_5Mg_6O_{17}$ has been unsuccessful so far. Table 4.9 summarizes the reaction conditions and results of the attempted synthesis approaches conducted in this study. The PXRD pattern obtained for Sample #1 after sintering is shown in Figure 4.8. All results have so far been nearly identical to this one. In every trial, the same phases are present in the product: $SrTiO_3$, $TiMg_2O_4$, and $TiMgO_3$.

Table 4.9			
Reaction Conditions and Products Produced in the Attempted Synthesis of $SrTi_5Mg_6O_{17}$			
Trial	**Reagents used (g)**	**Calcining/Sintering conditions**	**Products**
1	$SrCO_3$ – 1.4764 TiO_2 – 3.9884 MgO – 2.1783	1200 °C for 115 hours	$TiMgO_3$ $TiMg_2O_4$ $SrTiO_3$
2	$SrCO_3$ – 1.4788 TiO_2 – 4.0104 MgO – 2.2315	1400 °C for 115 hours	$TiMgO_3$ $TiMg_2O_4$ $SrTiO_3$
3	$TiMg_2O_4$ –1.6208 TiO_2 – 0.5310 $SrCO_3$ – 0.4993	1200 °C for 115 hours	$TiMgO_3$ $TiMg_2O_4$ $SrTiO_3$
4	$TiMg_2O_4$ –1.6591 TiO_2 – 0.5652 $SrCO_3$ – 0.5130	1400 °C for 115 hours	$TiMgO_3$ $TiMg_2O_4$ $SrTiO_3$
5	$TiMg_2O_4$ – 1.6402 TiO_2 – 0.5466 $SrCO_3$ -0.5022	1600 °C for 138 hours	$TiMgO_3$ $TiMg_2O_4$ $SrTiO_3$

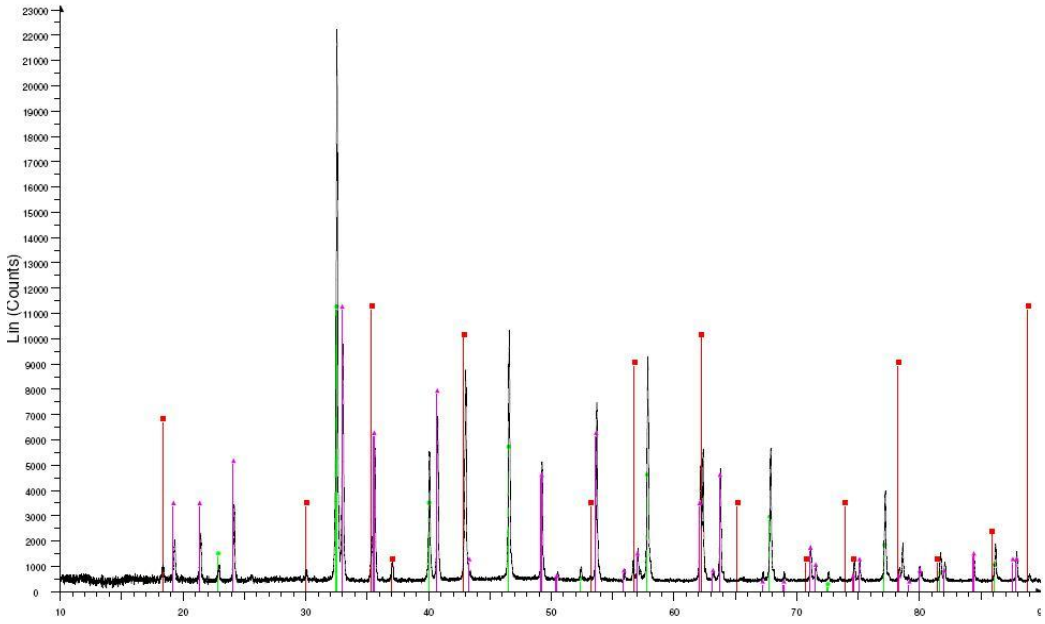

***Figure 4.8*. Powder XRD pattern of $SrTi_5Mg_6O_{17}$ Sample #1. No unidentifiable peaks are present, which indicates that the target novel compound was not produced. Instead, a mixture of $TiMgO_3$ (magenta, PDF File 00-002-0901), $TiMg_2O_4$ (red, PDF File 01-073-1723), and $SrTiO_3$ (green, PDF File 04-005-7016) is produced. Powder XRD patterns for all samples thus far were extremely similar to this one.**

It is clear that the currently attempted methods of producing this compound are not likely to be successful. However, it may still be possible to produce this compound by means of alternate reaction paths. For example, the reactions shown in Equations 4.7 and 4.8 above have not yet been attempted, and may have more success. In particular, Equation 4.7 may be successful since the reactants contain only one source of titanium, the stable ilmenite phase $MgTiO_3$. If none of the titanium involved in the sample is available as a binary precursor to produce the unwanted product $SrTiO_3$, it may be possible that the target compound $SrTi_5Mg_6O_{17}$ may form by thermodynamically "bypassing" the $SrTiO_3$ phase to produce the target compound. Trials involving altering the reagents composition will continue to be performed until the target compound is produced, or it is determined that it is not possible to synthesize this compound by conventional methods.

E. Synthesis of $TiMg_2O_4$

1. Background

The spinel compound $TiMg_2O_4$ was originally produced as a reagent for the synthesis of the novel β-alumina compound $SrTi_5Mg_6O_{17}$, which is discussed above in Section D of this chapter. In addition, to our knowledge, this compound itself has not been studied as a sacrificial oxide in reactive metal penetration, so it is also useful to react this compound under TCON conditions. Neither TiO_2 nor MgO can be used as TCON precursors. Although TiO_2 is thermodynamically usually predicted to react with

molten Al, it has poor wettability in the system, so no reaction takes place (28). The thermodynamics of a reaction between MgO and molten aluminum is not thermodynamically favorable (3). However, by using a compound such as $TiMg_2O_4$ as a TCON precursor, titanium and magnesium can both be incorporated into the composite material, hopefully alloyed in the metal phase with aluminum. The TCON transformation will be discussed in greater detail in Chapter 5.

Another important motivation for synthesizing $TiMg_2O_4$ and studying its transformation via the TCON process was for comparison to transformation of $SrTi_5Mg_6O_{17}$, once it is successfully prepared. The two compounds have similar composition, and differ mainly in the presence of conduction channels in $SrTi_5Mg_6O_{17}$. Thus, the comparison would illuminate the impact of the conduction layer on composite product microstructure, if any.

2. Synthesis Procedure

The production of $TiMg_2O_4$ is a relatively simple task, accomplished via traditional ceramic methods. Titanium dioxide and magnesium oxide are mixed in the desired molar ratios, and ground via mortar and pestel for ten minutes, and then ground for another ten minutes under acetone. The acetone is allowed to evaporate overnight, and the resulting powders are pelletized and sintered at 1400 °C for 16 hours. The resulting pellets are then ground back into powder form, and verified via powder XRD.

3. Results

Several sets of reaction conditions were used in an attempt to obtain the purest product, wherein reaction time and temperature was altered. It was found that the best reaction conditions for the production of $TiMg_2O_4$ were to sinter the pellets for 16 hours at 1400 °C. The purity of the product was determined via Rietveld refinement to be 94.60% by mass $TiMg_2O_4$, with the remaining 5.40% attributed to the impurity $TiMgO_3$. Starting atomic positions for the refinement were obtained from ICSD card 65792 for $TiMg_2O_4$ and ICSD card 55285 for $TiMgO_3$

F. Synthesis of $SrNiAl_{10}O_{17}$

1. Background

The next novel β-alumina compound targeted for synthesis was $SrNiAl_{10}O_{17}$. This compound was expected to be very similar in structure to $SrMgAl_{10}O_{17}$, which had previously been thoroughly studied in this research. Just as in its magnesium-containing counterpart, Ni^{2+} would act as a charge compensator in the spinel block, allowing a +2 charged cation such as Sr^{2+} to exist in the conduction plane of the β-alumina structure. In fact, Ni^{2+} has an ionic radius of 0.69 Å, in comparison to the Mg^{2+} ionic radius of 0.72 Å, which is a virtually insignificant difference (1). If this compound were to be successfully produced, and exposed to TCON transformation, the resulting composite would have a variety of beneficial properties. Strontium increases the strength and ductility of

aluminum alloys (12), and nickel increases the strength and conduction of aluminum alloys (14). And of course, there is also the possibility that a nano-scale composite material could be produced due to the presence of β-alumina conduction planes, as discussed previously.

2. Synthesis Procedure

The method of synthesis for this compound has been adapted from Fengxiang and Shengfu (29). This article describes the synthesis of a series of compounds of formula $MAl_{12}O_{19}$ and $MNAl_{11}O_{19}$, which adopt magnetoplumbite-type structure, where M and N are various metals. Magnetoplumbites and β-aluminas are similar in that both structures contain the definitive conduction planes, with β-alumina's being more open due to fewer atoms in the plane (i.e. SrO for β-alumina and $SrAlO_3^-$ for magnetoplumbite), and therefore of greater interest for the purpose of this research. The authors of the article synthesized these magnetoplumbite compounds by grinding metal nitrates in stoichiometric proportions, and combusting the mixture with urea as a fuel source to form the product (29). Therefore, we believed that through careful control of stoichiometry, we could use this method to instead produce the β-alumina type structure $SrNiAl_{10}O_{17}$.

The following metal nitrates were mixed and ground in the desired stoichiometric ratios to hopefully obtain $SrNiAl_{10}O_{17}$: $Al(NO_3)_3 \cdot 9\ H_2O$, $Sr(NO_3)_2$, and $Ni(NO_3)_2 \cdot 6\ H_2O$. Urea was added to the mixture, such that the molar ratio of urea to total metal ions was 3 to 1. The mixture was combusted at various times and temperatures (see next section) in a box furnace, with O_2 being streamed into the system and exhaust gases streamed out safely. Refer to Equations 4.9 and 4.10 for the proposed chemical reaction

for the production of the target compound, and for the combustion of urea, respectively. It is clear from these equations why it is necessary to vent gaseous byproducts out of the system. Upon completion of the synthesis, the product was verified in the usual way via powder XRD, and then pelletized and sintered. To be sure that sintering did not cause unwanted reactions to occur, the re-sintered pellet was verified again via powder XRD to still be the target compound. It should be noted that the re-sintering process is done at temperature high enough to be sure that the compound will be stable at TCON temperatures.

(4.9) $10\ Al(NO_3)_3 \cdot 9\ H_2O + 1\ Ni(NO_3)_2 \cdot 6\ H_2O + 1\ Sr(NO_3)_2 \rightarrow$

$$1\ SrNiAl_{10}O_{17} + 34\ NO_2 + 96\ H_2O$$

(4.10) $2\ CO(NH_2)_2 + 3O_2 \rightarrow 2\ CO_2 + 4\ H_2O + 2\ N_2$

Equation 4.9 and 4.10

3. Results

Synthesis of $SrNiAl_{10}O_{17}$ was met with immediate success. Not only is this significant for the purpose of using this compound as a TCON precursor, but this is also a novel compound. Table 4.10 summarizes reaction conditions for the formation of $SrNiAl_{10}O_{17}$.

Table 4.10		
Reaction Conditions for the Synthesis of $SrNiAl_{10}O_{17}$ via the Urea Combustion Method		
Sample #	**Reagents used in grams**	**Reaction Conditions**
1	$Al(NO_3)_3 \cdot 9H_2O$ – 16.346 $Ni(NO_2)_2 \cdot 6\ H_2O$ – 1.276 $Sr(NO_3)_2$ – 0.930 Urea – 10.10	Nitrates dissolved in H_2O, dried, ground, and mixed with urea. Combusted at 700 °C for 3 hours. Resintered at 1200 °C for 10 hours.
2	$Al(NO_3)_3 \cdot 9H_2O$ – 21.793 $Ni(NO_2)_2 \cdot 6\ H_2O$ – 1.711 $Sr(NO_3)_2$ – 1.238 Urea – 13.46	Nitrates dissolved in H_2O, dried, ground, and mixed with urea. Combusted at 700 °C for 3 hours. Resintered at 1200 °C for 10 hours.

After combustion, the resulting product was an extremely light, fluffy, fragile substance that is sky-blue in color. This powder was ground and verified via PXRD and Rietveld refinement. Because this is a novel compound, no previous powder pattern exists which can be compared to our pattern. However, we can compare our experimental pattern to that of $SrMgAl_{10}O_{17}$, as these two compounds are expected to have extremely similar unit cells, with the only difference being the presence of either Ni^{2+} or Mg^{2+} at the tetrahedral site in the spinel blocks. Additionally, Mg^{2+} and Ni^{2+} have extremely similar ionic radii, so the powder patterns of these two compounds should be very nearly identical.

The first PXRD pattern was taken before the sample was resintered. Because of the fluffy, extremely powdery nature of the compound, the peaks found within the pattern were very broad, indicating a very small average crystallite size. These peaks still matched up very well to those of $SrMgAl_{10}O_{17}$. A second phase was suspected to be

present, and was likely $NiAl_2O_4$. After the sample was resintered and another powder pattern was taken, much sharper peaks were found. The only identifiable phase was the β-alumina phase. It should be noted that magnetoplumbites have very similar structures to β-aluminas, so it is often possible to mistake a magnetoplumbites phase for a β-alumina phase. For this reason, the powder pattern was also compared to the magnetoplumbite phase $SrAl_{12}O_{19}$. Fortunately, none of these peaks matched up with the peaks of this phase, so we can be assured that a magnetoplumbite was not produced. Figure 4.9 shows the PXRD pattern of Sample 1, after resintering.

Rietveld refinement was performed on the compound, using the .cif file for $SrMgAl_{10}O_{17,}$ prepared from ICSD card 155524. The atomic positions parameter in the .cif file was changed so that Mg^{2+} was replaced with Ni^{2+}. The resulting refinement shows that the pattern for our sample was extremely similar to the one predicted by altering the .cif file of a similar compound. Figure 26 indicates the results of the Rietveld refinement of this sample, and proves that the target compound, $SrNiAl_{10}O_{17}$, was indeed produced. The refined unit cell parameters for $SrNiAl_{10}O_{17}$ are a = 5.6239 Å and c = 22.4285 Å, giving a ratio of c/a = 3.9881. As discussed previously, the c/a ratio of the similar magnetoplumbite phase $SrAl_{12}O_{19}$ is only 3.952 (from ICSD # 69020). Because our refined c/a ratio is significantly larger than that for the magnetoplumbite phase, this serves as further evidence that the produced phase $SrNiAl_{10}O_{17}$ has β-alumina structure. Further studies can be done in the future to formally solve the crystal structure, such as single crystal XRD if crystals of $SrNiAl_{10}O_{17}$ can be produced.

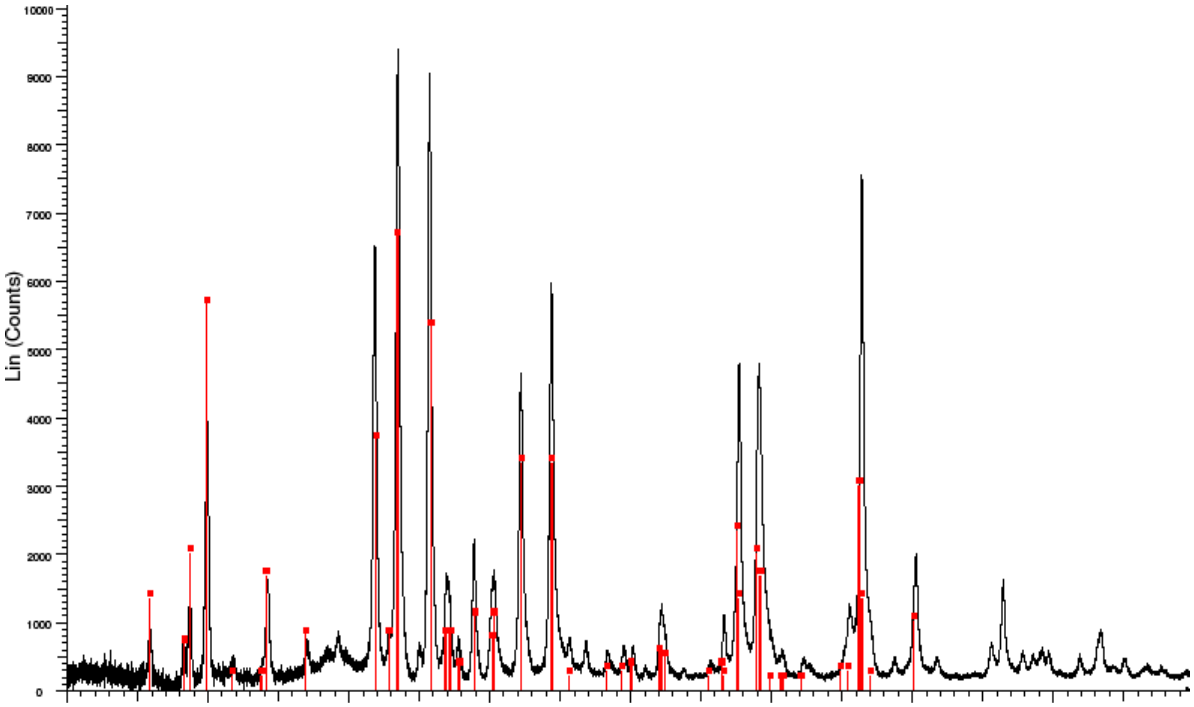

Figure 4.9. **PXRD pattern of $SrNiAl_{10}O_{17}$ Sample #1, taken after resintering. Red lines correspond to the powder pattern of $SrMgAl_{10}O_{17}$ (PDF File 04-010-0738), which is predicted to have a nearly identical structure to the target compound.**

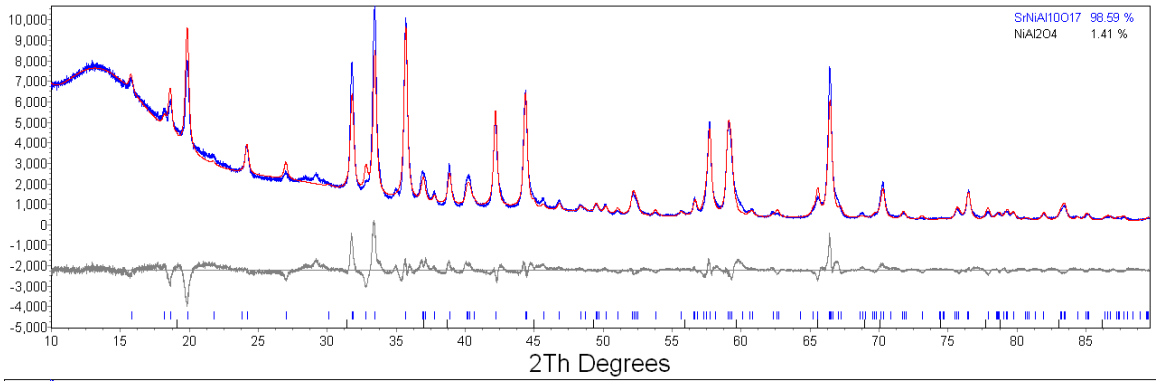

Figure 4.10. **Rietveld Refinement of $SrNiAl_{10}O_{17}$. The .cif file used was that of $SrMgAl_{10}O_{17}$, with the Mg^{2+} site replaced with Ni^{2+}. $NiAl_2O_4$ was originally suspected to be present, but was revealed to only present in very small amounts.**

G. $NiAl_2O_4$

1. Background

$NiAl_2O_4$ has already been reported to have been exposed to reactive metal penetration (28), so TCON transformation was predicted to yield similar results. The motive for synthesis and transformation of $NiAl_2O_4$ via the TCON process therefore is to obtain results for comparison with the transformation products of $SrNiAl_{10}O_{17}$. This comparison would be useful due to the fact that $NiAl_2O_4$ adopts the spinel structure, and $SrNiAl_{10}O_{17}$ effectively contains some $NiAl_2O_4$ related spinel blocks, separated by open conduction planes, the effect of which on final composite microstructure we wish to study.

2. Synthesis

$NiAl_2O_4$ was produced via the sol-gel method as adopted from Chokkaram and Srinivasan (30). Hydrated metal nitrates of aluminum and nickel were mixed in the desired molar ratios in a minimal amount of water. A solution of 1M ammonium carbonate was added until the pH was approximately 8. The resulting gel was filtered and washed with deionized water, and dried for 24 hours at 120°C. The powder obtained was ground, pelletized and sintered at 900 °C for 4 hours. The resulting pellets were verified via powder XRD (30).

3. Results

Several samples of $NiAl_2O_4$ were produced, each with identical reaction conditions and results. In every case, the only product verified via PXRD was the target compound.

CHAPTER V – TCON TRANSFORMATION AND CHARACTERIZATION RESULTS

After the contents of the oxide pellets are verified, the next step is to transform the pellets under TCON conditions. While the synthesis of the sacrificial oxides can be discussed in complete detail, it is necessary to omit many of the details about the TCON process itself, since this is proprietary information of Fireline TCON Inc. The concept of reactive metal penetration has been studied by many different research groups; however, Fireline has developed their own specific set of reaction conditions, equipment, and so on that makes the TCON process of reactive metal penetration unique.

A. $SrMgAl_{10}O_{17}$

1. TCON Transformation

Pellets of $SrMgAl_{10}O_{17}$ were given to Fireline TCON Inc. to react under TCON conditions with molten aluminum, with the hope of forming a ceramic/metallic composite material.

The resulting product was prepared for SEM and XRD analysis.

2. Characterization Results of TCON Product

The transformation of pellets of $SrMgAl_{10}O_{17}$ transformed under TCON conditions has had mixed success, and the results are summarized in Table 5.1. Only a very small portion of the pellets transformed in either case, with even less of TCON Sample 3 transforming than in Sample 2. Note that the table does not include results for Sample 1 because transformation was not attempted on this sample.

$SrMgAl_{10}O_{17}$ TCON Sample 2 was rather porous likely due to the CO_2 released from the $SrCO_3$ precursor during calcining, and this is undesirable for obtaining SEM images of composite morphology. Therefore, Sample 3 was prepared by regrinding and resintering $SrMgAl_{10}O_{17}$ from Sample 2 in order to remove the voids. Also, Sample 3 was reacted under TCON conditions for twice as long as Sample 2 was, with the hope of obtaining a more complete reaction. However, Sample 3 reacted even less completely than the case for Sample 2. It is possible that the porous nature of Sample 2 helped enable the reaction by providing more surface area for the molten Al to react with the specimen. Nevertheless, SEM data was obtained from both Samples 2 and 3, as discussed next.

Table 5.1			
Description of TCON Transformed $SrMgAl_{10}O_{17}$ Samples			
$SrMgAl_{10}O_{17}$ Oxide Sample	**Description of Sacrificial Oxide**	**Description of TCON reaction**	**Initial Visual Description of SEM-prepared sample**
1	~95% by mass target compound, ~5% $SrAl_2O_4$ Pellets were not reground and resintered for densification	Not TCON Transformed	N/A
2	~95% by mass target compound, ~5% $SrAl_2O_4$ Pellets were not reground and resintered for densification	Standard TCON reaction conditions	Very little reaction, medium grey color, porous, large pore in center
3	~95% by mass target compound, ~5% $SrAl_2O_4$ Pellets were reground and resintered for densification	Standard TCON reaction conditions, with twice the reaction time	Very little reaction, less than Sample #2. Very light grey color, less porous.

Two SEM samples were prepared from the sample 2 TCON pellet, one containing a layer of complete reaction (referred to as Sample 2.1), the other one being approximately half-transformed, with one side being the composite, and the other the ceramic sacrificial oxide (referred to as Sample 2.2). Note that while there were varying degrees of how much of the samples actually transformed, PXRD data indicated for each sample that the transformed region was indeed a combination of two main phases, aluminum metal and Al_2O_3 as corundum. Refer to Figure 5.1 for the PXRD pattern of transformed $SrMgAl_{10}O_{17}$, Sample #2.1, as an example. It is important to note that this PXRD pattern was obtained by collecting X-rays diffracted from the surface of the transformed pellet. When the pellet is pulverized and the bulk material analyzed, mostly untransformed material is detected.

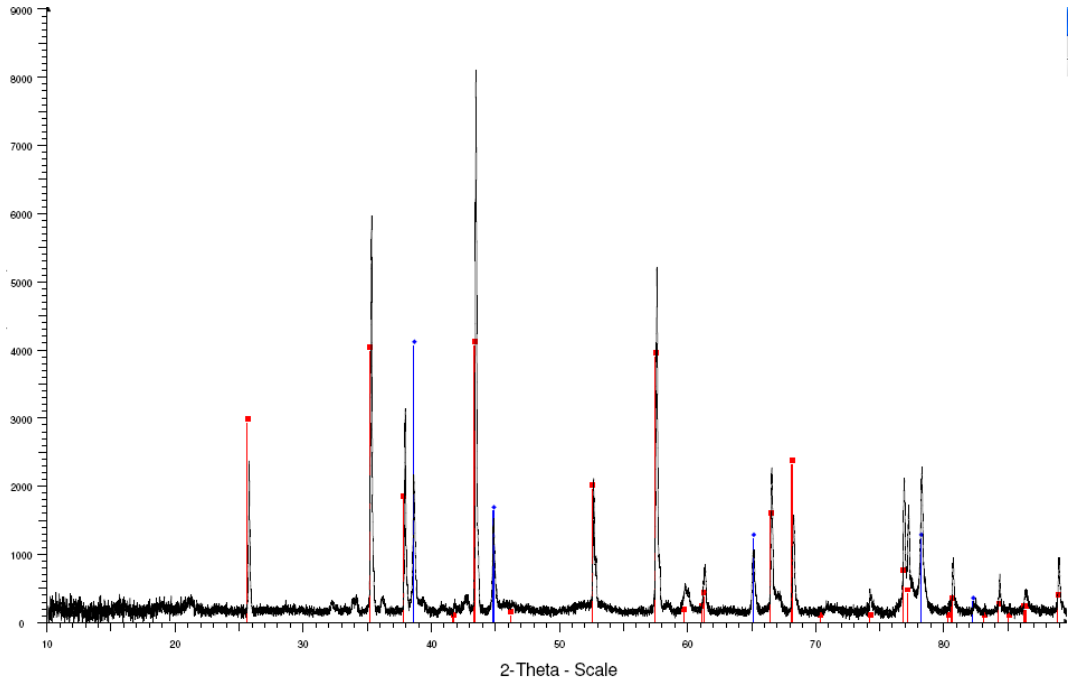

***Figure 5.1*. PXRD Pattern of TCON transformed $SrMgAl_{10}O_{17}$, sample #2.1. Blue lines correspond to Al metal (PDF File 00-001-1180) , Red lines to corundum, Al_2O_3 (PDF File 00-043-1484).**

The SEM micrographs for Sample 2.1 are shown in Figures 5.2 – 5.5. The voids present in the sample are quite noticeable in Figures 5.2 and 5.3, and Figure 5.4 then shows the sample at a still larger magnification. The regions of different contrast represent the ceramic (lighter) and metallic (darker) phases of the composite. Figure 5.5 then shows images taken within a void at different magnifications. Since the features within the void are not ground and polished, the 3-dimensional morphology of ceramic and metallic components becomes evident.

SEM Micrographs of Transformed $SrMgAl_{10}O_{17}$ Sample #2.1

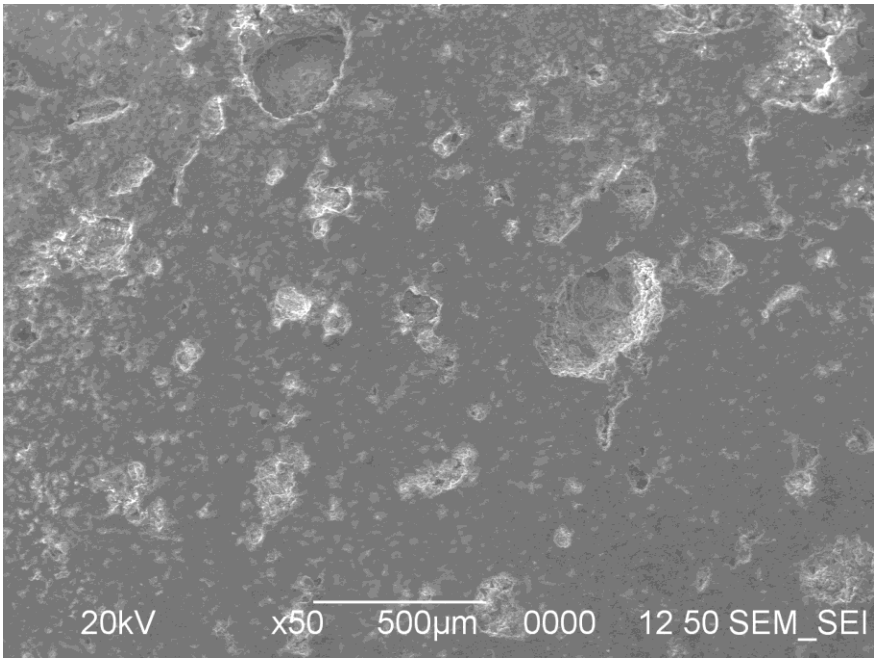

Figure 5.2. **SEM secondary electron micrograph of $SrMgAl_{10}O_{17}$ Sample #2.1, shown at x50 magnification. The most noticeable features here are the voids in the structure; however, at closer magnification the different phases present become more noticeable.**

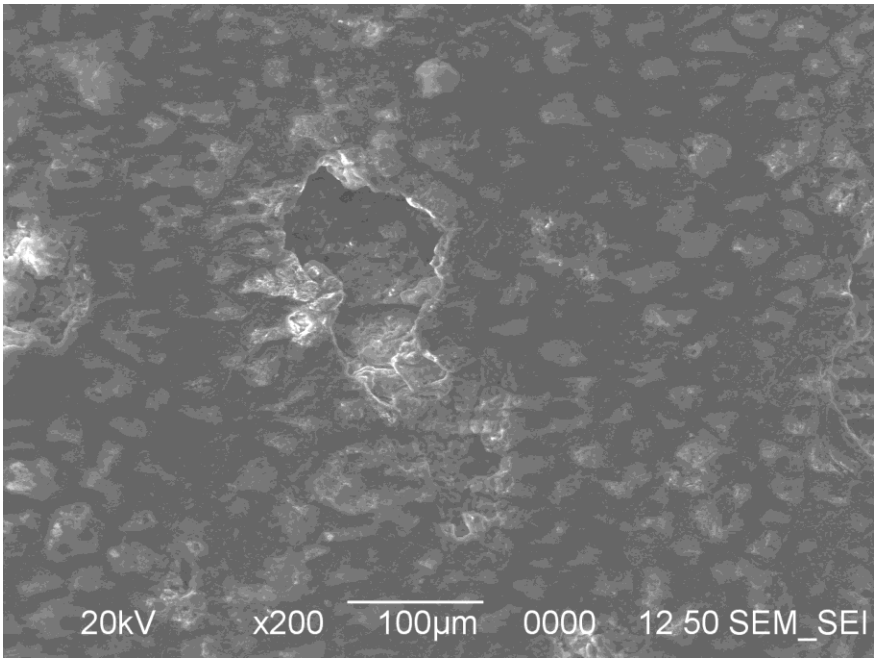

Figure 5.3. **SEM secondary electron micrograph of $SrMgAl_{10}O_{17}$ Sample #2.1, shown at x200 magnification. The most noticeable features here are still the voids in the structure; however, at closer magnification the different phases present become more noticeable.**

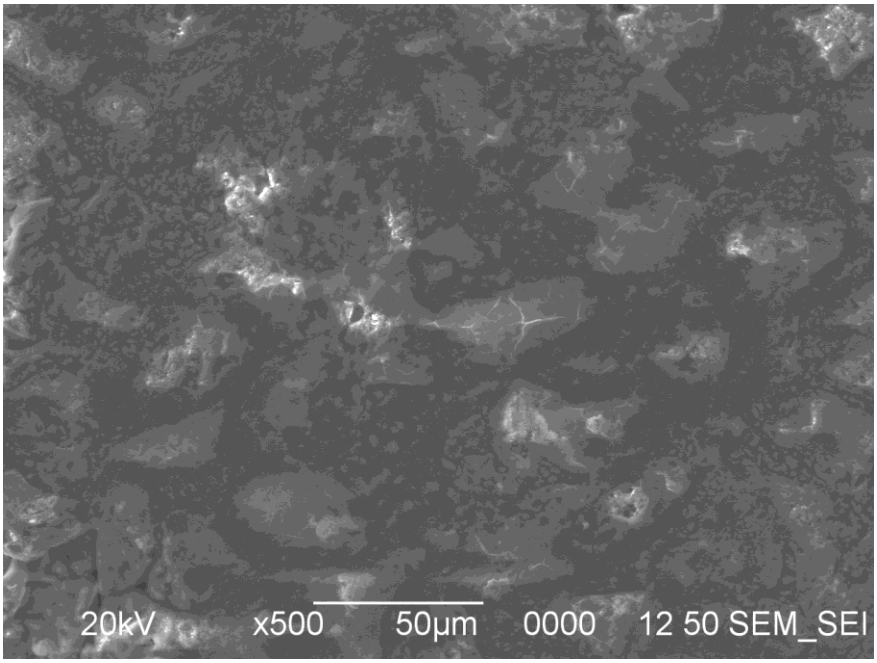

Figure 5.4. **SEM secondary electron micrograph of $SrMgAl_{10}O_{17}$ Sample #2.1, shown at x500 magnification. At this magnification the different phases present can be distinguished.**

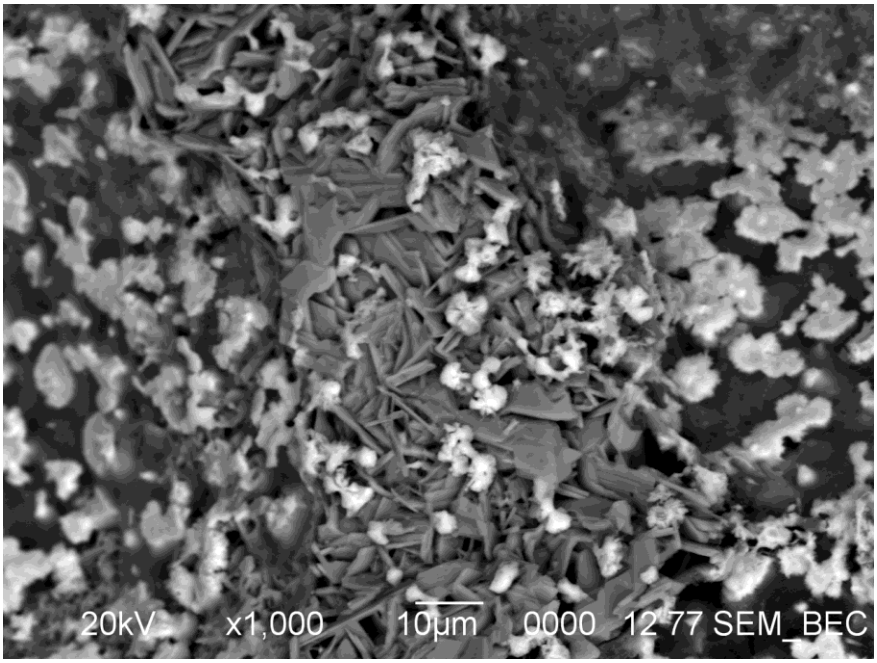

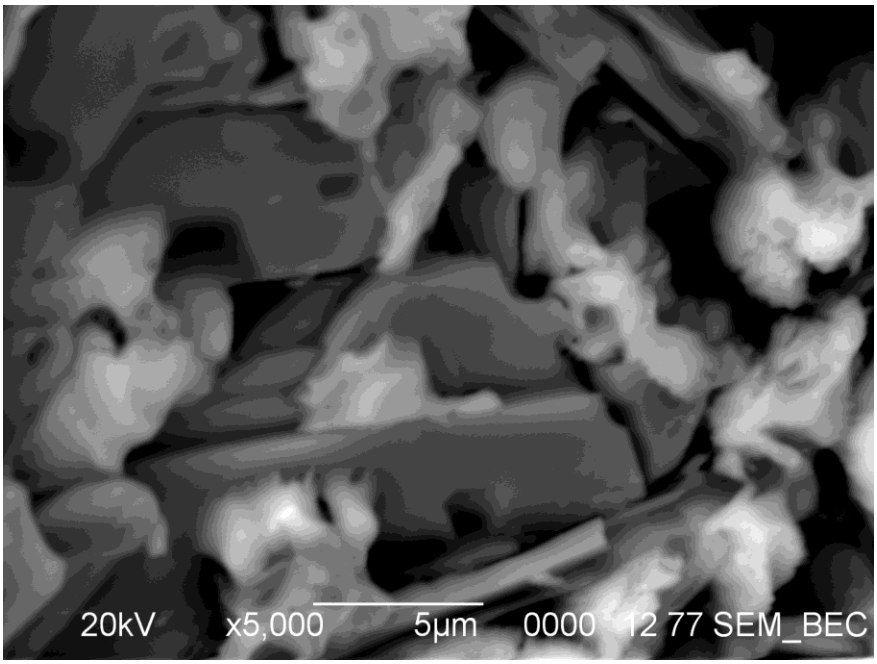

***Figures 5.5a (top) and 5.5b (bottom)*. SEM backscattered micrograph of $SrMgAl_{10}O_{17}$, Sample 2.1, taken of a large void in the sample, so the features here are not ground and polished. The image clearly shows long, thin crystals of ceramic material, and globules of metal. Images were taken at magnification of (a) x1000 and (b) x5000. This is the highest degree of magnification that was obtainable on these features where the micrograph is still clear and not grainy. The globules of metal were found to contain between 3.00 and 6.48 percent abundance by mole strontium. This was the only appreciable source of strontium that was found in the sample.**

An SEM micrograph obtained from a second specimen prepared from the reaction 2 pellet, i.e. Sample 2.2, is shown in Figure 5.6. This image clearly shows the ceramic-metallic phase of the composite where lighter regions are Al_2O_3, and the darker regions are Al metal. Comparison of this Figure to the one shown in Chapter 1, Figure 1.4 indicates that this composite consists of the ceramic phase embedded in a continuous metal matrix, rather than the co-continuous system usually observed for TCON composites. This will be discussed further later.

SEM images pertaining to a specimen prepared from Sample 3 are shown in Figures 5.7 – 5.9, and very clearly depict distinct ceramic and metallic phases of the composite. Figures 5.10 – 5.16 then show EDS data for Sample 3, and verify that the ceramic phase is mainly aluminum oxide (i.e. Al_2O_3), while the metallic phase is mainly Al.

SEM Micrographs of Transformed $SrMgAl_{10}O_{17}$ Sample # 2.2

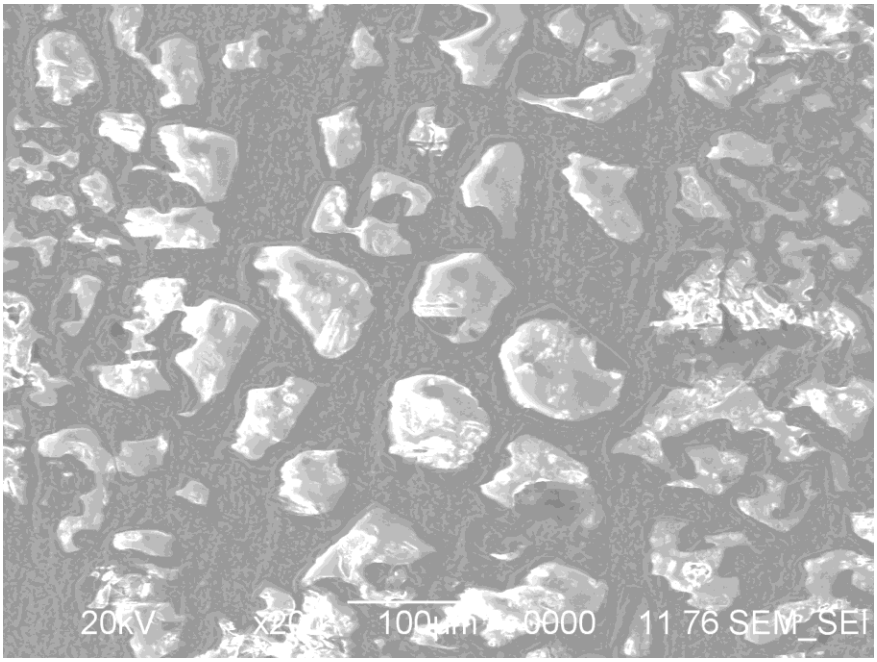

***Figure 5.6*. SEM secondary electron micrograph of $SrMgAl_{10}O_{17}$ Sample #2.2, shown at x200 magnification. Lighter areas are aluminum oxide, darker areas are aluminum metal.**

SEM Micrographs of Transformed $SrMgAl_{10}O_{17}$ Sample #3

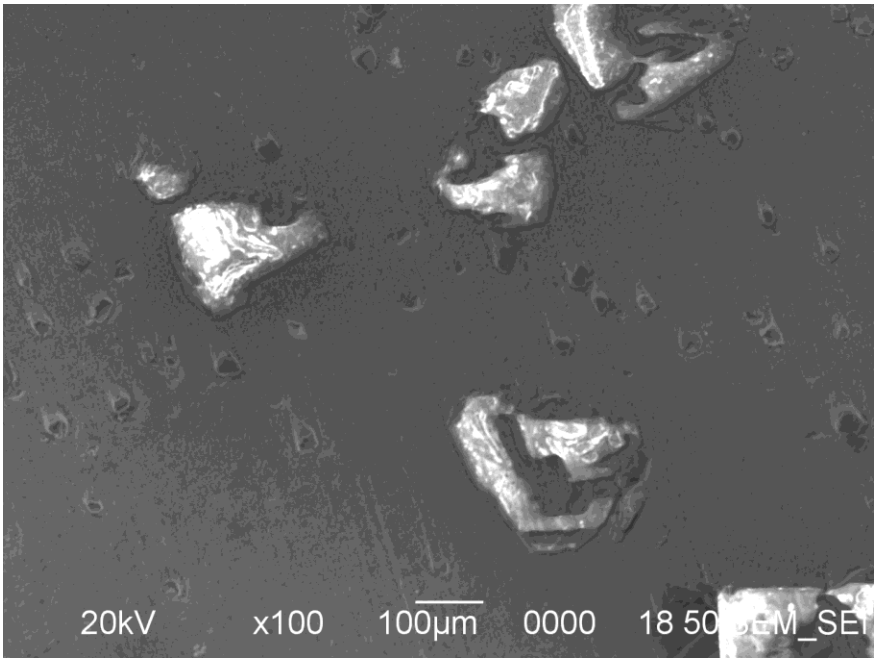

Figure 5.7. **SEM secondary electron micrograph of $SrMgAl_{10}O_{17}$ Sample #3, shown at x100 magnification. Lighter, rougher areas are the ceramic phase, and darker, smoother areas are the metal phase. This micrograph displays the lack of homogeneity in the sample, as in this region, the metal phase is much more abundant than the ceramic phase, despite the lower magnification in relation to Figure 5.8, for example**

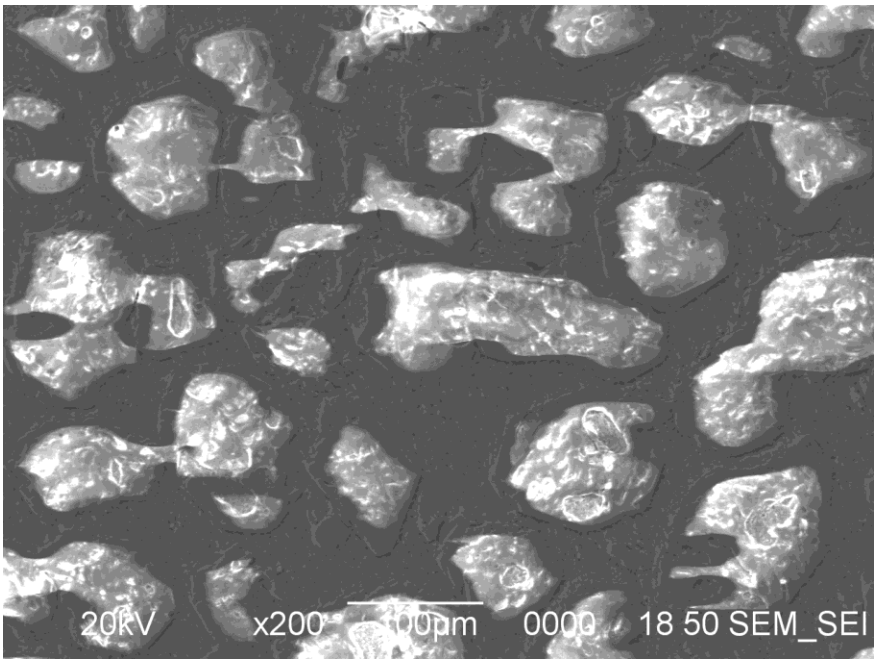

Figure 5.8. **SEM secondary electron micrograph of $SrMgAl_{10}O_{17}$ Sample #3, shown at x200 magnification. Lighter areas are the ceramic phase, darker areas are the metallic phase.**

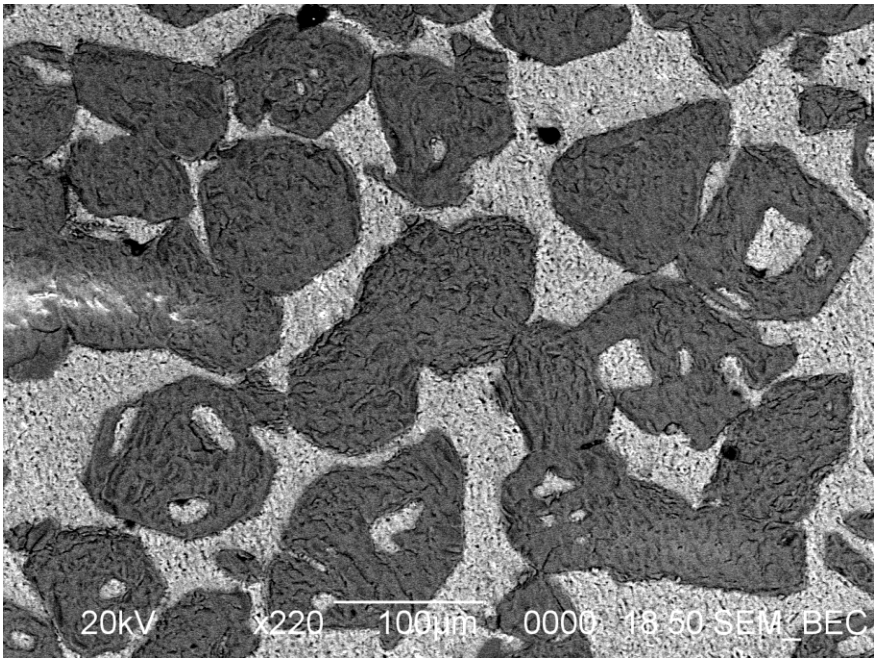

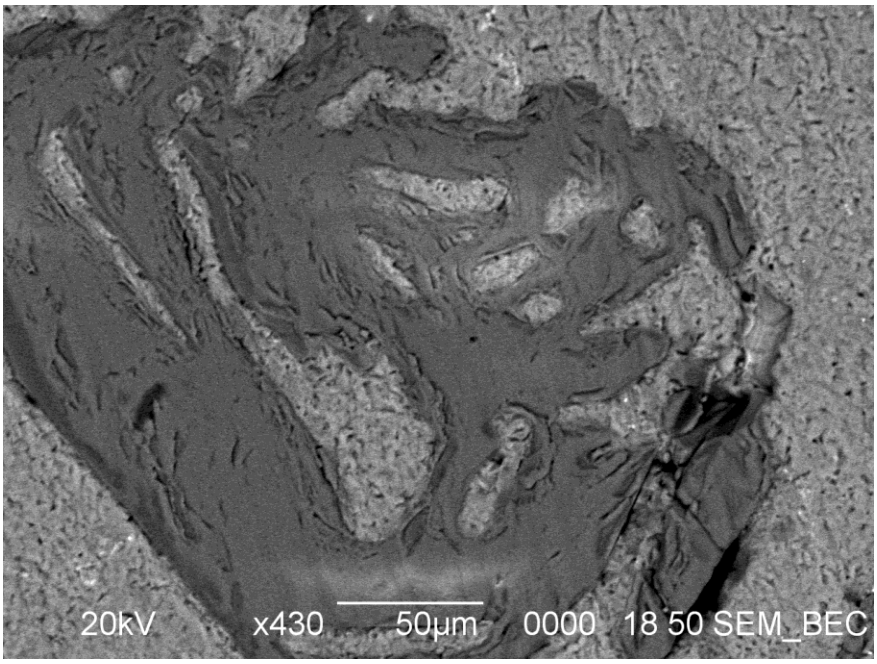

Figure 5.9a (top) and 5.9b (bottom). **SEM backscattered micrograph of $SrMgAl_{10}O_{17}$ Sample #3. Dark areas are the ceramic phase, lighter areas are the metallic phase. White areas are contaminants, black areas are voids. The images were taken at magnifications of x220 and x430.**

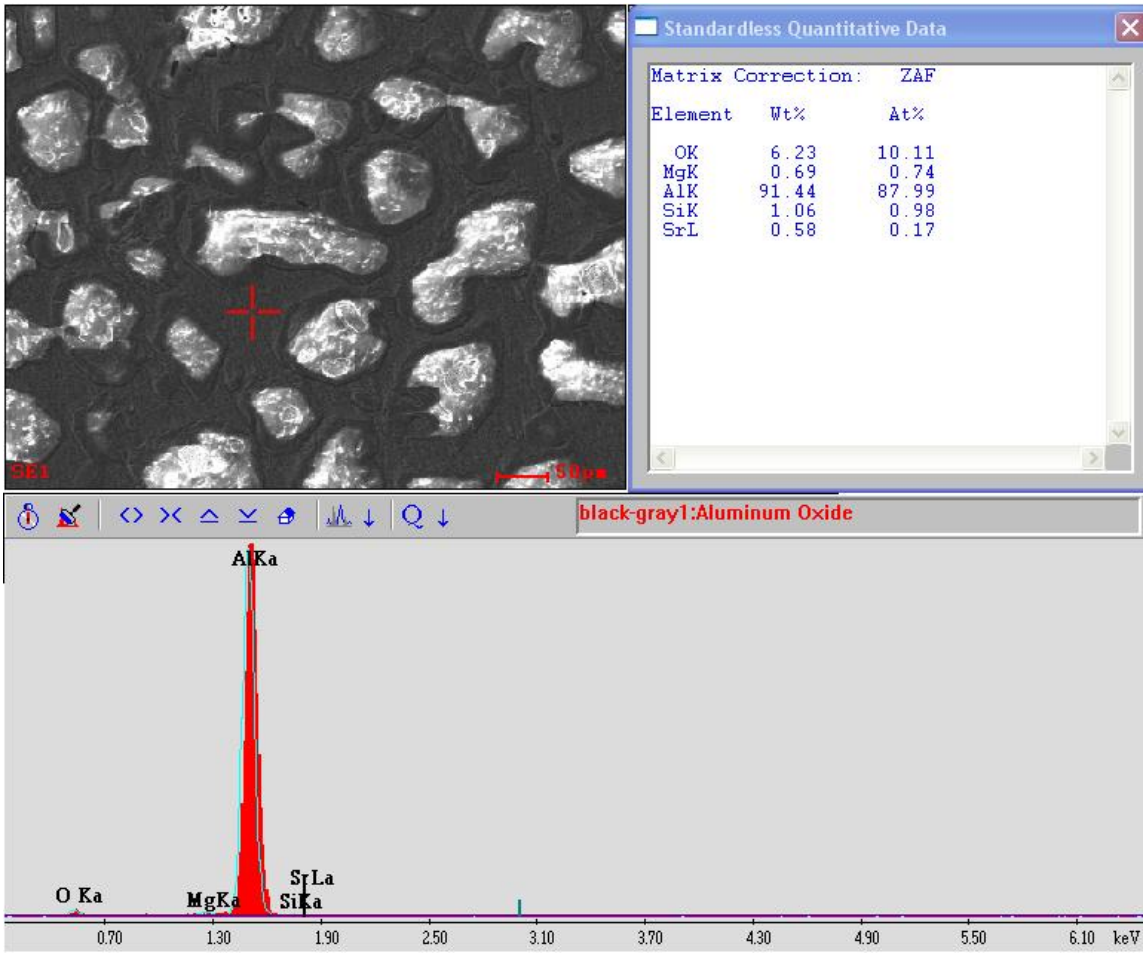

Figure 5.10. **EDS micrograph and data of a region in $SrMgAl_{10}O_{17}$ Sample #3. The analyzed portion is verified to be the metal phase, containing mostly aluminum. Oxygen's presence is most likely due to oxide formation on the surface of the sample. Silicon was a contaminant of the sample. It is unclear whether magnesium or strontium measured exist as oxides or metals, or are even really present since the miniscule amounts measured would simply be noise from the aluminum or silicon peaks.**

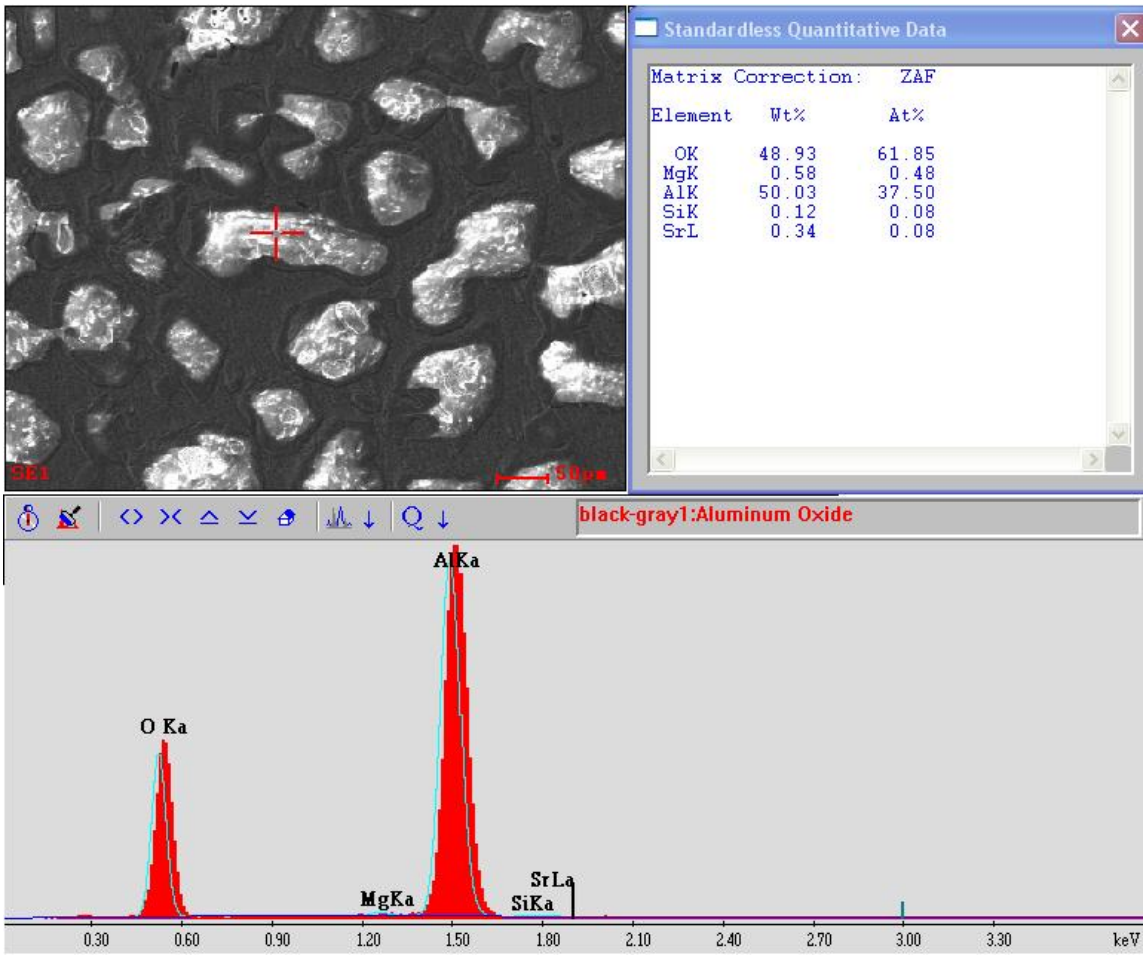

***Figure 5.11*. EDS micrograph and data of a region in $SrMgAl_{10}O_{17}$ Sample #3. The region analyzed is verified to be the ceramic phase. The main elements present are aluminum and oxygen, which indicate the presence of aluminum oxide. Silicon is a contaminant. It is unclear whether strontium or magnesium measured is in the metallic or ceramic phase, or if they are even present at all, since the miniscule amounts measured could simply just be noise from the aluminum or silicon peaks.**

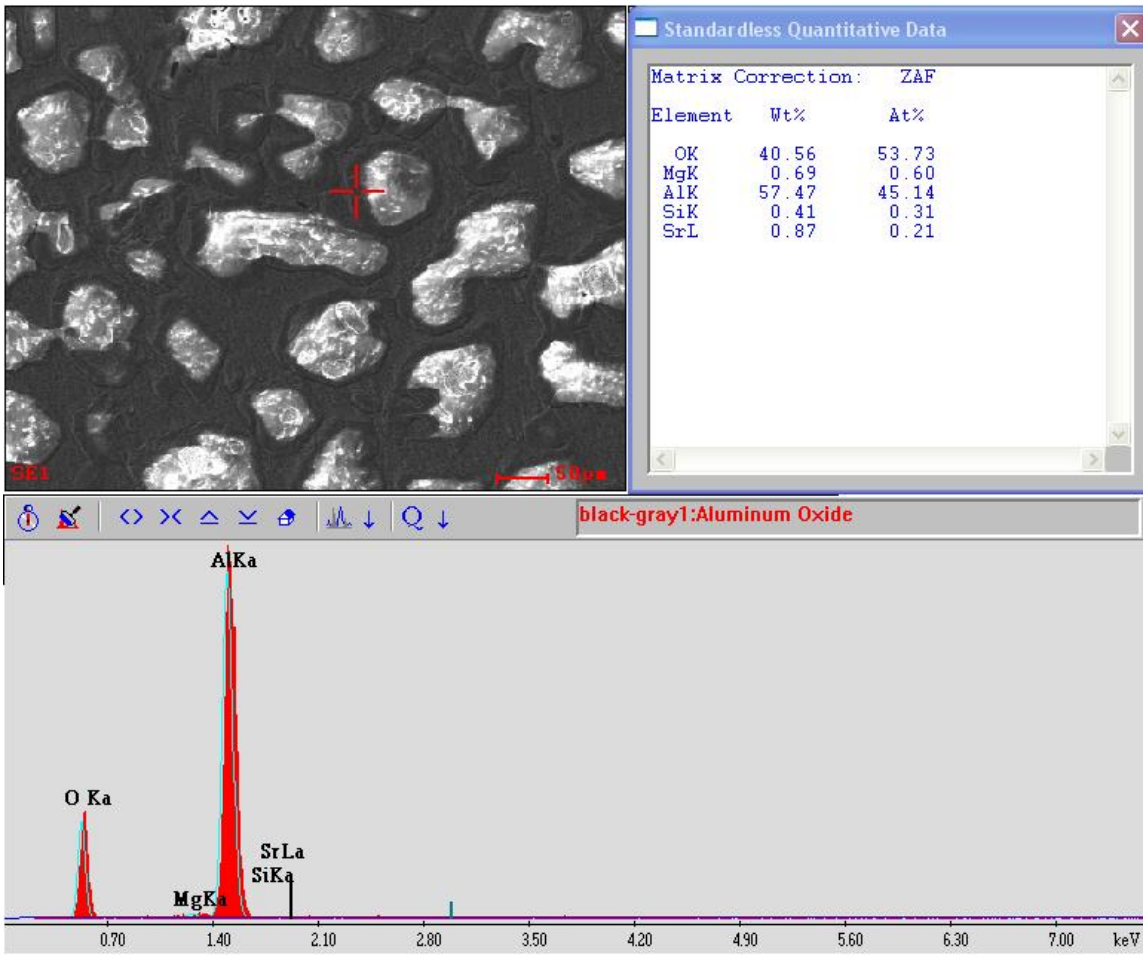

Figure 5.12. **EDS data for $SrMgAl_{10}O_{17}$ Sample #3. Analysis of interphase region reveals that it is a combination of both the metallic and ceramic phases. This could be due to the penetration of EDS analysis, as the measured region appears visually to be more similar to the metal phase.**

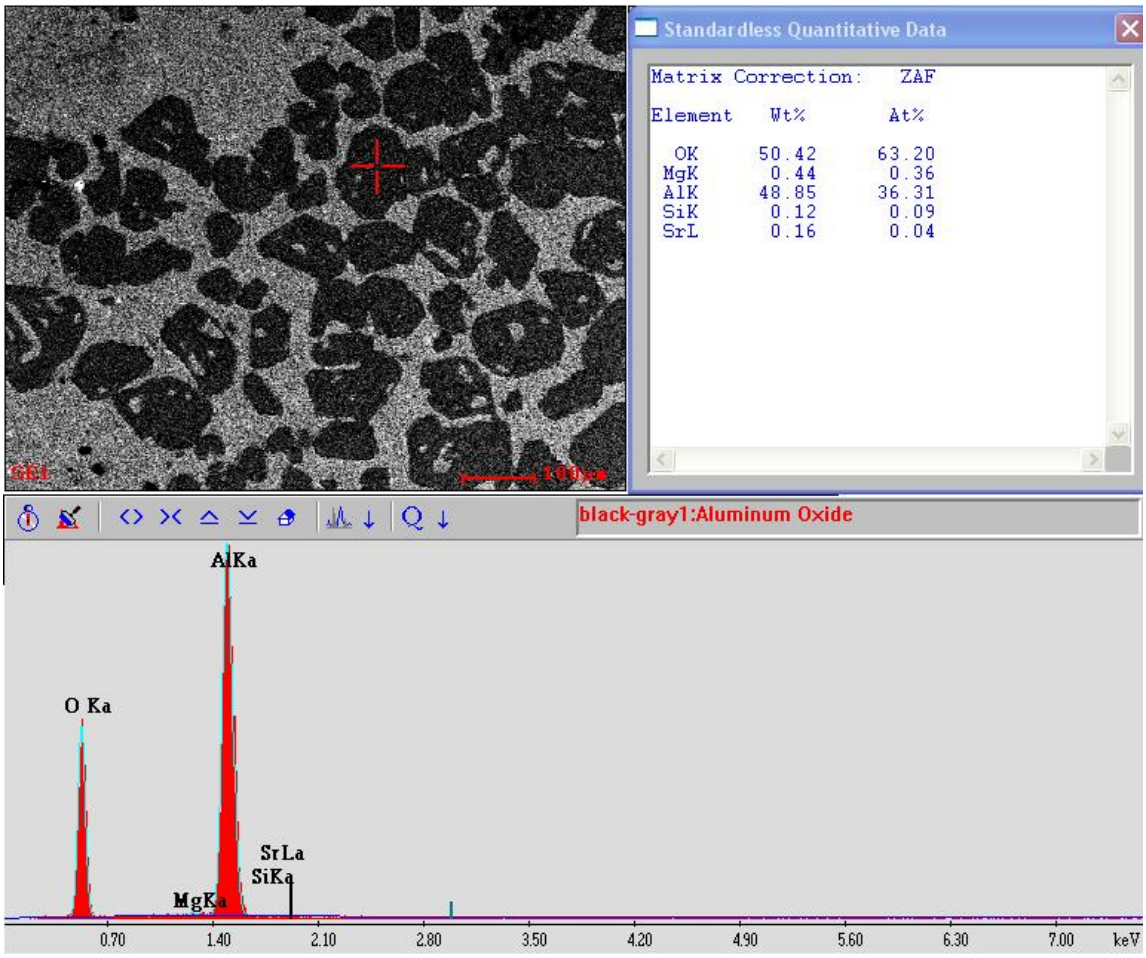

Figure 5.13. **EDS data on an SEM backscattered micrograph of $SrMgAl_{10}O_{17}$. Analysis of the darker region confirms that this is the ceramic phase, as the atomic ratio of Al to O is approximately 2 to 3. Silicon is a contaminant, and strontium and magnesium may or may not be oxidized.**

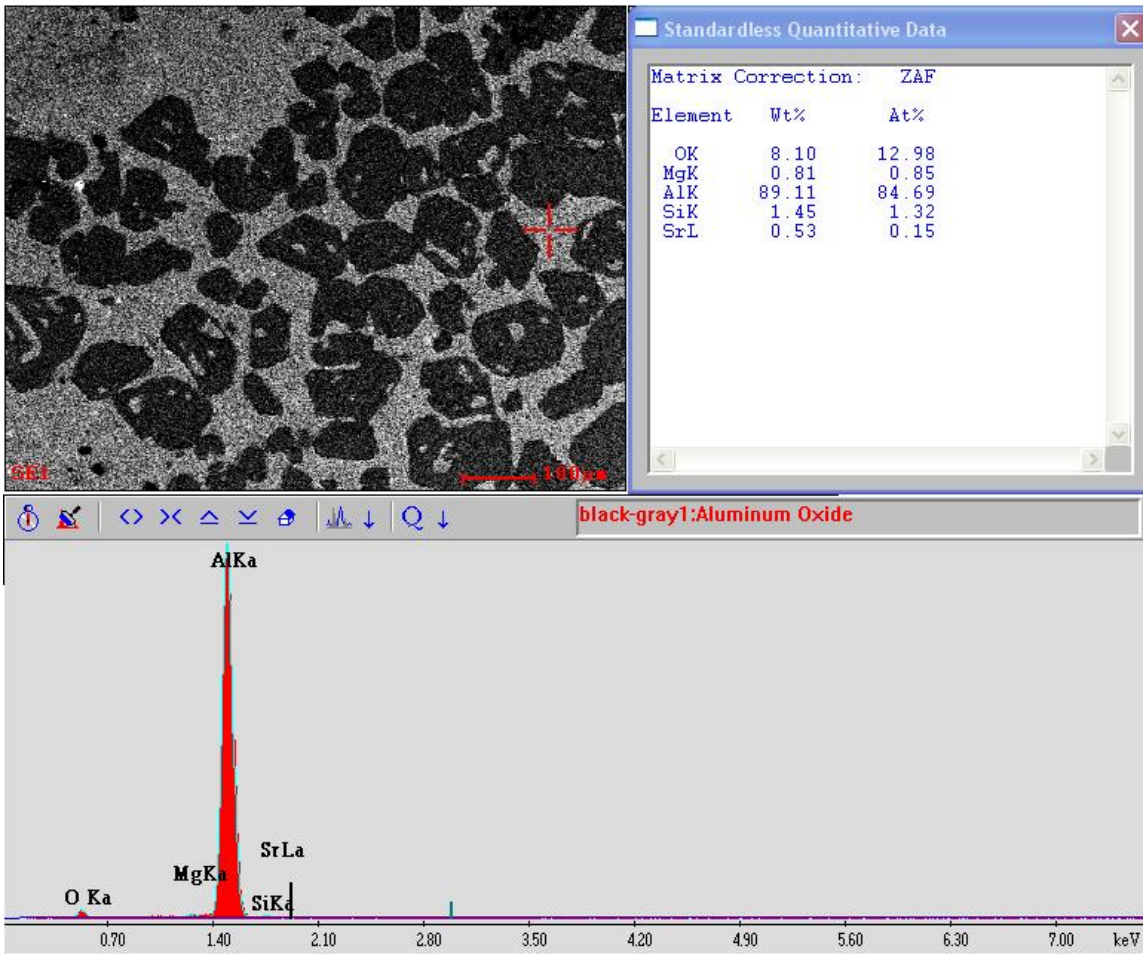

Figure 5.14. **EDS data on an SEM backscattered micrograph of $SrMgAl_{10}O_{17}$. Analysis of the lighter region confirms that this is the metal phase, containing mostly aluminum. Oxygen present is most likely due to a thin oxide layer forming on the surface. Silicon is a contaminant. It is unclear whether magnesium and strontium exist as metals or oxides.**

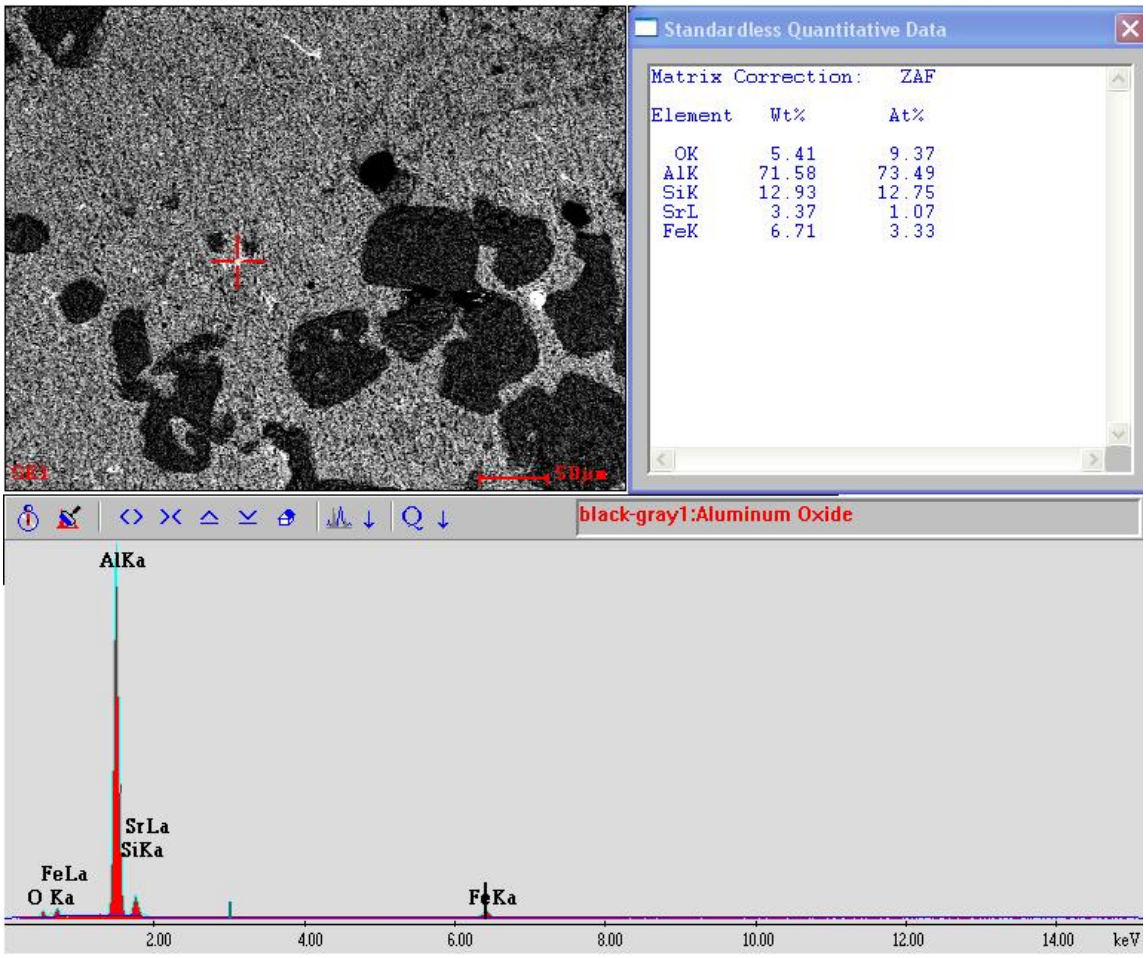

Figure 5.15. **EDS analysis of one of the many white spots found in backscattered mode, showing that these spots are simply iron or other metal contaminants.**

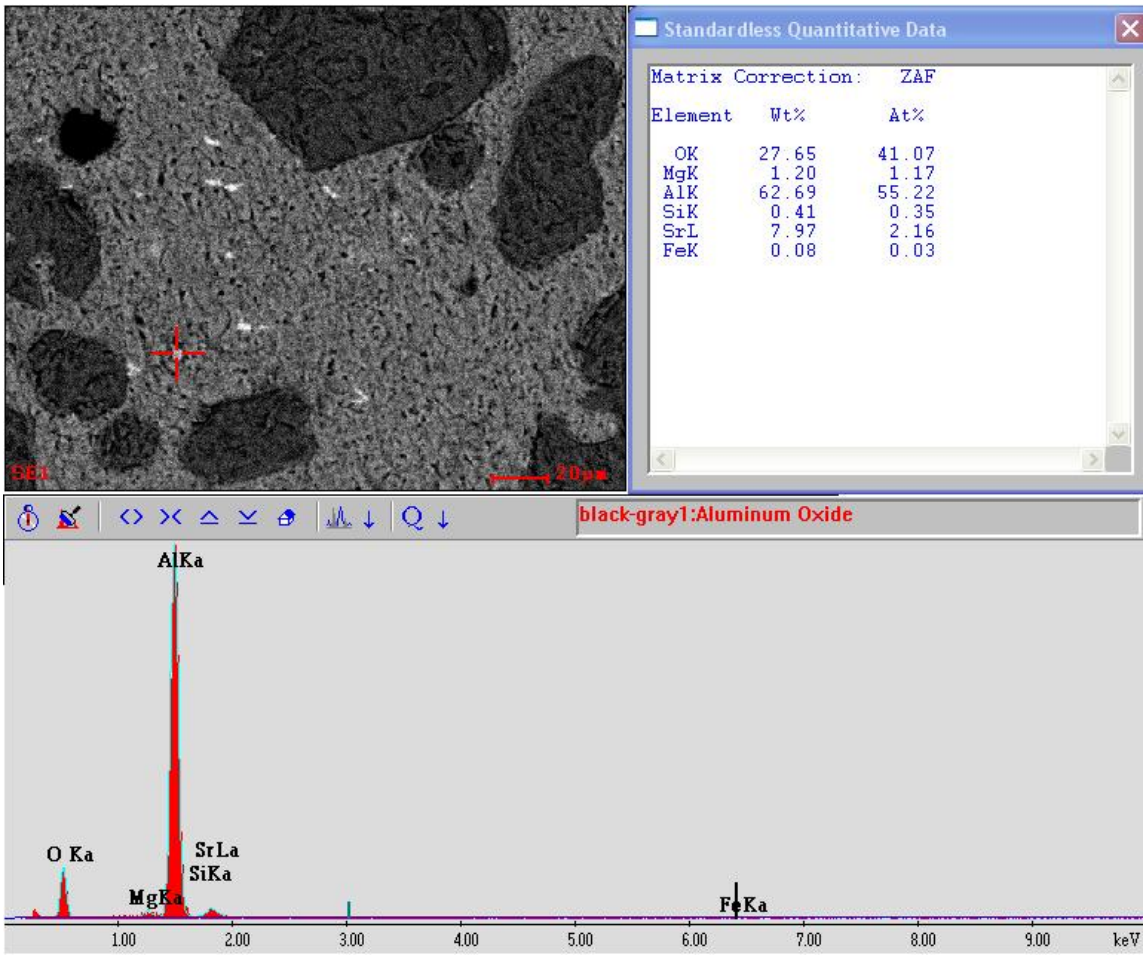

Figure 5.16. **EDS data on an SEM backscattered micrograph of $SrMgAl_{10}O_{17}$. Measured area is confirmed to be one of the few white areas that's brightness can be attributed to the presence of strontium, not a contaminant.**

From these results, we can determine that while only a very small portion of the samples of $SrMgAl_{10}O_{17}$ transformed, a transformation did indeed occur. This is verified by PXRD, where the identifiable phases present were corundum Al_2O_3, and metallic Al. No $SrMgAl_{10}O_{17}$ was identified via PXRD in the reacted portion of the pellet.

It is important to note that in all three of these samples, very little strontium or magnesium was found in the transformed regions. It was hypothesized that these elements would alloy with aluminum; however, they did not appear in appreciable

amounts in either the metallic or ceramic phases. It is possible that these elements simply diffused out of the sample into the Al bath during transformation, or were present in amounts too low to detect.

It is also clear from the SEM micrographs that a co-continuous composite was not formed. Instead, the micrographs were more similar to that of a composite continuous in only one phase, wherein particles of the ceramic Al_2O_3 phase are embedded in a continuous matrix of aluminum metal. Also, it is clear that a micro-scale composite was formed, as phases present are several tens to hundreds micrometers thick. However, this does not necessarily rule out the possibility of nano-scale features being present. It is possible that some nano-scale morphology exists, particularly at phase boundary regions, but these types of features would be undetectable with SEM, which cannot magnify greatly enough to examine nano-level morphology. TEM analysis would be required to definitively verify the presence or absence of any nanostructural features.

Finally, it should be noted that there may actually be applications in which a complete transformation is not necessary, and where only the outermost layer of the product is transformed with the inner core remaining a pure ceramic phase. For example, such an application may be one in which the inner surface of a container to be used for molten metal transfer is transformed as a cost effective protection layer against corrosion. Transformation of $SrMgAl_{10}O_{17}$ could therefore be useful in an application such as this.

B. $SrNiAl_{10}O_{17}$

1. TCON Transformation

Pellets of $SrNiAl_{10}O_{17}$ were given to Fireline TCON Inc., to react under TCON conditions with molten aluminum, with the hope of forming a ceramic/metallic composite material.

The resulting product was prepared for SEM and XRD analysis.

2. Characterization Results of the TCON Product

Unfortunately, a TCON transformation did not occur with the compound $SrNiAl_{10}O_{17}$. Upon examination of the pellets, excess molten aluminum that adhered to the pellet simply peeled or flaked off, revealing the underlying ceramic material. This ceramic material was analyzed by PXRD , in order to verify that the phase present was still that of the $SrNiAl_{10}O_{17}$ β-alumina phase. Figure 5.17 shows the for the PXRD pattern of the sample after attempted TCON transformation.

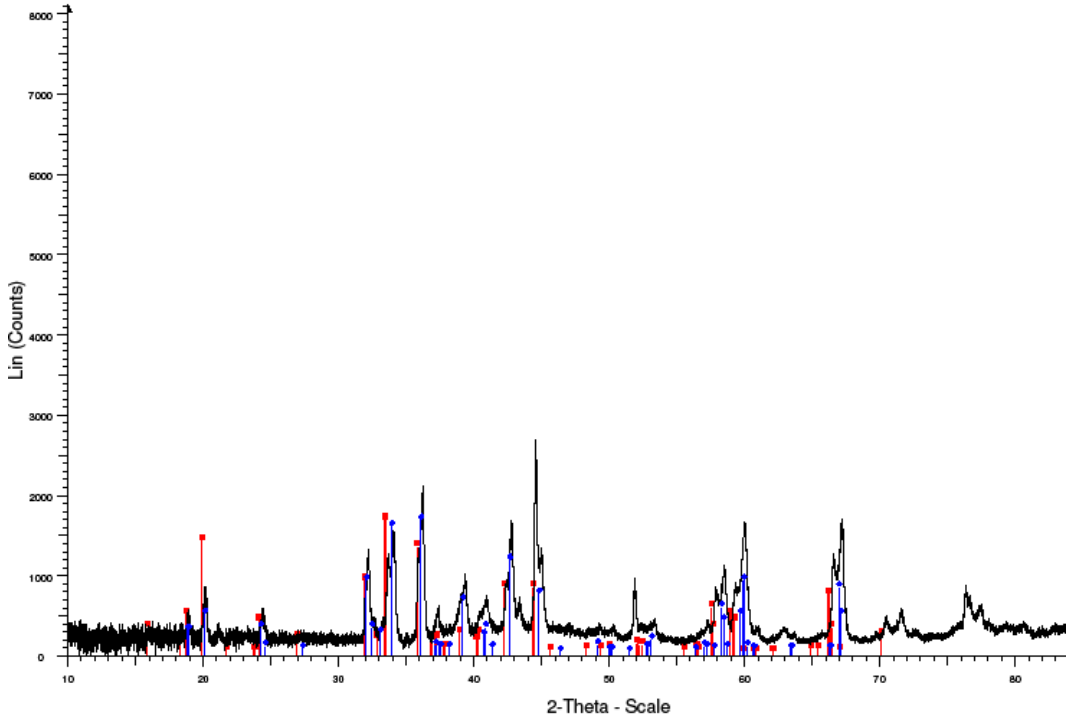

Figure 5.17. **Attempt at TCON transformation of $SrNiAl_{10}O_{17}$, which did not appear to transform. Red peaks indicate the β-alumina phase $SrNiAl_{10}O_{17}$ (PDF File of $SrMgAl_{10}O_{17}$ used, 04-010-0738) . Blue peaks indicate the magnetoplumbite phase, $SrAl_{12}O_{19}$. (PDF File 00-026-0976).**

Two possible phases were identified in the sample, one of which does appear to be the original β-alumina phase $SrNiAl_{10}O_{17}$. However, the more intense peaks seem to match up better with the magnetoplumbite phase, $SrAl_{12}O_{19}$. Thus, it appears that much of the β-alumina converted to magnetoplumbite-type structure during TCON transformation. It is not clear why this reaction occurred, as $SrNiAl_{10}O_{17}$ was confirmed by this research group to be stable at TCON temperatures. In any case, we can be sure that a TCON transformation did not occur, as PXRD confirms that neither corundum nor aluminum metal is present in the sample.

C. $TiMg_2O_4$

1. TCON Transformation

Pellets of $TiMg_2O_4$ were given to Fireline TCON Inc., to react under TCON conditions with molten aluminum, with the hope of forming a ceramic/metallic composite material.

The resulting product was prepared for SEM and XRD analysis.

2. Characterization Results of TCON Transformation

The transformation of $TiMg_2O_4$ pellets under TCON at first appeared to be a great success. A complete transformation of the pellets occurred, with little volume change of the pellets themselves. The SEM-prepared sample was analyzed via SEM as well as PXRD. Refer to Figure 5.18 for a PXRD pattern of the transformed sample, and to Figures 5.19 through 5.23 for SEM micrographs and EDS data of the sample. The X-ray powder pattern in Figure 5.18 as well as the SEM micrographs in Figures 5.19 – 5.21 clearly depict the presence of the ceramic and metal phase regions characteristic of TCON composites. Further verification is provided by the EDS data in Figures 5.22 and 5.23.

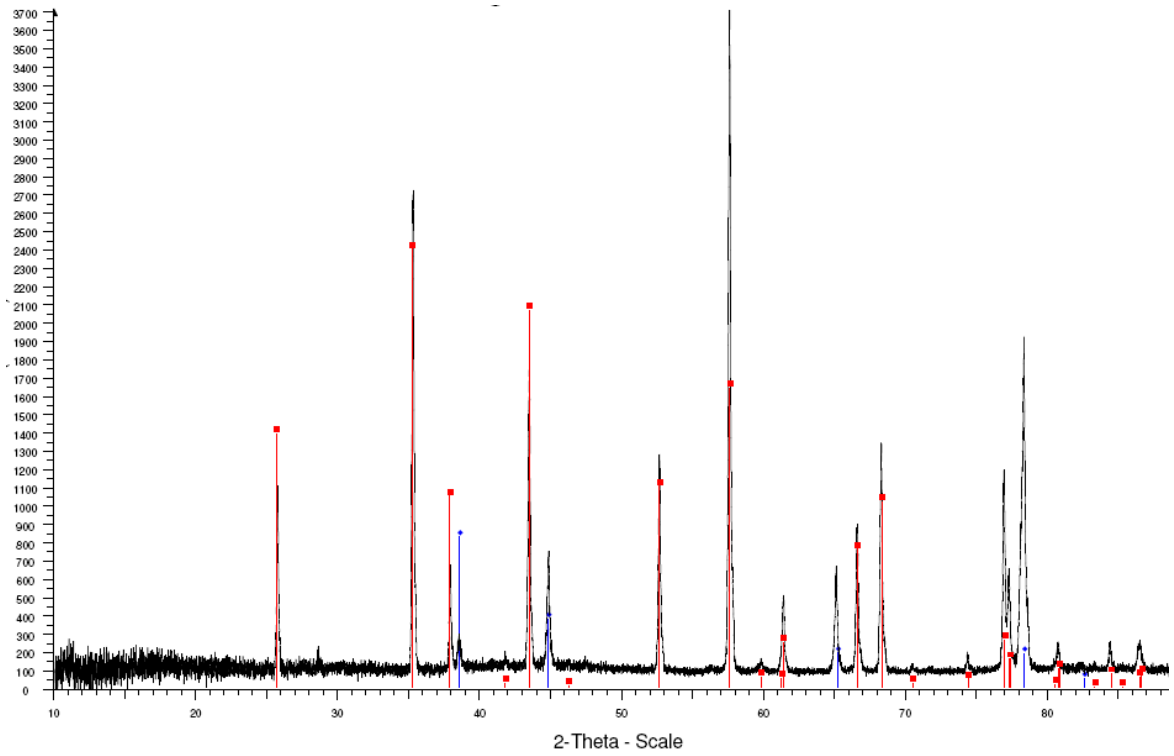

Figure 5.18. **PXRD pattern of TCON transformed $TiMg_2O_4$. Blue lines correspond to Al metal (PDF File 00-001-1180), red lines correspond to corundum, Al_2O_3, (PDF File 00-043-1484).**

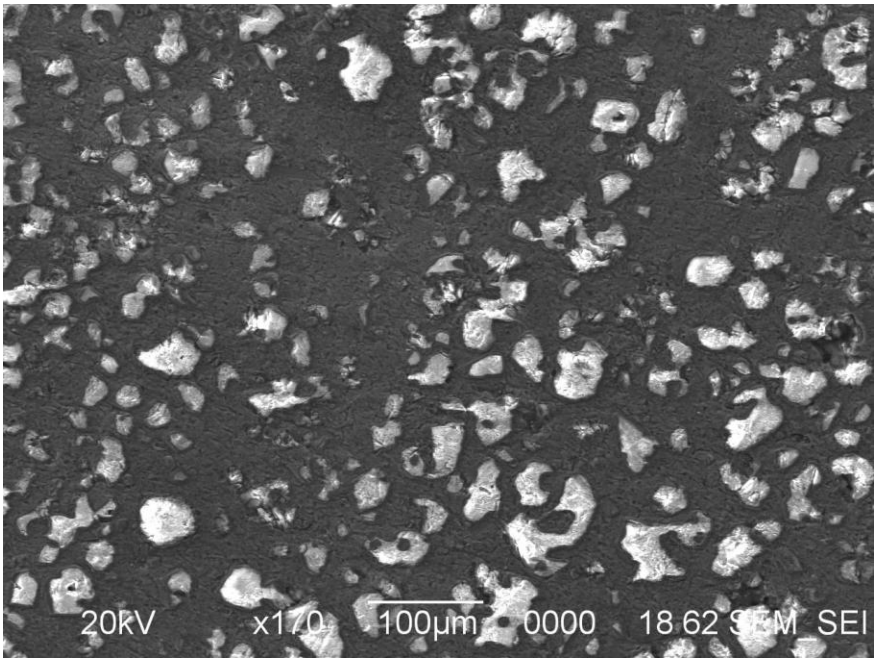

Figure 5.19. **SEM micrograph of TCON transformed $TiMg_2O_4$ Sample 9, shown at x170 magnification. Lighter areas are the ceramic phase, darker areas are the metallic phase.**

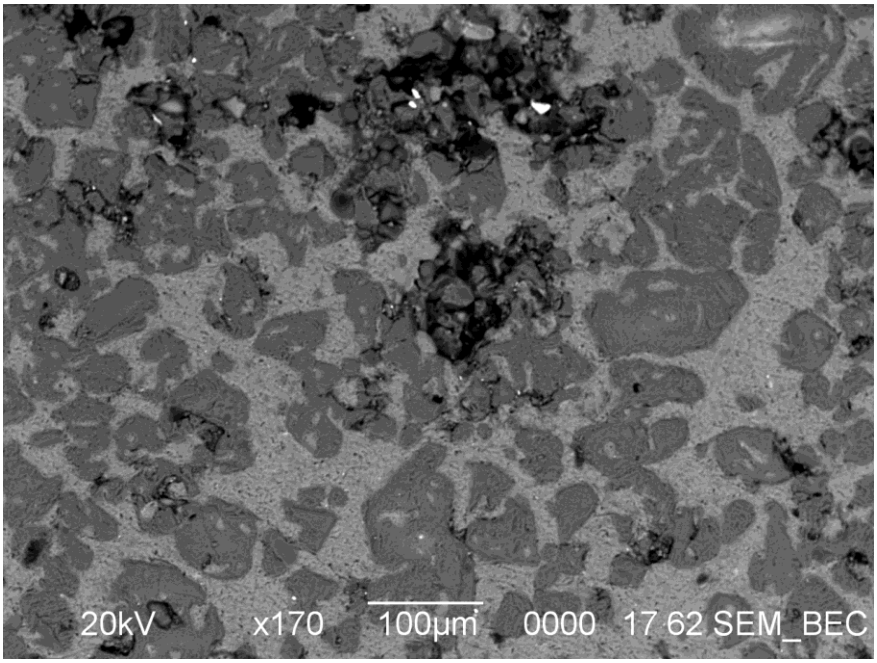

***Figure 5.20*. SEM Backscattered micrograph of TCON transformed $TiMg_2O_4$ Sample 9, shown at x170 magnification. Lighter areas are the metal phase, darker areas are the ceramic phase. White specks are contamination, black areas are voids in the structure.**

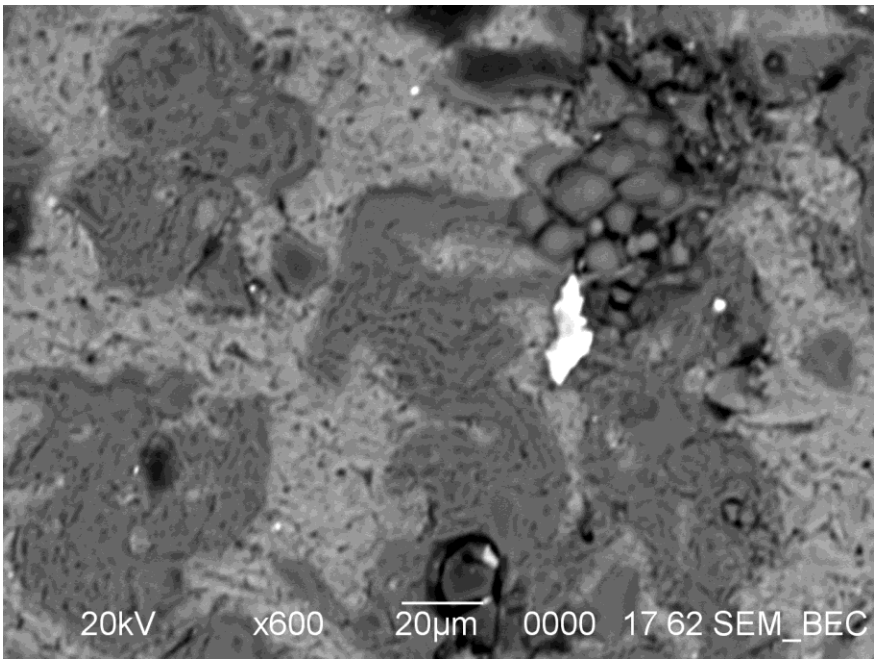

***Figure 5.21*. SEM Backscattered micrograph of TCON transformed $TiMg_2O_4$ Sample 9, shown at x600 magnification. Lighter areas are the metal phase, darker areas are the ceramic phase. White specks are contamination, black areas are voids in the structure.**

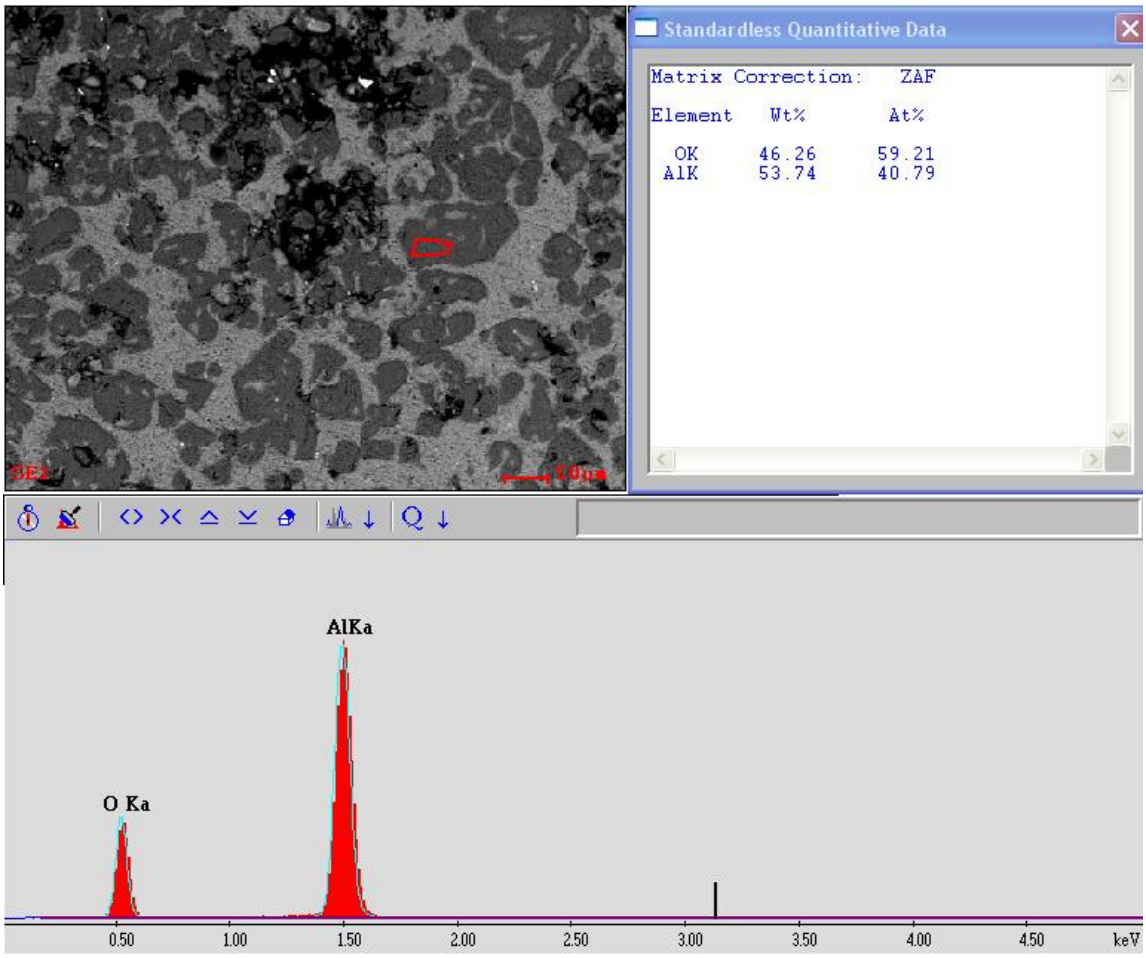

Figure 5.22. **EDS micrograph of TCON transformed $TiMg_2O_4$ Sample 9, displaying fluorescence peaks and elemental abundance. The red outline indicates the portion of the micrograph that was measured. Elemental abundance confirms that this is indeed the ceramic phase, since the atomic molar percentage of Al_2O_3 should be 40% Al, 60% O.**

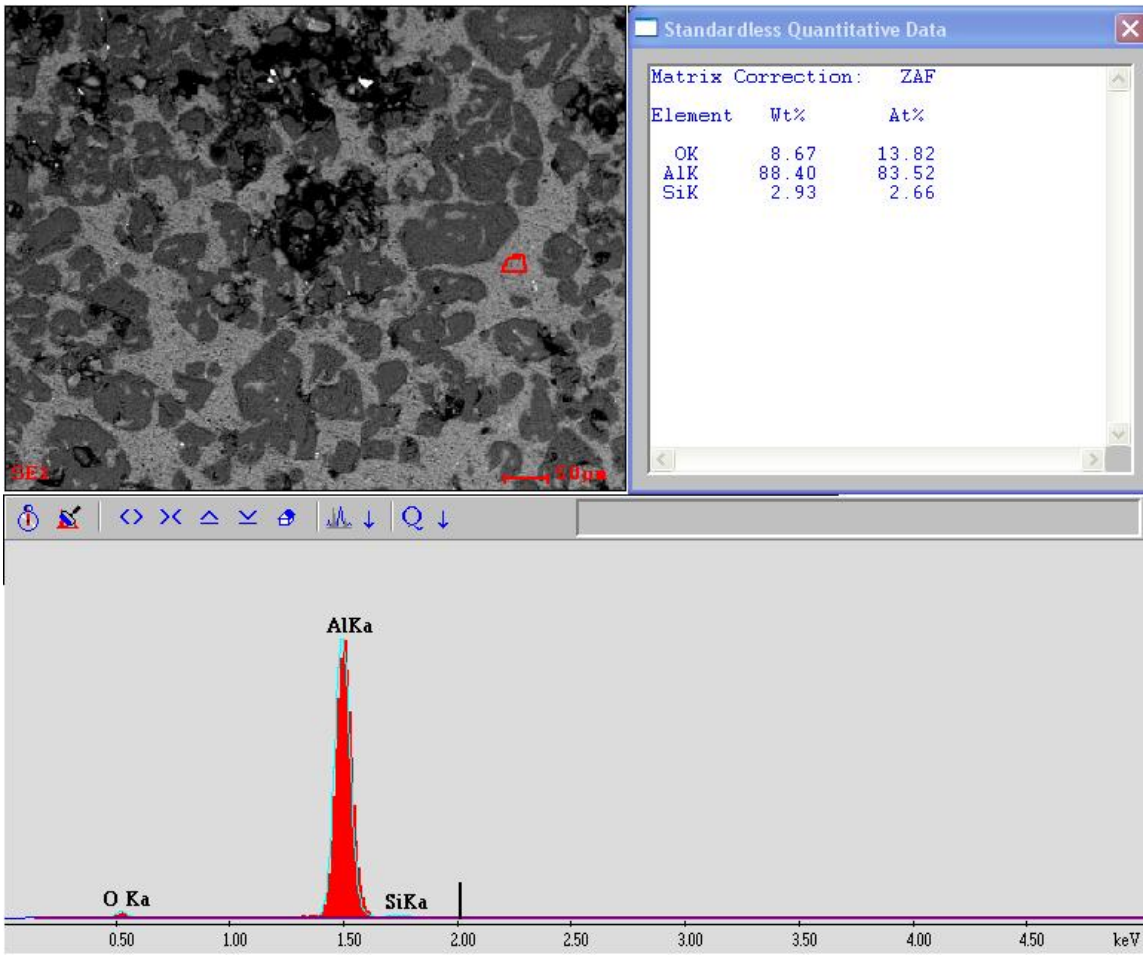

Figure 5.23. **EDS micrograph of TCON transformed $TiMg_2O_4$ Sample 9, displaying fluorescence peaks and elemental abundance. The red outline indicates the portion of the micrograph that was measured. This confirms that the lighter area is the metal phase, as it should be mostly aluminum and other metals. The small amount of oxygen measured can be attributed either to a thin oxide film forming on the surface of the aluminum metal, or to a layer of aluminum oxide just below the surface of the sample, since EDS penetrates the sample to a certain degree, measuring more than what is visible. The presence of silicon can be attributed to contamination.**

Despite successful transformation of the $TiMg_2O_4$ precursor to a ceramic-metallic TCON composite as depicted in the data above for Sample 9, the results are somewhat puzzling in the sense that there seems to be virtually no titanium or magnesium present in the TCON product. Theoretically, a transformation of this material would follow the chemical reaction shown in Equation 5.1, in which molten aluminum reacts with

$TiMg_2O_4$ to produce aluminum oxide and aluminum metal, and the reduced Ti and Mg remain in the sample as part of an Al-Ti-Mg alloy system;

$$3\ TiMg_2O_4 + (8 + x)\ Al \rightarrow 4\ Al_2O_3 + (\ x\ )Al_{(Ti,\ Mg)}$$

Equation 5.1

Aluminum metal is definitely present, and aluminum oxide is present in the form of corundum, which was verified via powder XRD; however, no evidence of titanium or magnesium was found. Heavier elements such as titanium are easily found in SEM backscattering mode, since heavy atoms appear whiter; however, every light spot on the micrograph was found to be iron or copper, and can be attributed to contamination of the sample from the tools used to prepare the SEM sample. No titanium or magnesium was found when using EDS. No titanium or magnesium containing phases were identified via powder XRD, and no titanium or magnesium was found when the sample was analyzed via XRF.

One possible explanation for this result is simply that all of the titanium and magnesium diffused out of the sample and into the surrounding molten Al while in the TCON furnace. If this had been the case, the concentration of Ti and Mg metals in the molten bath would be too small to detect by the available methods listed above. In order to further investigate this possible diffusion of displaced metals into the molten Al, a TCON-like reaction on a laboratory scale is required. Dispersion of the Ti and Mg atoms into a much smaller quantity of originally pure Al should ensure their detection via XRF or EDS techniques. Alternatively, a shorter reaction time or larger sample size may serve to somewhat better control diffusion.

D. $NiAl_2O_4$

1. TCON Transformation

Pellets of $NiAl_2O_4$ were given to Fireline TCON Inc., to react under TCON conditions with molten aluminum, with the hope of forming a ceramic/metallic composite material.

The resulting product was prepared for SEM and XRD analysis.

2. Characterization Results of TCON Product

While reactive metal penetration has been studied with $NiAl_2O_4$ as the sacrificial oxide in the past, this compound was still transformed via TCON conditions for several reasons. First, transformation of this compound will yield good data on the morphology of a typical TCON transformation of a spinel-like compound. Actual spinel itself, $MgAl_2O_4$, is not thermodynamically suitable for reaction under TCON conditions, so other spinels must be transformed. Second, transformation of $NiAl_2O_4$ will be a good comparison to transformation of $SrNiAl_{10}O_{17}$. Finally, as the TCON process of reactive metal penetration is unique, transformation of this compound via TCON conditions may actually yield different results from those previously reported.

$NiAl_2O_4$ was reacted under standard TCON conditions. Refer to Figure 5.24 for a PXRD pattern of the transformed pellet, revealing the corundum and aluminum metal

phases to be present. Figures 5.25 through 5.27 then show SEM and EDS micrographs of transformed $NiAl_2O_4$.

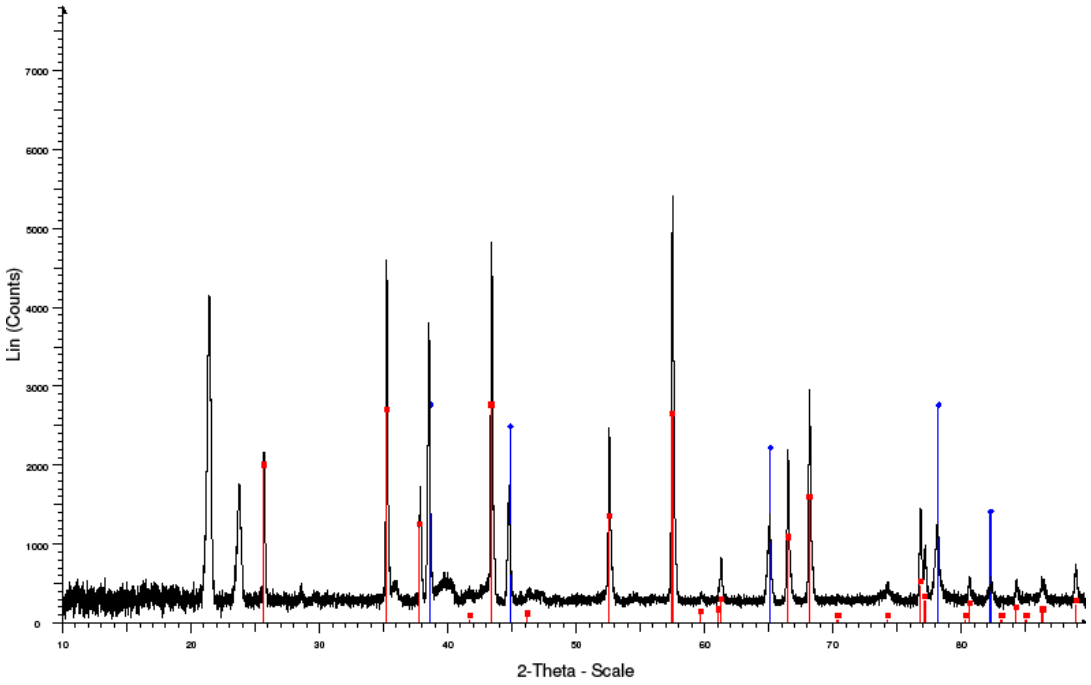

Figure 5.24. **PXRD pattern of TCON transformed $NiAl_2O_4$. The two identifiable phases present are corundum (PDF File 00-043-1484) and aluminum metal (PDF File 00-001-1180).**

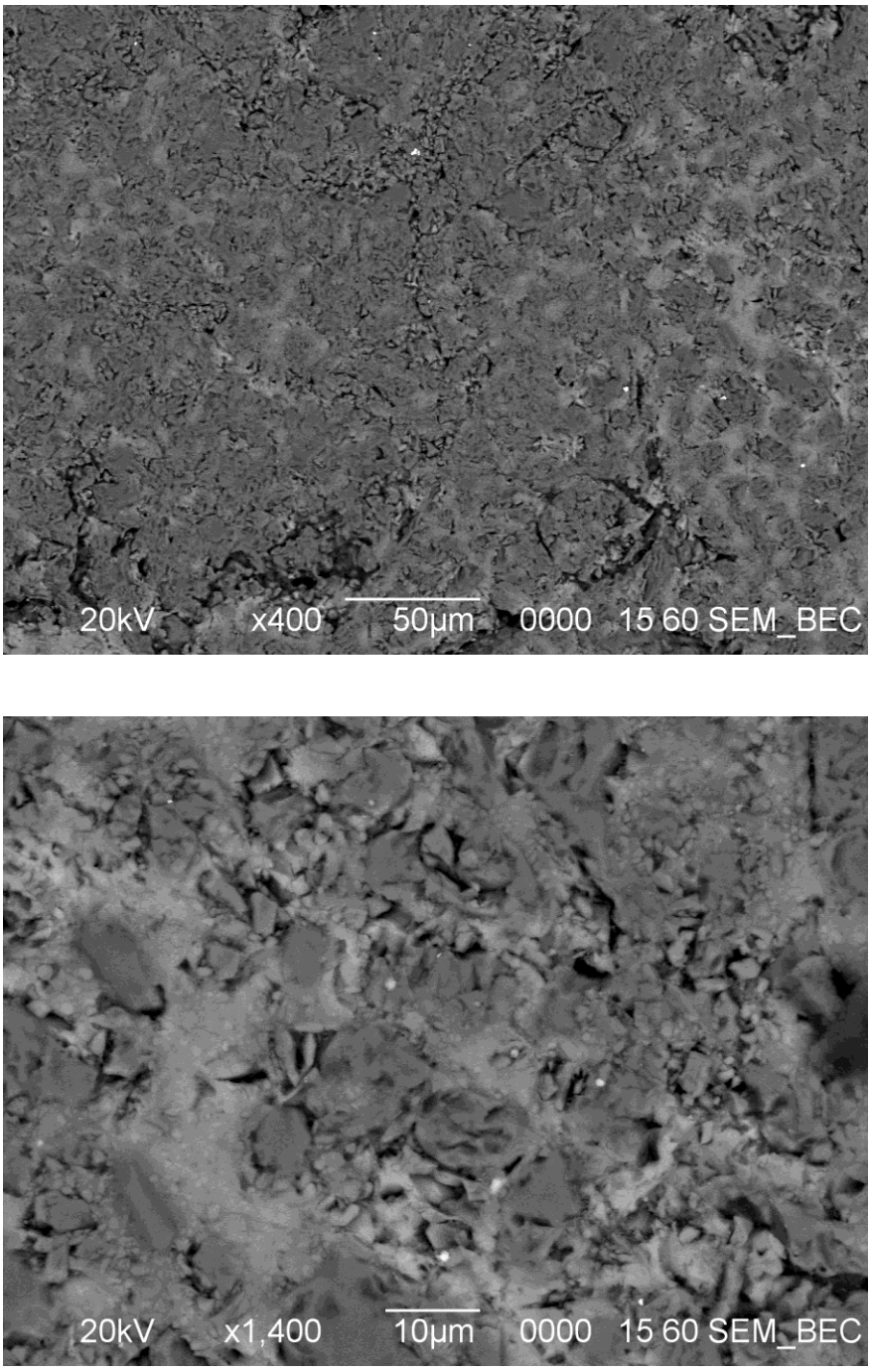

***Figure 5.25a (top) and 5.25b (bottom)*. SEM backscattered micrograph of transformed $NiAl_2O_4$. Lighter areas are aluminum, darker grey areas are aluminum oxide. Black areas are voids. White specks are likely impurities from cutting tools, or nickel (see text). Images were taken at magnifications of x400 (a) and x1400 (b).**

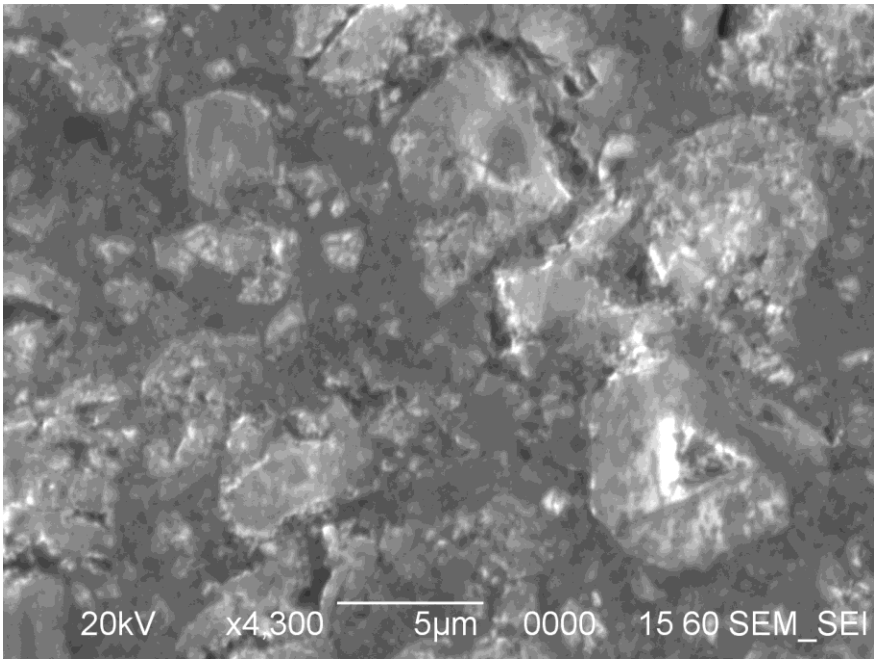

***Figure 5.26*. SEM secondary electron micrograph of transformed $NiAl_2O_4$, shown at x4300 magnification. Slightly darker areas are aluminum metal, lighter, blockier areas are the ceramic phase.**

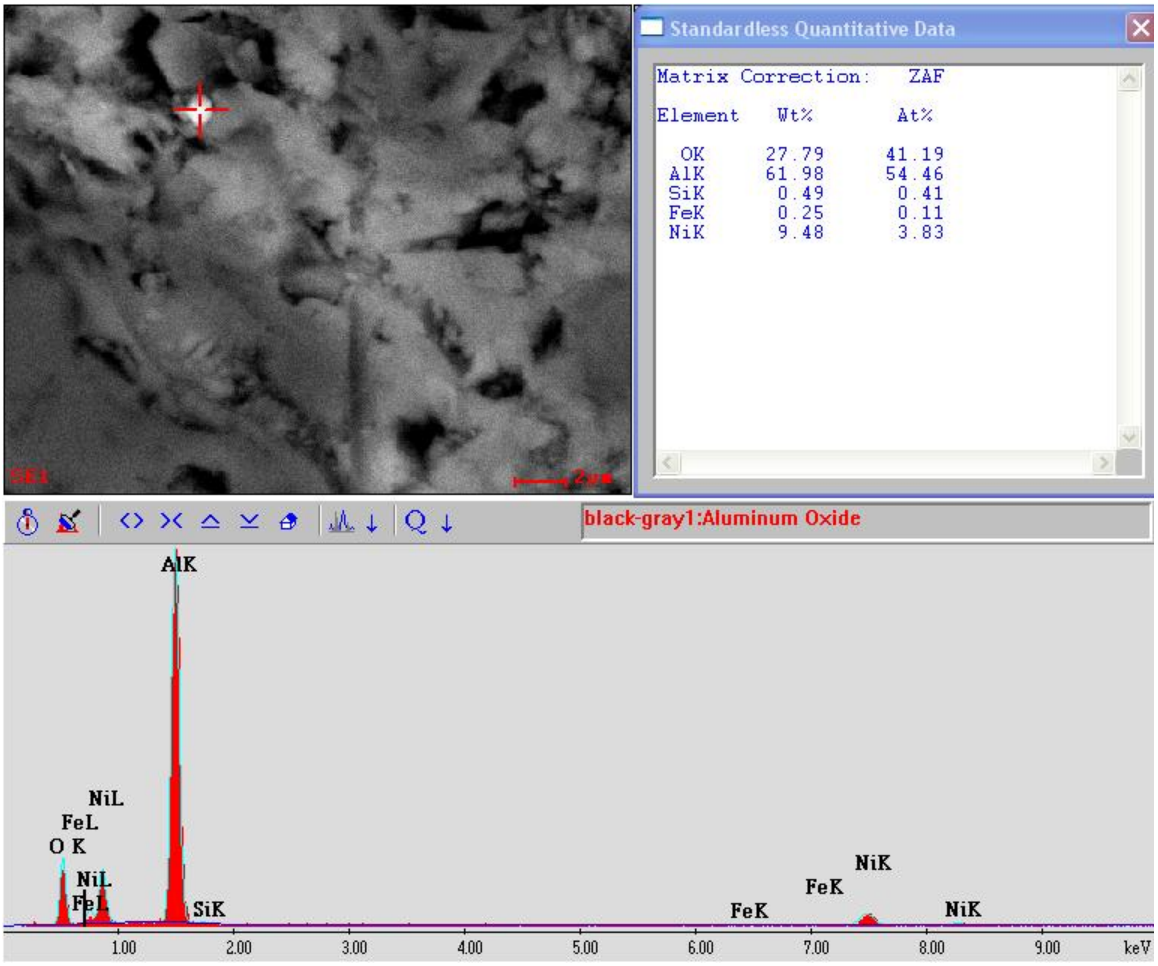

Figure 5.27. **EDS data measuring a light spot on transformed $NiAl_2O_4$, confirming presence of nickel. Iron was also measured, to confirm that the spot isn't just an artifact from cutting with a steel blade.**

SEM micrographs of transformed $NiAl_2O_4$ display a co-continuous morphology between the two phases present, aluminum oxide and aluminum metal. Phase boundaries are often only tens of micrometers apart, which is similar to results found in traditional TCON materials wherein silica is transformed. This is especially evident in Figure 5.25. However, transformed $NiAl_2O_4$ also has the issue of only small quantities of nickel being present after transformation. While there is indeed some nickel present, there isn't nearly as much as would be expected. Nickel is only found in appreciable amounts in tiny

clusters of about a micrometer or so in diameter, and only at around 3-4 percent atomic abundance. In the above backscattered micrographs, more than half of the white specks found are actually iron, not nickel. This is due to iron fragments being imbedded in the sample from grinding and cutting during SEM sample preparation. It is possible that nickel simply diffused out of the sample during transformation, much like titanium and magnesium appeared to have done in transformed $TiMg_2O_4$. Future studies can be done here as well where $NiAl_2O_4$ is transformed in a minimal amount of molten aluminum.

It is important to note, however, that while PXRD revealed that the two main phases present are corundum and aluminum metal, two large unidentifiable peaks are observed at relatively small 2θ values in the pattern. SEM and EDS confirm that there are indeed distinct phases of aluminum metal and some form of Al_2O_3 present, but these peaks do not belong to other phases. We were unable to identify any obvious phase that accounts for these peaks, although it is possible that they represent an undetected Ni-containing phase.

Also, the sample was revealed to be quite porous. Porosity is an undesirable trait when studying the morphology of TCON samples, and is usually due to porosity of sacrificial oxides. This can be avoided in the future by regrinding and resintering the sacrificial oxide, in order to produce a denser, less porous product.

Finally, it should be noted that transformed $NiAl_2O_4$ experienced significant volume reduction when compared to the original volume of the sacrificial pellets, despite the voids still present in the transformed material. One of the main advantages of the standard TCON process of transforming silica is that little to no volume reduction is

noted between sacrificial oxide and produced pellets. This is a highly desirable trait for the manufacture of TCON objects, and may result in production issues if this process would be altered to accommodate $NiAl_2O_4$. Further studies can be done to see if this volume reduction is avoidable, as a densified pellet may not undergo the same volume reduction.

CHAPTER VI – CONCLUSION

Overall, this research has yielded rather positive results. Despite the fact that $MgAl_2O_4$ does not transform via TCON-like reactions according to the literature, $SrMgAl_{10}O_{17}$ was at least partially TCON transformed, yielding a mixed phase of aluminum metal and corundum. However, with isolated regions of corundum embedded in an Al matrix, the transformed regions of these samples appeared to be more like a traditional composite material, in which only one phase is continuous. This is unlike the case for TCON composites, in which the phases are co-continuous. While no evidence of nano-scale features was found so far, further analysis must be performed via TEM, as SEM is not capable of nano-level magnification. Another issue with this transformation is that strontium and magnesium were present in very minute amounts, somewhat less than expected.

Thus the results for the first transformation of a β-alumina phase via the TCON process did not match our hypothesis. It was predicted that the open channels within the β-alumina-type structure would facilitate the mobility of molten Al into the lattice, where Sr^{2+} and Mg^{2+} would be displaced, and the aluminum oxide phase of the spinel blocks would be transformed to corundum. We further hypothesized that the nano-scale features of the β-alumina lattice would be reflected in the composite microstructure, and so we were at first somewhat surprised to find that the composite consisted of the relatively large "islands" of Al_2O_3 embedded in a matrix of Al. In hindsight, however, this could be related to the fact that using a $SrMgAl_{10}O_{17}$ precursor involves more of a phase transformation from the aluminum oxide phase of the spinel blocks, rather than a

reductive metal displacement process that occurs in the typical TCON reaction with SiO_2, for example. Thus, since the Al_2O_3 phase essentially grows continuously as the Al diffuses into the sample in the typical TCON reaction, for this case there is no mechanism for continual growth during the process. Finally, it must be noted that the possibility of some nano-structural features in the material cannot be ruled out until TEM analysis can be completed, as SEM does not possess the magnification capability to confirm or deny the presence of these nano-scale features.

The use of $TiMg_2O_4$ as a sacrificial oxide yielded positive results in that a transformation occurred. This compound was confirmed to react completely to form a composite of aluminum metal and corundum. The resulting morphology between the two phases appears to possibly be co-continuous in nature (see Figure 5.34). The only problem with this transformation was that titanium and magnesium were not found in the finished product, and further studies are planned to first find out whether or not these metals diffused into the melt, and second to alter reaction conditions (e.g. reaction time) to attempt to alloy Ti and Mg with the metal phase in the composite.

The use of $NiAl_2O_4$ as a sacrificial oxide also yielded very positive results. This compound was confirmed to react completely to form a composite of aluminum metal and corundum. The resulting morphology between the two phases was almost certainly co-continuous in nature. As with other sacrificial oxides; however, nickel was not found in appreciable amounts throughout the sample, and perhaps diffused into the melt.

The synthesis of $SrTi_5Mg_6O_{17}$ has yielded disappointing results so far. In both reaction schemes attempted, none of the target compound was produced. However,

alternate reaction paths can be attempted, which could yield more positive results. And of course, attempts to synthesize this compound have not been completely in vain, as precursors such as $TiMg_2O_4$ which are produced along the way can be transformed as well.

The synthesis of $SrNiAl_{10}O_{17}$ yielded immediate, positive results. Because of the ease of synthesis of this compound via urea combustion as a source of heat energy to drive the reaction, it is probable that other, similar β-alumina compounds may be synthesized in the same fashion. Compounds with the formula $SrMAl_{10}O_{17}$, where M is a transition element such as Fe^{2+}, Co^{2+}, Cu^{2+}, or Mn^{2+} may very well be possible. If so, these compounds could have beneficial effects on TCON composites if used as sacrificial oxides, especially if the M^{2+} ions can be incorporated into the TCON composite's metal phase upon reduction.

It is interesting that $SrNiAl_{10}O_{17}$ did not transform via the TCON process, despite the fact that $NiAl_2O_4$ did so easily. Perhaps the $SrNiAl_{10}O_{17}$ phase is relatively too stable thermodynamically for the TCON process to occur, so that instead all that occurs is a partial phase transformation to magnetoplumbite-type $SrAl_{12}O_{19}$, which is energetically very similar to the β-alumina-type $SrNiAl_{10}O_{17}$ phase.

CHAPTER VI – FUTURE WORK

In a research project such as the one described herein, there is a nearly unlimited potential for studies that could be done in the future. Most obviously, perhaps, is the fact that so many different oxides can be reacted under TCON conditions. Because this research focused primarily on the TCON transformation of β-alumina type compounds, other β-aluminas can be produced in the lab and exposed to TCON transformation.

It is possible to even further broaden the range of β-alumina compounds that can be used in this process by replacing an O^{2-} anion with an N^{3-} anion. This allows for more variety when choosing cations to be used to these compounds, since an additional +1 charge can be compensated for by the presence of nitrogen. Compounds such as $SrAl_{11}O_{16}N$ are possible (31), as well as novel compounds which have not yet been studied. In addition, compounds similar to β-aluminas can be produced and transformed, such as magnetoplumbites, which also have channel-like structures. These compounds could therefore possibly have some of the beneficial properties that β-alumina compounds are theorized to display when transformed.

Because ion-exchange is such an excellent platform for producing a wide variety of β-aluminas from $NaAl_{11}O_{17}$, a number of other β-aluminas could be produced in this way, and TCON transformed to yield interesting aluminum alloys in the metal phase. Also, the process of creating $NaAl_{11}O_{17}$ itself can be improved upon, as the samples created throughout the course of this research were only 92% pure by mass at best. It is

probable that by altering reaction conditions and stoichiometric ratios of reagents, a higher level of purity can be obtained.

Further studies can be done on the TCON transformation of $LiAl_{11}O_{17}$, specifically, how much $LiAl_{11}O_{17}$ actually remains in the sample directly before transformation, as Li β-alumina is unstable at high temperatures and converts to $LiAl_5O_8$. For that matter, Youngstown State University will soon be receiving its own lab-scale TCON-type furnace, with which we will have complete control over reaction conditions such as temperature. Therefore, in the future we will be able to react Li β-alumina with molten aluminum at temperatures at which the compound is more stable.

Further studies can also be done on the synthesis of the novel β-alumina compound $SrTi_5Mg_6O_{17}$. Several alternative reactions have been proposed that may have more success than those already attempted. Another benefit to pursuing the synthesis of this compound is that all precursors produced can also be exposed to TCON transformation, much like $TiMg_2O_4$ has been. $TiMgO_3$ and Ti_2MgO_5, two other compounds in the Ti-Mg-O system could also act as excellent sacrificial oxides, possibly allowing for titanium and magnesium to alloy with aluminum in the metal phase.

A common problem that occurred throughout the course of this research is that metal elements involved in the sacrificial oxide compounds were not actually observed in appreciable amounts, if at all, in the finished TCON product. This was observed in $SrMgAl_{10}O_{17}$, $TiMg_2O_4$, and $NiAl_2O_4$. Theoretically, these elements should exist in the metal phase along with aluminum; however, they were either found in too small quantities, or not at all. This is most likely due to these elements simply diffusing out of

the sample during transformation, and dissolving into the excess molten aluminum in the furnace. Because one of the primary reasons that these compounds were chosen for transformation in the first place is due to the potential to form useful alloys with aluminum, this is very undesirable. Therefore, it will be necessary to study these reactions further, and to try to find ways to retain more of these elements in the produced TCON pellets. This may not be difficult, as it could simply involve use of a minimal amount of molten aluminum in the reaction, or shorter reaction times. Also, the excess aluminum itself can be tested for presence of these elements.

References

1. **Douglas, B., McDaniel, D. and Alexander, J.** *Concepts and Models of Inorganic Chemistry.* s.l. : Malloy Lithographing, Inc., 1994.

2. **Wagner, Tim.** Synthesis, Characterization, and Applications of Mixed-Anion Inorganic Materials. Youngstown, OH : s.n., September 2009.

3. *Criteria for Formation of Interpenetrating Oxide/Metal - Composites by Immersing Sacrificial Oxide Preforms in Molten Metals.* **W. Liu, U. Koster.** 1996, Scripta Materialia, pp. Vol. 35, No. 1, pp 35 - 40.

4. **Budworth, D.W.** *An Introduction to Ceramic Science.* s.l. : Pergamon Press, 1970.

5. *Structure of Spinels.* **Sickafus, K. and Wills, J.** 1999, Journal of the American Ceramic Society, pp. Volume 82, pages 3279 - 3292.

6. *The Crystal Structure of Na2O*MgO*5Al2O3 with Reference to Na2O*5Al2O3 and other Isotypal Compounds.* **Bettman, M. and Peters, C.R.** 1969, Journal of Physical Chemistry, pp. 1774-1780.

7. *Crystal Chemistry of Hexaaluminates; β-Alumina and Magnetoplumbites.* **Iyi, N., Takekawa, S. and Kimura, S.** 1989, Journal of Solid State Chemistry, pp. Volume 83, pages 8-19.

8. *Advanced materials for sodium-beta alumina batteries; Status, challenges, and perspectives.* **Lu, Xiaochuan, et al.** s.l. : Journal of Power Sources, 2010, Vol. 195, pp. 2431 - 2442.

9. *The Metals Red Book; Nonferrous Metals, 2nd Ed.* **Bringas, John and Wayman, Michael.** s.l. : CASTI publishing, June 1998.

10. *Lithium Aluminum Alloys - The New Generation Aerospace Alloys.* **Joshi, Amit.** Bombay : Mechanical Engineering Department, Indian Institute of Technology.

11. *Effect of Titanium on the Structure and Properties of Aluminum.* **Parkhutik, P.A. and Lubenskii, M.Z.** 1967, Metal Science and Heat Treatment, Vol. 9, pp. 940-942.

12. *Effects of Strontium on the Structure and Properties of Aluminum-Silicon Alloys.* **Haque, M.M.** 1994, Journal of Materials Processing Technology, Vol. 55, pp. 193-198.

13. **Noordegraaf, Jan, Krahmer, Piet and Donnelly, Martin.** *Aluminum-Strontium Master Alloy and the Process of Making the Alloy. 5,205,986* United States, April 27, 1993.

14. *Wrought Aluminum-Nickel Alloys for High-Strength, High-Conductivity Applications.* **Rohatgi, P.K. and Prabhakar, K.V.** 5, s.l. : Metallurgical and Materials , 1975, Vol. 6.

15. **Holliday, Leslie (editor).** *Composite Materials, Elsevier Materials Science Series.* s.l. : Elsevier Publishing Company, 1966.

16. *The Sol-Gel Process.* **Hench, Larry and West, Jon.** 1, 1990, Chemical Reviews, Vol. 90, pp. 33-72.

17. **Skoog, D., Holler, F. and Nieman, T.** *Principles of Instrumental Analysis.* s.l. : Saunders College Publishing, 1998.

18. *X-ray Diffraction from a Crystal Lattice.* **Shlotz, Reinhold.** s.l. : Bruker-AXS, 2006.

19. *Investigation of Novel Routes in the Synthesis of TiNF and Compounds in the Ti-N-O-F System.* **Ngendahimana, Aimable.** Youngstown, OH : Youngstown State University, 2010.

20. *Crystal Structure of the New Magnetoplumbite-Related Compound in the system SrO - Al2O3 - MgO.* **Iyi, Nobuo and Gobbels, Matthias.** 1996, Journal of Solid State Chemistry, Vol. 122, pp. 46-52.

21. *Preparation of Lithium B" Alumina by the Ion-Exchange Reaction.* **V. Jayaraman, G. Periaswami, T.R.N. Kutty.** 1999, Materials Research Bullitin, pp. 1811-1820.

22. *Gel to Crystallite conversion technique for the syntheses of M-B/B"-Alumina.* **V. Jayaraman, G. Periaswami, T.R.N. Kutty.** 2008, Materials Research Bulletin, pp. 2527-2537.

23. *Preparation of beta-alumina powder from kaolin-derived aluminium sulphate solution.* **Kang, H.K., Park, H.C. and Kim, K.H.** 1996, Journal of Materials Science, Vol. Materials in Electronics 7, pp. 385-389.

24. **Wells, A.F.** *Structural Inorganic Chemistry.* s.l. : Clarendon Press, 1975.

25. **Shriver, Duward.** *Inorganic Synthesis, Volume XIX.* New York : Wiley, 1979.

26. *Preparation of Lithium B"-Alumina by the Ion-Exchange Reaction.* **Jayaraman, V., Periaswami, G. and Kutty, T.R.N.** 12, s.l. : Materials Research Bullitin, 1998, Vol. 33, pp. 1811-1820.

27. *Progress in Solid State Chemistry.* **Kummer, J.T.** 1972, Vol. 7, pp. 141 - 175.

28. *Formation of Structural Intermetallics by Reactive Metal Penetration of Ti and Ni Oxides and Aluminates.* **Fahrenholtz, William, et al.** s.l. : Metallurgical and Materials Transactions, 1996, Vol. 27A.

29. *Preparation, Characterization, and methane total oxidation of AAl12O19 and AMAl11O19 hexaaluminate catalysts prepared by the urea combustion method.* **Yin, Fengxiang, et al.** s.l. : Journal of Molecular Catalysis, 2008, Vol. 294, pp. 27-36.

30. *Conversion of 2-octanol over nickel-alumina, cobalt-alumina, and alumina catalysts.* **Chokkaram, Sivaraj, et al.** 121, s.l. : Journal of Molecular Catalysts, 1997, pp. 157-169.

31. *Incorporation of Nitrogen in Alkaline-Earth Hexaaluminates with B-Alumina or Magnetoplumbite-type Structure.* **Jansen, S.R., de Haan, J.W.** 7, 1997, Chemistry of Materials, Vol. 9, pp. 1516-1523.